Durham E-Theses

An examination of regge cut models in high energy scattering processes

Fitton, Alec

How to cite:

Fitton, Alec (1974) *An examination of regge cut models in high energy scattering processes*, Durham theses, Durham University. Available at Durham E-Theses Online: http://etheses.dur.ac.uk/8272/

Use policy

AN EXAMINATION OF REGGE CUT MODELS

IN

HIGH ENERGY SCATTERING PROCESSES

AN EXAMINATION OF REGGE CUT MODELS

IN

HIGH ENERGY SCATTERING PROCESSES

THESIS SUBMITTED TO THE

UNIVERSITY OF DURHAM

BY

ALEC FITTON B. Sc. (DUNELM)

FOR THE DEGREE OF DOCTOR OF PHILOSOPHY

DEPARTMENT OF PHYSICS   OCTOBER 1974

UNIVERSITY OF DURHAM

ABSTRACT

A phenomenolgical analysis of two body scattering data
with particular emphasis on the phase and energy dependence of
Regge cut corrections is presented.

After a brief summary of the Regge philosophy and approach,
we survey the experimental data in chapter two. We note that all
hadronic processes, as distinct from photoproduction appear to
exhibit strong Regge shrinkage at large $|t|$.

In chapter three, we motivate the eikonal model approach
and show how it is used to calculate cuts in πN charge exchange
and in photoproduction. Most of the phase problems encountered in
the naive absorption models can be overcome, provided we use the
true elastic amplitude (which we represent as a sum of $P + P'$
poles) to generate the absorptive corrections. We conclude this
chapter by discussing how the shrinkage of the eikonal model cuts
is inconsistent with the α_{eff}'s of chapter two for hadronic
processes.

We digress a little in chapter four to examine the important
role played by t-channel unitarity and show how it can solve some
of the problems outlined in the previous chapter by peaking the
cut discontinuity at the position of the pole.

Finally, we propose a new scheme for calculating Regge cuts
and in the last chapter construct a specific model for πN CEX
and π° photoproduction. A detailed examination of the cut discont-
inuity provides a possible explanation for the different energy
dependence of these ostensibly similar processes.

In conclusion, we discuss the implications of our model for
the traditional (Michigan and Argonne) approaches to Regge cut
phenomenology and suggest some areas which may provide interesting
tests of the model.

PREFACE

Part of the work reported here has been done in collaboration with Dr. P. D. B. Collins and is published in Nuclear Physics B68 125 (1974).

No part of this work has been submitted for a degree in this or any other university.

CONTENTS

INTRODUCTION

The strong interaction is characterised, as its name suggests, by the strength of the force as compared with the other fundamental forces which exist in nature - Electromagnetic, Weak and Gravitational. In nuclear physics it provides the binding force which holds the nucleus together against the repulsive effect of the coulomb interaction. The short range nature of the nuclear force prompted Yukawa to postulate the existance of the π meson. Low energy (~ 1 kev/c) nuclear reactions show a rapid variation in the cross section plotted as a function of centre of mass energy, which is well described by a sum of resonances given by the simple Breit-Wigner formula. As the energy increases ($\sim 10 - 20$ Mev/c) the resonances merge to form a continuum which can, nevertheless, still be interpreted as a sum of overlapping Breit-Wigner resonances.

In elementary particle physics the strong interaction also accounts for the forces between a group of particles known collectively as hadrons. A striking feature is the richness of the hadronic spectrum compared to the limited number of particles which do not experience strong interactions (leptons). As in nuclear physics, the cross section up to a few Gev/c shows prominant resonance bumps which at higher energies begin to overlap into a continuum. Hadronic resonances can be grouped into SU(3) singlets, octets and decuplets for baryons and singlets and octets for mesons, whose quantum numbers may be generated by the quark model. There are as yet no firmly established exotic resonances (i.e. those which

cannot be constructed in the quark model from $q\bar{q}$ for mesons and qqq for baryons).

The successes of field theories in describing Electromagnetic interactions cannot be carried over with any confidence into the strong interaction situation. One reason is simply the strength of the interaction which prohibits the utilisation of the normal perturbation expansion techniques. A further problem is the complexity of the hadronic spectrum, which makes it extremely difficult to formulate a theory in which each particle necessitates the introduction of a new field operator. If we try to construct a theory in terms of a limited set of operators, we violate the democracy which appears to exist amongst the hadrons by imposing the view that some particles are more elementary than others.

A more appealing approach to strong interactions is in terms of the S-matrix, where the aim is to formulate a theory from a few general postulates such as crossing, Lorentz invarience, conservation of probability etc.. Here the main interest is in the scattering amplitude and by including some additional assumptions about the analytic properties of the S-matrix we arrive at the Regge approach which has been so successful in describing experimental data.

High energy two-body or quasi two-body processes are known to be peripheral, with the angular distributions often showing prominent peaks in the forward (or backward) direction. Their presence or absence is strongly correlated with the presence or absence of particles

(or resonances) in the crossed t (or u) channel. The
integrated cross section also exhibits a power law dependence
as a function of centre of mass energy. Both of these
experimental facts can be understood within the Regge framework ,
which places the known hadronic states on trajectories which
are approximately linear functions of the square of the particle
masses. The prediction that the differential cross section
should "shrink" (become increasingly concentrated in the forward
direction) with increasing energy, is also well verified
experimentally.

As accurate data has become available for a wide range
of experimental observables (polarisations, spin rotation
parameters, asymmetries, decay correlations, etc.) the
emphasis in Regge phenomenology has shifted towards a direct
study of the amplitudes themselves. In one particular process
it has become possible to extract the amplitudes in a model
independent way. However, many features of the data cannot be
adequately described in terms of the leading set of Regge poles
alone. We here adopt the most logical solution to the problems
of simple pole models - namely that Regge cuts are also
important in the full scattering amplitude.

The most fundamental difficulty with Regge cuts is
the lack of knowledge of the discontinuity function.
Most phenomenologists work in the absorptive/eikonal model
where the analogy to nuclear physics is once again strong.
There is also considerable debate about the structure of the
input Regge pole residue and the mechanism which produces the

observed dips in differential cross sections.

Phenomenologists are continually appealing for
higher energy data against which to test their models. In
recent years this cry has been answered by the abundance of
data at sufficiently high energies to allow the symbol $\gg$
to take on its full meaning. The Serpukhov machine provides
for the collision of up to 70 Gev/c proton beams with a
stationary target, whilst NAL extends the range up to 400
Gev/c. The CERN Intersecting Storage Ring (ISR) facility
provides a centre of mass energy equivalent to a 3000 Gev/c
proton beam striking a stationary target. At such ultra-high
energies, the number of final state particles is so large as to
prohibit a detailed analysis of the energy and momentum of each.
This has led to the study of "inclusive reactions" in which
one observes only a limited number (usually one) of the
final state particles.

Much of the data, which has already come out of the
new accelerators, such as the rising total cross sections
and appearance of structure in the pp differential cross
section, provides a fascinating challenge to the ingenuity of
Regge phenomenologists. In this thesis we concentrate on the
quasi two-body data over the whole of the currently available
energy range and look at its interpretation in the light of
various Regge cut models.

CHAPTER   ONE

1.1 INTRODUCTION

We approach the problems of high energy scattering through the framework of S-matrix theory [1], where the S-matrix is defined to be the operator which transforms the incoming system of particles into the out-going system. The probability for the transition to occur is then given by the square modulus of S, and conservation of probability then demands that S be unitary. By explicitly removing that part of S which represents the physically uninteresting situation in which the particles do not inter-act, we arrive at a definition of the reaction or scattering amplitude (A). Maximal analiticity of the First Kind [1] now states that the only singularities of A are those poles corresponding to physical particles and the cuts generated from them through the unitarity equation

$$A - A^\dagger = 2 A A^\dagger \qquad (1.1)$$

In appendix one we define the s,t and u channels for a general two particle scattering process. In the simple case of equal masses, A(s,t,u) is the physical amplitude for the s-channel reaction when

$$s > 4m^2 \quad ; \quad t \leqslant 0 \quad ; \quad u \leqslant 0$$

where s,t and u are all real.

It is possible to define an analytic continuation [2] of the amplitude into the t-channel physical region.

$$t > 4m^2 \quad ; \quad s \leqslant 0 \quad ; \quad u \leqslant 0$$

The postulate of crossing symmetry asserts that the amplitude thus obtained is the physical amplitude for the t-channel process. Therefore the s,t and u channel reactions may each be described by the same analytic function $A(s,t,u)$ evaluated in the appropriate region of phase space.

1.2 THE CONTINUATION TO COMPLEX ANGULAR MOMENTUM

The angular momentum structure of scattering amplitudes has long formed a basis for experimental and theoretical investigation. Following the work of Regge in potential scattering, it was recognised that the continuation to complex values of angular momentum provided, via the crossing postulate , a link between the asymptotic behaviour of the amplitude and its angular momentum structure. It is the extension and development of this idea that forms the basic content of Regge thoery, where the high energy behaviour in the direct channel is interpreted in terms of the exchange of one or more composite particles, or Regge poles, in the crossed (t or u) channel.

The problem therefore, is to extend the range of validity of the t-channel partial wave series, which for spinless particles may be written in the form

$$A(s,t) = 16\pi \sum_{\ell=0}^{\infty} (2\ell+1) A_\ell(t) P_\ell(z_t) \qquad (1.2)$$

where $A(t)$ is the partial wave amplitude of angular momentum ℓ, and $P(Z_t)$ is the Legendre function of the First Kind.

The inverse of (1.2) is

$$A_\ell(t) = \frac{1}{32\pi} \int_{-1}^{1} A(s,t) P_\ell(z_t) \, dz_t \qquad (1.3)$$

This representation breaks down as soon as we encounter the first s (or u) channel singularity - that is outside the enlarged Martin-Lehmann ellipse [3]. To obtain information about the analytic properties of A(s,t) outside this region, we replace the summation in (1.2) by a contour integral in the complex angular momentum plane [1]. The partial wave amplitudes are now (complex) analytic functions of ℓ close to the real axis, which are subject to the constraint

$$A_\ell(t) = A(\ell,t) \qquad \ell = 0, 1, 2 \ldots \qquad (1.4)$$

In order that the new representation be unique (equation (1.4) does not gaurantee this) the continued partial wave amplitudes must satisfy Carlson's Theorem [3]. We shall, for the moment, assume that a suitable definition of $A(\ell,t)$ exists.

The step of replacing (1.2) by a contour integral in the complex ℓ-plane is known as the Sommerfeld-Watson transform [1].

$$A(s,t) = \frac{-16\pi}{2i} \int_{C_1} \frac{(2\ell+1) A(\ell,t) P_\ell(-z_t)}{\sin \pi\ell} \, d\ell \qquad (1.5)$$

A(ℓ,t) is assumed to be analytic in the region close to the real axis enclosed by the contour C_1 (shown below) so

only singularities of the integrand come from the vanishing of the denominator at integer values of ℓ. The argument of the Legendre Function is taken to be $-Z_t$ to compensate for the factor $(-1)^\ell$ appearing in the residue of the poles at integer ℓ.

The crucial step in the Regge analysis is to deform the contour $C_1 \longrightarrow C_2$ to expose the singularities of $A(\ell, t)$, such as poles and cuts, for $\mathrm{Re}(\ell) > -\tfrac{1}{2}$.
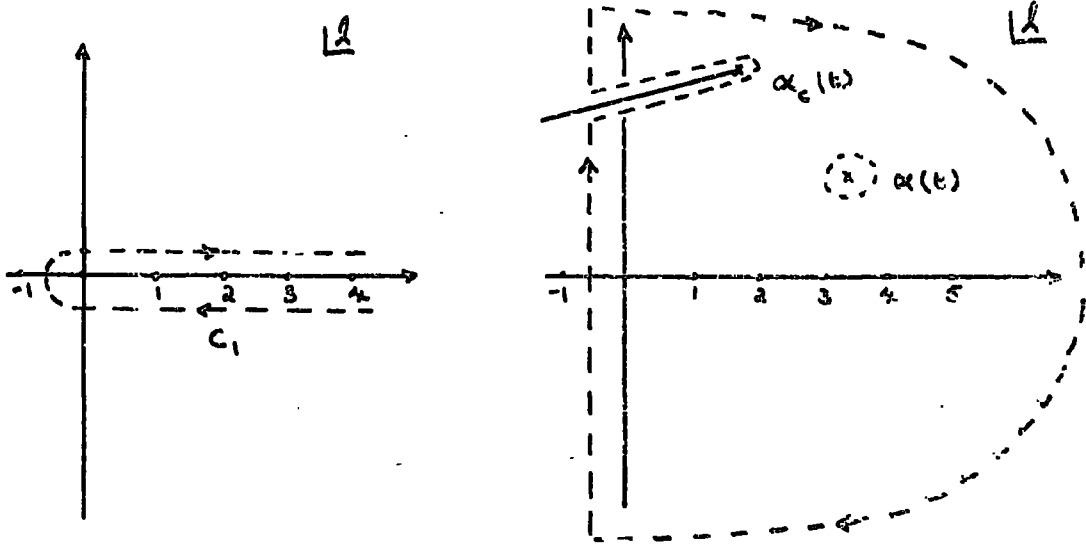
Provided the behaviour of the partial wave amplitudes is such that the contribution from the large semicircle ($|\ell| \to \infty$, $\mathrm{Re}(\ell) > -\tfrac{1}{2}$) can be neglected, then

$$A(s,t) = -\frac{(2\ell+1)\,\beta_\alpha(t)\,P_\alpha(-z_t)}{\sin \pi\alpha} - \frac{16\pi}{2i}\int_{\text{cut}} \frac{(2\ell+1)\,\Delta(\ell,t)\,P_\ell(-z_t)}{\sin \pi\ell} \tag{1.6}$$

+ fixed poles + background.

In (1.6) we have exhibited the contribution from a single Regge pole at $\alpha(t)$ with residue $\beta_\alpha(t)$ and a single branch cut running from $\ell = \alpha_c(t)$ to $\ell = -\infty$ with discontinuity $\Delta(\ell,t)$.

The background integral is the contribution from the line $-i\infty - \frac{1}{2}$ to $+ i\infty - \frac{1}{2}$ which vanishes as $Z^{-\frac{1}{2}}$ for $Z \to \infty$.[1]. Mandelstam has shown how it is possible to push the background to the left $(\mathrm{Re}(\lambda) < -\frac{1}{2})$ so that the Regge terms always dominate the background asymptotically. This procedure is well known [1,3] and alters non of the conclusions which we shall draw from (1.6).

The interesting situation is one in which $s \to \infty$ (the s-channel physical region). In this limit

$$P_{\ell}(-z_t) \xrightarrow[s \to \infty]{} (-z_t)^{\ell} \tag{1.7}$$

and using the kinematics of Appendix one, equation (1.6) becomes (neglecting the non Regge terms)

$$A(s,t) \underset{s \to \infty}{=} - \frac{\beta(\alpha,t)\left(s/s_0\, e^{-i\pi}\right)^{\alpha(t)}}{\sin \pi \alpha(t)}$$

$$- \int_{-\infty}^{\alpha_c(t)} \frac{\Delta(\ell,t)\left(s/s_0\, e^{-i\pi}\right)^{\ell}}{\sin \pi \ell}\, d\ell \tag{1.8}$$

where s_0 is a scale factor, and we have absorbed all extraneous factors into the residue and discontinuity functions β and Δ . Thus the trajectory $\alpha(t)$ completely determines the energy dependence of the first term in (1.8), the Regge pole term.

We now return to the problem of obtaining a suitable definition of the partial wave amplitudes in which to make the continuation provided by the Sommerfeld-Watson transform. (A full account of this procedure for the general case of particles

with spin can be found in reference (4)). Froissart and Gribov have shown that a sufficient condition for the required continuation to exist is that the Mandelstam representation [3] holds for the amplitude $A(s,t)$. We proceed therefore by writing a dispersion relation in s at fixed t, involving both the s and u singularities of A.

$$A(s,t) = \frac{1}{\pi} \int_{z_{t_0}}^{\infty} \frac{D_s(z_t', t)}{(z_t' - z_t)} dz_t' + \frac{1}{\pi} \int_{-z_{u_0}}^{-\infty} \frac{D_u(z_t', t)}{(z_t' - z_t)} dz_t' \quad (1.9)$$

D_s and D_u are the discontinuities across the right and left hand cuts respectively. (1.9) is only valid up to the number of subtractions required to make the integrals converge. Substituting (1.9) in (1.3) and interchanging the order of integration gives

$$A_\ell(t) = \frac{1}{16\pi^2} \int_{z_0}^{\infty} \left[D_s(z', t) + (-1)^\ell D_u(-z', t) \right] Q_\ell(z') dz' \quad (1.10)$$

where $Q_\ell(Z)$ is the Legendre function of the second kind and

$$Z_0 = \min \left\{ z_{t_0}, z_{u_0} \right\}$$

As we have already discussed, for the continuation (1.5) to be unique the large ℓ behaviour of the amplitude must satisfy Carlson's theorem. The exchange forces represented by the u-singularities in (1.10) involve the usual factor $(-1)^\ell$ which also appears in potential scattering (Majorana forces). This violates Carlson's theorem. The way out of the difficulty is to define amplitudes of definite signature $\mathcal{S}(= \pm 1)$ [4].

$$A_\ell^\pm(s,t) = \frac{1}{16\pi^2} \int_{z_0}^{\infty} \left[D_s(z',t) \pm D_u(-z',t) \right] Q_\ell(z') \, dz' \qquad (1.11)$$

Thus the signatured partial wave amplitudes $A_\ell^\pm(t)$ coincide with the physical amplitudes for even/odd values of ℓ respectively.

Looking at the pole term in (1.6), we need to replace the factor $\left[\dfrac{P_\alpha(-z_t)}{\sin \pi \alpha} \right]$ by $\left[\dfrac{\delta P_\alpha(z_t) + P_\alpha(-z_t)}{\sin \pi \alpha} \right]$ which, in the high energy limit, becomes

$$\frac{\delta + e^{-i\pi\alpha(t)}}{\sin \pi \alpha(t)} \qquad (1.12)$$

((1.12) is often called the "signature factor")

So the effect of introducing signature is to replace $\left[\dfrac{e^{-i\pi\alpha}}{\sin \pi\alpha} \right]$ by (1.12) in equation (1.8) with a similar replacement in the cut term, giving

$$A(s,t) = -\beta(\alpha,t) \left(\frac{\delta + e^{-i\pi\alpha(t)}}{\sin \pi \alpha(t)} \right) \left(\frac{s}{s_0} \right)^{\alpha(t)}$$

$$- \int_{-\infty}^{\alpha_c(t)} \Delta(\ell,t) \left(\frac{\delta + e^{-i\pi\ell}}{\sin \pi\ell} \right) \left(\frac{s}{s_0} \right)^\ell d\ell \qquad (1.13)$$

All of the Regge formalism outlined above may be generalised to the case of particles with spin. Problems such as the need for amplitudes of definite parity, kinematic singularities and constraints and the analytic properties of the

trajectory and residue functions are dealt with in detail in reference (4).

1.3 REGGE POLES IN S-CHANNEL HELICITY AMPLITUDES

The first term in (1.13) is the contribution of a single Regge pole to a t-channel helicity amplitude. For many purposes (particularly when considering absorptive corrections) it is convenient to work in terms of s-channel helicity amplitudes. In principle the connection between the two sets of amplitudes is provided by the helicity crossing matrix[2]. Cohen-Tannoudji et al[5] write the contribution of a t-channel Regge pole to an s-channel helicity amplitude as

$$A_{H_s}(s,t) = \left(-\frac{t}{s_0}\right)^{\frac{x}{2}} \left(\frac{t_0-t}{s_0}\right)^{\frac{N}{2}} \gamma_{H_s}(t) \, F_{H_s}(\alpha) \left(\frac{8+e^{-i\pi\alpha(t)}}{\sin\pi\alpha(t)}\right)\left(\frac{s}{s_0}\right)^{\alpha(t)} \quad (1.14)$$

where N is the net s-channel helicity flip.

$$N = |(\mu_1-\mu_3)-(\mu_3-\mu_4)| \quad (1.15)$$

and

$$x = |\mu_1-\mu_3| + |\mu_2-\mu_4| - N \quad (1.16)$$

The quantity t_0 is the value of t when $\theta_s = 0$ and is defined in Appendix one. S_0 is usually taken to be 1 Gev/c and the function $F_{H_s}(\alpha(t))$ depends on whether the pole chooses sense, nonsense, etc..

1.4 EXCHANGE DEGENERACY AND NONSENSE WRONG SIGNATURE ZEROS

Phenomenologically, Regge poles of opposite signature appear to occur in (exchange degenerate) pairs such that

$$\alpha^+(t) = \alpha^-(t) \equiv \alpha(t) \qquad (1.17)$$

where the superscripts relate to even or odd signature.

Equation (1.17) is a statement of weak exchange degeneracy (EXD). Strong EXD also demands equality of the residues.

$$\gamma^+(t) = \gamma^-(t) \equiv \gamma(t) \qquad (1.18)$$

Strong EXD therefore imposes a severe restriction on the pole terms in reactions where a pair of EXD Regge poles may be exchanged. For example consider

(A) $K^-p \to \bar{K}^0 n$ where the full amplitude is $A_2 + \rho$

(B) $K^+n \to K^0 p$ where the full amplitude is $A_2 - \rho$

(The sign change in the rho contribution reflects the property that the rho is odd under charge conjugation.) If strong EXD holds, then (see(1.14))

$$\rho(s,t) = \gamma(t) \left(-1 + e^{-i\pi\alpha} \right) s^\alpha \qquad \text{odd signature}$$

$$A_2(s,t) = \gamma(t) \left(1 + e^{-i\pi\alpha} \right) s^\alpha \qquad \text{even signature}$$

(We represent the contribution of a Regge pole to the full amplitude by its trajectory label.)

Now assuming that $\alpha(t)$ and $\gamma(t)$ are real for $t < t_0$, we see that the amplitude for (B) is purely real, whilst that for (A) is the same apart from a rotating phase factor.

$$A(K^-p \to \bar{K}^0 n) \sim 2\gamma(t) e^{-i\pi\alpha} s^\alpha$$

$$A(K^+n \to K^0 p) \sim 2\gamma(t) s^\alpha$$

Strong EXD therefore predicts equality for the cross sections and zero for the polarization in both reactions. Similar results are obtained for pairs of processes connected by "line reversal" [4,6].

For example :-

$$K^-p \to \pi^- \Sigma^+ \qquad K^{**} - K^{*} \qquad \text{Real}$$

$$\pi^+p \to K^+ \Sigma^+ \qquad K^{**} + K^{*} \qquad \text{Rotating}$$

$$K^-p \to \pi^0 \Lambda \qquad K^{**} - K^{*} \qquad \text{Real}$$

$$\pi^-p \to K^0 \Lambda \qquad K^{**} + K^{*} \qquad \text{Rotating}$$

$$K^+p \to K^0 \Delta^{++} \qquad K^{**} - K^{*} \qquad \text{Real}$$

$$K^-n \to \bar{K}^0 \Delta^- \qquad K^{**} + K^{*} \qquad \text{Rotating}$$

Finally consider the signature factor (1.12). At right signature points (α even for δ even etc.), the denominator gives a pole which is not removed by the numerator and must therefore be cancelled by a zero in the residue γ (t). Strong EXD means that we must use the same residue for both signatures, so γ (t) must have a zero at the wrong signature points also (since this is a right signature point for the other EXD trajectory). But the cancellation of numerator and denominator in (1.12) occurs automatically at wrong signature points leaving an overall amplitude zero, known as a wrong signature nonsense zero.

1.5 PREDICTIONS OF PURE REGGE POLE MODELS

In (1.14) we have a simple formula which can be directly confronted with the experimental data. It is most easily tested in the few reactions where the t-channel quantum numbers are sufficiently restrictive to allow the exchange of only a single Regge pole. In one such process, pion nucleon charge exchange (CEX), enough data exists to allow a complete separation of the amplitudes (see chapter two). We list below other processes of this nature together with the upper limit of the available energy range.

Reaction	Exchange(s)	Max P_{lab} (Gev/c)
$\pi^- p \to \pi^o n$	ρ	48 (200)
$\pi^- p \to \eta^o n$	A_2	50 (200)
$K_L^o p \to K_S^o p$	$\omega (\rho)^{(3)}$	10
$K^- p \to \eta^o n$	$K^*(K^{o*})$	4.25
$K^- p \to \eta^o n$	$K^*(K^{*o})$	4.25

We have indicated in brackets after the first two react-
ions the energy range which will soon be available from the NAL
machine.

Returning to (1.14), both the phase and energy depend-
ence of the Regge pole contribution are completely fixed once
we have specified the trajectory $\alpha(t)$, provided $\alpha(t)$ and
$\gamma(t)$ are both real. Furthermore, they are independent of all
helicity labels, so that in a given reaction, all helicity
amplitudes corresponding to the exchange of a particular Regge
pole have identical phase and energy dependence. We shall
return to the question of determining $\alpha(t)$ from the experiment-
al data in chapter two. The phase restriction predicts that
the polarization should be zero in the process shown in the
table above, if we allow only Regge pole exchange. This simply is
because polarizations depend on the relative phases of helicity
amplitudes through formulae such as (A1.12).

The experimental data provides many severe tests of
(1.14). There is now overwhelming evidence to support the
conjecture that Regge poles alone are not the only singularities
which contribute to high energy scattering amplitudes, and that
Regge cuts arising from the second term in (1.13), are also
important. We list below some of the predictions of pure Regge

pole exchange which are in direct conflict with the data[8].

(i) The non zero polarization oberseved in πN CEX[9] is a direct indication of some other contribution besides the rho pole. This could be a secondary trajectory or it could be a cut.

(ii) The failure of the omega "crossover zero" (see chapter two) in pp and $\bar{p}p$ to propagate, via factorisation, into other processes such as $\pi N \rightarrow \rho N$ or $\gamma p \rightarrow \pi^e p$ which are also dominated by omega exchange. Since cuts do not need to factorise, the addition of a destructive cut which generates the zero by pole-cut interference obviates this. Alternatively we could invoke a lower lying ω' trajectory and form the zero by interference between it and the ω . In this case we would expect the zero to move to larger values of $|t|$ as the energy increased.

(iii) The high energy ($P_{lab} \gtrsim 20$ Gev/c) total cross section data[10] disagrees with the extrapolation of low energy energy fits done with simple pole models. In particular, these fits predict a constant total cross section at high energy coming from Pomeron (P) exchange, whilst the data exhibits a broad minimum ($\sigma_{tot}(pp)$) over the Serpukhov energy range, followed by a distinct rise through the NAL and ISR ranges. One explanation is the presence of destructive cuts which die away logarithmically to isolate the Pomeron pole contribution. However $\alpha_p(o) > 1$ is also a possible, if slightly more controversial explanation[11].

(iv) The failure of NWSZ to appear in reactions related by factorisation is also evidence to support the inclusion of important (non factorising) cut contributions. For example the NWSZ of the rho trajectory, which in pole models accounts for

the dip at $t \sim 0.6$ (Gev/c)^2 in $\pi^- p \to \pi^0 n$ does not appear in $\gamma p \to \eta^0 p$ which is also dominated by rho exchange. The presense of a lower lying B contribution in the latter reaction has also been invoked to explain the absense of a dip[12].

(v) The data on $\gamma p \to \pi^+ n$ and $np \to pn$ shows a prominant peak in the forward direction of width $\sim m_\pi{}^2$. Both processes are dominated by π exchange which, because of its parity must decouple at $t=0$. The pole model therefore predicts a forward dip. A pion conspirator seems to violate factorisation, but a destructive $\pi \otimes P$ cut again provides an answer.

(vi) As we have mentioned, strong EXD predicts equality of the differential cross sections for pairs of processes connected by line reversal. Experimentally the rotating phase reaction lies above the real reaction in most cases[6] by an amount which requires a substantial breaking of EXD in pole models. Furthermore, to explain the polarization requires secondary trajectories. We might hope that cuts would violate EXD in such a way as to reconcile theory and experiment.

1.6 REGGE CUTS

As we have seen, Regge cuts are very desirable objects phenomenologically, providing at first sight a simple and appealing way out of several problems inherent in the pure pole models. Most of the theoretical understanding of Regge cuts has relied upon the Feynman diagram approach[13]. The most common method is to use the "weak coupling limit" to examine the analytic structure of the diagrams in perturbation theory and to hope that the results may hold true in the strong interaction context.

In addition to the obvious argument that there is no reason why Regge cuts should not be present and furthermore give

important contributions to the full scattering amplitude,
Mandelstam[14]demonstrated that cuts are instrumental in removing
many of the difficulties caused by fixed J-plane singularities
at nonsense points of the amplitude[4]. These arise from any
diagram which has a third double spectral function (d.s.f.).
A third d.s.f. is also essential if we are to generate a true
Regge cut. The simplest Feynman diagram which does this is the
"double cross" graph shown below, where the "bubbles" are
complex scattering amplitudes.
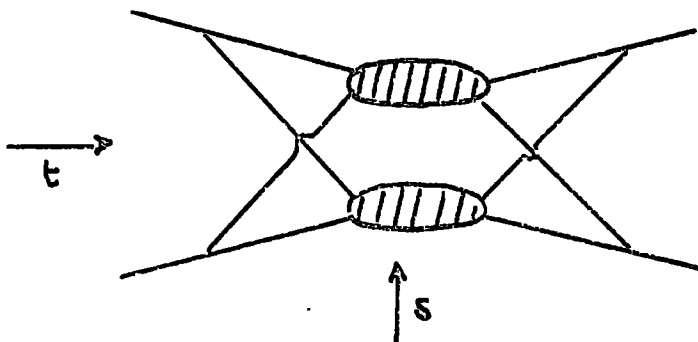
If the asymptotic contribution to the bubbles is taken
to be Regge pole exchange, then the full diagram gives a two-
Reggeon cut.

It has been demonstrated[15] that the t-iterations of
this diagram are important in "softening" the nature of the cut
(i.e. forcing the discontinuity to vanish at the tip of the cut)
and in removing the difficulties presented by the singularities
mentioned above - in particular the Gribov-Pomeranchuk fixed pole
at J=-1. The insertion of such a singularity into the t-channel
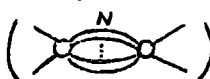unitarity equation for the partial wave amplitudes,

$$A_J(t) - A_{J^*}^*(t) = \rho_J(t) \, A_J(t) \, A_{J^*}^*(t) \tag{1.19}$$

means that it iterates util it eventually becomes incompatible

with Maximal Analiticity in J [8]. Apart from giving a Regge cut, diagrams such as the one above have branch points which lie along the unitarity cut in such a way that A_J and A_{J^*} must be evaluated on opposite sides of the cut. Since the fixed pole is present only in A_J, it remains a pole and is eventually cancelled in the physical amplitude by the signature factor.

Amati, Fubini and Stanghellini [16] (AFS) looked at Feynman diagrams of the type shown below, the essential feature of which is their planar topology.
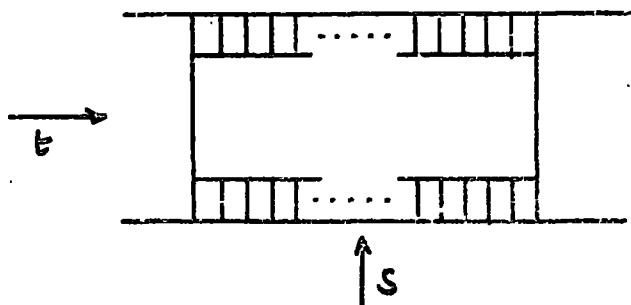
That this diagram does not generate a Regge cut on the physical sheet was demonstrated explicitly by Mandelstam [14]. In fact it gives a contribution which, asymptotically, goes like $s^{-3} \log(s)$ [17]. The AFS mistake was in taking just the two-particle discontinuity term $\left(\rangle\!\!\bowtie\!\!\langle \right)$ in the unitarity equation, which in fact behaves like $(\log(s))^{-1} s^{\alpha_c(t)}$ (moving cut). Including the full spectrum of intermediate states $\left(\rangle\!\!\overset{N}{\ominus}\!\!\langle \right)$ sees a cancellation of this term and the diagram has the fixed cut behaviour given above.

There are therefore, general arguments in favour of Regge cuts in any theory which has a non zero third d.s.f.. Mandelstam's analysis details the following specific properties of Regge cuts:-

(i) If the individual exchanges in the two Reggeon cut are represented by Regge poles with trajectories $\alpha_1(t)$ and $\alpha_2(t)$

then the branch point trajectory is given by

$$\alpha_c(t) = \text{Max}\left(\alpha_1(t_1) + \alpha_2(t_2) - 1\right) \qquad (1.20)$$

where

$$\sqrt{-t} = \sqrt{-t_1} + \sqrt{-t_2} \qquad (1.21)$$

If the input trajectories are linear functions of t

$$\alpha_i(t) = \alpha_i(0) + \alpha_i' t \qquad (1.22)$$

then it can easily be shown that the constraint (1.20) leads to the cut trajectory

$$\alpha_c(t) = \alpha_1(0) + \alpha_2(0) - 1 + \left(\frac{\alpha_1' \alpha_2'}{\alpha_1' + \alpha_2'}\right) t \qquad (1.23)$$

Thus if one (or both) of the exchanged Reggeons is the Pomeron which has $\alpha_P(0) = 1$, then the position of pole and cut coincide at $t = 0$. Equation (1.23) can readily be generalised to the case where more than two Reggeons are exchanged. Again, the Regge pole (R) and its n-Pomeron cut $(R \boxtimes P^n)$ coincide at $t = 0$.

Taking the typical Reggeon and Pomeron trajectories

$$\alpha_R(t) = 0.5 + t$$

$$\alpha_P(t) = 1.0 + 0.3 t$$

we obtain the relative energy dependences (up to possible factors of $\log(s)$) shown below for the two-Pomeron, Reggeon-Pomeron and two-Reggeon cuts.
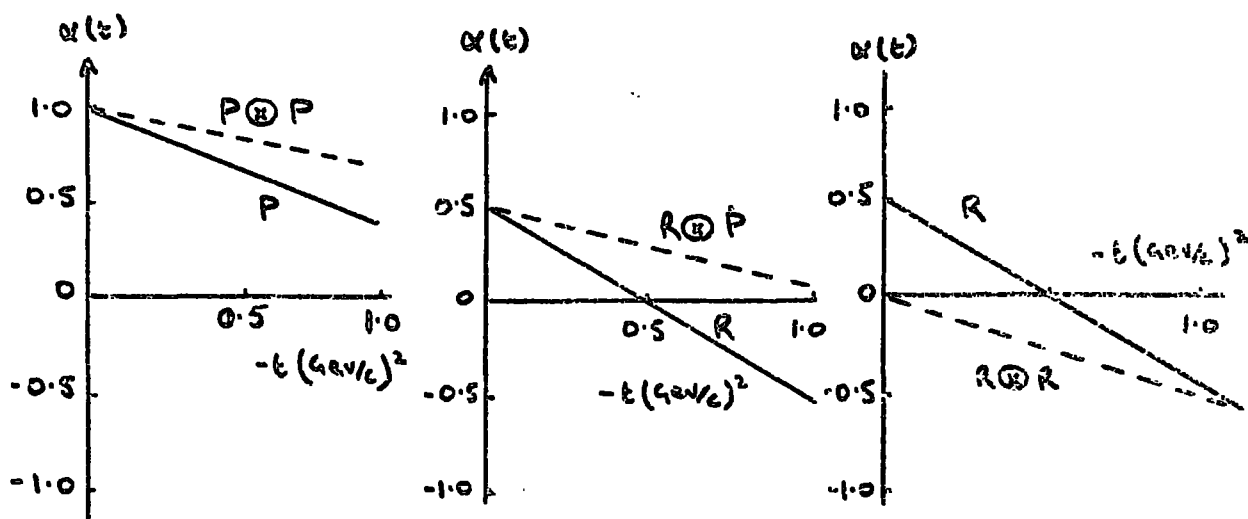
(ii) The signature of the two-boson cut is simply the product of the signature factors for the individual exchanges.

$$\mathcal{S}_c = \mathcal{S}_1 \, \mathcal{S}_2 \qquad\qquad (1.21)$$

(For the two-baryon cut $\mathcal{S}_c = -\mathcal{S}_1 \mathcal{S}_2$)

(iii) Although Regge poles have definite parity, cuts may contribute to both parities because of the orbital angular momentum $(-1)^{\ell}$.

(iv) Cuts do not factorise.

1.7 ABSORPTIVE CORRECTIONS TO REGGE POLES

A conceptually appealing way of thinking about Regge cuts, is in terms of multiple rescattering or absorptive corrections. The basic Regge pole exchange is modified by elastic scattering - usually represented by the Pomeron - in either the initial or final state. For example, we consider diagrams such as
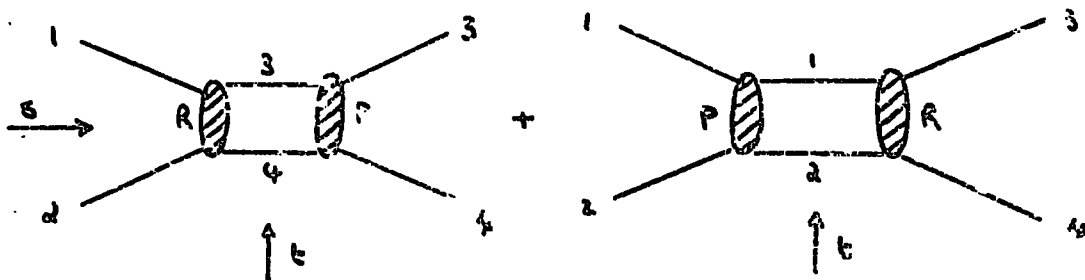
Experimentally, most of the inelastic two-body cross section is peripheral i.e. the dominant contribution is from impact parameters corresponding to the surface of the target hadron ($b \sim 1$ fm.). Conversely, high multiplicity collisions result from the projectile striking the centre of the target. Now, the impact parameter decomposition of a Regge pole amplitude such as (1.14) with net helicity flip N is

$$A_N(t) \sim \int_0^\infty b\,db\, A_N(b)\, J_M(b\sqrt{-t})$$ (1.25)

This formula will be derived in detail in chapter three. However, for a simple exponential residue, a Regge pole has an impact parameter profile $A_N(b)$, which is peaked at small b. The addition of absorptive corrections, which allow for the possibility of creating high multiplicity final states at small b, tends to damp out the low partial waves to give an impact parameter profile which is more peripheral (coming from a ring of radius R, with $R \sim 1$ fm).

The resulting t dependence is characteristic of the Bessel function, producing a typical diffraction structure with the positions of the dips controlled by the index of the Bessel function and the parameter R. In fact for $R \sim 1$ fm, the first zero of the Bessel function with N=0 occurs at $t \sim -0.2$ (Gev/c)^2, whilst for N=1 it is at $t \sim -0.6$ (Gev/c)^2. These are in remarkable agreement with the position of the crossover zero and the dip in the pion-nucleon CEX differential cross section. There is also evidence to support a further zero in the imaginary part of the non flip amplitude at $t \sim -1.2$ (Gev/c)^2 [18] which again correlates nicely with the second zero of J_0.

Also, the strongest low energy resonances appear to occur in the peripheral band of partial waves, by which we mean those for which $\ell \sim P_{cm}R$, with $R \sim 1$ fm. Duality then leads us to expect strong corrections to Regge poles, which alone are non-peripheral.

The early attempts to calculate absorptive corrections were based on the Sopkovich prescription[4], in which the quantum numbers are carried by the Regge pole and absorption is included by multiplying each partial wave by the square root of the elastic S-matrix to account for elastic scattering in the initial and final states. Typically, this is assumed to be adequately described by the Pomeron and we end up with (schematically)[19]

$$A(s,t) = A_R + i\, A_P(s,t) \otimes A_R(s,t) \qquad (1.26)$$

In this equation, the symbol '$\otimes$' represents a convolution such as

$$A \otimes B \sim \frac{1}{8\pi^2 s} \int dt_1\, dt_2\, A(t_1) B(t_2)\, \frac{\theta(\tau)}{\tau^{1/2}} \qquad (1.27)$$

where

$$\tau = -t^2 - t_1^2 - t_2^2 + 2tt_1 + 2tt_2 + 2t_1 t_2 \qquad (1.28)$$

The result of convoluting two exponentials, such as appear in a typical Regge residue, is

$$\exp(a_1 t) \otimes \exp(a_2 t) \sim \exp\left(\frac{a_1 a_2}{a_1 + a_2}\, t\right) \qquad (1.29)$$

A final point concerns the structure of the residue $\gamma_{H_s}(t)$ in the basic Regge pole term (1.14). There are two possibilities, which give rise to two different cut models.

(i) The strong cut model:

The Michigan group argue that the t structure observed in two-body scattering is mainly a geometric effect, characteristic of diffraction from the surface of the target hadron. The pole residues are then simple, exponentially decreasing functions of t and all structure is a product of pole-cut interference. To fit the data it is then necessary to multiply the cuts (the second term in (1.26) for example) by a constant, λ, which is interpreted as allowing for the possibility of diffractively produced intermediate states. Typically, $\lambda \sim 1.5 - 3.0$ to fit the data, hence the name " Strong Cut Reggeised Absorption Model " or SCRAM [19].

(ii) The weak cut model:

An alternative approach [20] is to assert that the Regge pole is the main contribution to the scattering amplitude and as such dictates the t dependence, which is only slightly modified by the (weaker) cuts. NWSZ's in the poles are filled in by the cuts to yield dips in the differential cross section; EXD adds predictive power to this approach. The nonsense factors mean that the pole changes sign within the region of integration in (1.26) giving rise to cancellations within the integral, and cuts that are weaker than in SCRAM.

It is now clear from (1.26) how cuts interfere with the pole terms in a destructive fashion. Since the Pomeron is mainly imaginary (at least near to $t = 0$), the rescattering corrections will be approximately 180° out of phase with the pole. Also (1.29) suggests that the cuts will die away less rapidly than the pole as we go to larger values of $|t|$. We therefore have a model in which the pole dominates near $t = 0$,

with the cuts becomming relatively more important and possibly cancelling the pole at large $|t|$.

However, there are several technical difficulties inherent in the absorption model approach. Mandelstam's work has emphasised the importance of the non planar nature of the rescattering diagrams in obtaining a true moving cut in the J-plane instead of a fixed (AFS) cut. The diagrams which we drew to motivate the absorption model are nonetheless definitely planar.

The absorption model also generates "hard cuts". This means that the discontinuity $\Delta(J,t)$ in (1.13) is finite at the tip of the cut $J=\alpha_c(t)$. Bronzan and Jones[15] have shown that such a behaviour is incompatible with t-channel unitarity which in fact forces the discontinuity to vanish at this point.

Finally, there is also the problem of whether the input Regge pole already includes (in principle) some absorptive corrections, since this already receives contributions from multiparticle intermediate states in the unitarity integral. In the Optical Potential Model developed by Arnold[21], the eikonal phase shift, χ, (to be defined in chapter three) is linearly related to the optical potential. A Regge pole gives a contribution to $\text{Im}\,\chi$, which therefore corresponds to absorption of flux from the input beam into various other competing channels besides the one under consideration. Thus including both the Regge pole and absorptive corrections may lead to double counting. In the eikonal model, the non planar structure of the diagrams avoids this problem.

To conclude this chapter we mention two predictions of the absorption model. The failure of these to be substantiated by

experiment (as we shall see in the next chapter), indicates the kind of phase modifications required by the model.

(i) The naive absorption model predicts approximately equal absorption at small $|t|$ in both the real and imaginary part of the input pole amplitude. Consequently, if we use the $\rho \boxtimes P$ cut to produce the crossover zero ($\text{Im } A_{++} = 0$ at $t \sim -0.2$ (Gev/c)^2) in pion-nucleon CEX, we are forced to accept a similar zero in the real part of the non flip amplitude. One consequence of this is a large negative spike in the predicted polarization in the region $0.2 \leqslant |t| \leqslant 0.6$ (Gev/c)^2 [19,20].

(ii) In section 4 we listed pairs of reactions involving vector and tensor meson exchanges which are connected by line reversal. From equation (1.26), it is clear that in the "real" process, pole and cut will be exactly 180° out of phase (the Pomeron is assumed to be pure imaginary). This will clearly not be so in the rotating case. In addition, cancellations may occur within the integrals ((1.27)) in the latter case which will further reduce the effectiveness of the pole-cut cancellation. We therefore expect the full amplitude (pole plus destructive cut) to be larger in the rotating case. The data shows

$$\frac{d\sigma}{dt} \left(real \right) \approx \alpha \frac{d\sigma}{dt} \left(rotating \right) \tag{1.30}$$

for the hypercharge exchange cases[6], in direct contradiction to the predicted behaviour. The pair

$$K^- p \to \bar{K}^0 \wedge \qquad \text{rotating}$$

$$K^+ n \to K^0 p \qquad \text{real}$$

achieve equality at about 5.0 Gev/c consistent with strong EXD, but below this energy the disagreement is in the same direction as (1.30).

CHAPTER TWO

2.1 INTRODUCTION

In the major part of this work we shall seek to use the abundance of good data which now exists over a wide range of s and t on the two reactions

(A) $\pi^- p \to \pi^0 n$ (πN CEX)

(B) $\gamma p \to \pi^0 p$

to critically examine various Regge cut models. Polarisation measurements and Finite Energy Sum Rule (FESR) analysis, both useful in fixing the detailed phase structure of the amplitudes, exist for both reactions. Kinematically the two reactions are very similar - the dominant amplitude being spin flip (N=1) in both cases. However, in (B) the flip occurs at the $\gamma\pi$ vertex ensuring that a different relationship between pole and cut is required to obtain the correct phases. The photoproduction reaction can have N=0, 1 or 2, and this rich amplitude structure is a severe test of any cut model.

We shall apply our models mainly to (A) and (B), but will infer from other global fits [22-24] that, given SU(3) and approximate exchange degeneracy, any model which successfully describes these two processes also gives a reasonable fit to the wider class of $0^- + \frac{1}{2}^+ \to 0^- + \frac{1}{2}^+$ reactions and those related to (B) by SU(3) and vector dominance. However, to support arguments which we shall present concerning the energy dependence of Regge cuts, it will be useful to consider data from a much wider set of processes.

2.2 THE REACTION $\pi^- p \to \pi^0 n$

The differential cross section for this process is remarkably well fitted in both its s and t dependence, by a simple pole model in which the rho chooses sense[25]. Then the presence of $\alpha_\rho(t)$ in the dominant spin flip amplitude accounts for the observed dip at $t \sim -0.6$ $(Gev/c)^2$, and the flip to non-flip ratio provides the marked turnover in the forward direction. The new data for the Serpukhov accelerator range[26] ($P_{lab} \lesssim 50$ Gev/c, $|t| \lesssim 1.5$ $(Gev/c)^2$) is still in good agreement with this picture. In particular the dip remains fixed at $t \sim -0.6$ $(Gev/c)^2$, strongly suggesting that it is not due to a pole-cut cancellation mechanism in the spin flip amplitude (SCRAM). In this case we would expect the dip to move to smaller values of $|t|$ as the relative importance of the cut increased with energy.

This is supported by the energy dependence of the differential cross section as represented by the quantity $\alpha_{eff}(t)$ defined in appendix two. A plot of this "effective" trajectory for the Serpukhov and other low energy data is shown in fig. (2.1) [26]. Whithin the errors it is in complete agreement with a linear rho trajectory. Two interesting conclusions can be drawn from fig. (2.1) :-

(i) In all the "convential" eikonal/absorptive models of Regge cuts, the dominant $\rho \boxtimes P$ cut has the approximate trajectory

$$\alpha_c(t) \approx 0.5 + 0.2 \, t \tag{2.1}$$

if, as in chapter one, we take $\alpha_\rho(t) = 0.5 + t$ and $\alpha_P(t) = 1.0 + 0.3 \, t$. The α_{eff} data is inconsistent with either a weak or strong cut model in which the cuts have the branch

point trajectory (2.1). In particular the (strong cut) model of Collins and Swetman[27], discussed in more detail in chapter three, gives the α_{eff} shown in fig.(2.2). For $|t| > 0.6$ (Gev/c)^2 the shrinkage observed in the data is much stronger than is anticipated on the basis of this model.

(ii) The structure in fig.(2.2) in the dip region $t \sim -0.6$ (Gev/c)^2 is a general feature of all convential cut models[28], whilst the data exhibits no such deviation from linearity.

Using the large $|t|$ data available at 3.67 and 4.83 Gev/c, Barger and Phillips have obtained an α_{eff} for $\pi^- p \to \pi^\circ n$ out to $t \sim -5.0$ (Gev/c)^2 [29]. Their trajectory is reproduced in fig.(2.3). Again the slope is in remarkable agreement with $\alpha'_\rho \sim 1$ (Gev/c)$^{-2}$. However, one must be careful when seeking to apply Regge theory at such large values of $|t|$, for such low values of s. For example, at $P_{lab} \sim 5$ Gev/c, $\theta_s = 60^\circ$ corresponds to $t \sim -2.3$ (Gev/c)^2, whilst $t \sim -5.0$ (Gev/c)^2 is well into the backward direction.

Thus, in pion nucleon CEX there is good evidence to suggest that the ρ trajectory continues to "shrink" out to very large values of $|t|$, in apparent contradiction to traditional cut models. We shall see later in this chapter, that this appears to be a universal feature of all $0^- + \frac{1}{2}^+ \to 0^- + \frac{1}{2}^+$ data.

As we mentioned in chapter one, the measurement of a non zero polarization in πN CEX[30] was instrumental in forcing phenomenologists to think seriously about Regge cuts. Furthermore, the fact that the polarization is positive for $0 \lesssim |t| \lesssim 0.5$ (Gev/c)^2, means that the amplitude phases predicted on the basis of the absorption model using weak or strong cuts[19,20] are also

incorrect. Sufficient data now exists at 6.0 Gev/c for the elastic and charge exchange reactions to allow a complete decomposition of the isospin amplitudes (defined in appendix one) up to an overall phase[31]. We shall attempt to outline briefly, how the data fixes the structure of the $I_t = 1$ amplitude.

In πN scattering, the $I_t = 0$ amplitude is well described by a sum of P and P' exchanges. As expected $|A^0_{++}| \gg |A^0_{+-}|$, and also $|ReA^0_{++}| \ll |ImA^0_{++}|$; ImA^0_{++} is strongly peaked in the forward direction and has no zeros at least out to $t \sim -0.8$ $(Gev/c)^2$. With this behaviour of the $I_t = 0$ amplitude, the data forces the $I_t = 1$ exchange amplitude to exhibit the following qualitative features:-

(i) The crossover zero.

The $\pi^\pm p$ elastic differential cross sections are equal at $t \sim -0.2$ $(Gev/c)^2$. If the $I_t = 0$ component has the gross features indicated above, then

$$\frac{d\sigma}{dt}(\pi^- p) - \frac{d\sigma}{dt}(\pi^+ p) \sim Im\, A^0_{++}\, Im\, A'_{++} \qquad (2.2)$$

where all the relevant amplitudes are defined in appendix one. The lack of structure in A^0_{++} forces a zero in ImA^1_{++} in order to explain this effect. This is the crossover zero which is also observed at $0.1 \leqslant |t| \leqslant 0.2$ $(Gev/c)^2$ in FESR analysis.

(ii) Using similar reasoning, the elastic polarizations are given approximately by

$$P(\pi^\pm p) \sim Im\, A^0_{++}\, Re\, A^c_{+-} \mp Re\, A'_{+-}\, Im\, A^c_{++} \qquad (2.3)$$

The data has two striking features[32]. Firstly, there is almost perfect mirror symmetry between the $\pi^+ p$ and the $\pi^- p$ which implies that the second term in (2.3) dominates. Secondly, there

is an approximate double zero in the data near $t \sim -0.5$ (Gev/c)^2 indicating a similar behaviour for Re A^1_{+-}.

(iii) The CEX polarisation is given "exactly" by

$$P(\pi^- p \to \pi^\circ n) \sim Im A'_{++} \, Re A'_{+-} - Re A'_{++} \, Im A'_{+-} \qquad (2.4)$$

Now since the crossover zero forces the first term to vanish at $t \sim -0.2$ (Gev/c)^2, the sign of the polarisation gives us directly the sign of the second term. All Regge models have a single zero in $Im A^1_{+-}$ to explain the dip in the differential cross section at $t \sim -0.6$ (Gev/c)^2, but no zero for $|t| \lesssim 0.5$ (Gev/c)^2. Therefore, the large positive polarisation observed in πN CEX for $|t| \lesssim 0.5$ (Gev/c)^2 means that $Re A^1_{++}$ must not change sign in this region. We shall comment on the consequences this has for cut models later in this chapter.

Hence, the $I_t = 1$ amplitudes which we shall take to be given by the rho pole plus its cuts, must have the following structure at 6.0 Gev/c.

Im A^1_{++}	:	A zero at $t \sim -0.2$ (Gev/c)^2
Re A^1_{++}	:	No zero for $|t| \lesssim 0.5$ (Gev/c)^2
Im A^1_{+-}	:	A zero at $t \sim -0.6$ (Gev/c)^2
Re A^1_{+-}	:	An approximate double zero near $t \sim -0.5$ (Gev/c)^2

It is immediately apparent that the flip amplitude has exactly the phase structure expected of a nonsense choosing ρ pole, with relatively minor modifications coming from the cuts. The non flip amplitude has no such interpretation and so presumably receives appreciable cut corrections. This supports the view that absorption is more important in non flip amplitudes[33].

The FESR analysis of Elvakajeer, Inami and Ringland[18], suggests that the rho pole continues to dominate the non flip amplitude out to $t \sim -2.5$ $(\text{Gev/c})^2$. In fact they observe zeros in $\text{Im } A^1_{+-}$ at $t \sim -0.5$, -1.4 and -2.5 $(\text{Gev/c})^2$, with double zeros at $t \sim -0.5$ and -2.5 $(\text{Gev/c})^2$. Again, this is precisely the behaviour we expect from a nonsense choosing rho pole with negligible cut corrections.

Beyond $t \sim -0.6$ $(\text{Gev/c})^2$ there does not exist a complete set of experimental observables with which to perform a model independent analysis of the amplitudes. However, in view of the pole dominance of the flip amplitude, it is possible to use a model dependent approach. Elvakajeer et al[34] assumed that the phase of the spin flip amplitude is well represented by the rho signature factor with $\alpha_\rho(t) = 0.5 + t$. They were then able to extract the non flip amplitude for $0.8 \lesssim |t| \lesssim 1.4$ $(\text{Gev/c})^2$. Two of their conclusions are relevant to this discussion.

(i) There is evidence of a second zero in $\text{Im } A^1_{++}$ at $t \sim -1.2$ $(\text{Gev/c})^2$.

(ii) With some extra assumptions it is possible to estimate $\alpha_{\text{eff}}(t)$ for just the non flip amplitude A^1_{++}. Within understandably large errors this is again consistent with the normal rho trajectory and shows strong shrinkage in this region. i.e.

$$\alpha_{\text{eff}}(t)\Big|_{\text{non flip}} \sim \alpha_\rho(t) \qquad (0.8 \lesssim |t| \lesssim 1.4 \ (\text{Gev/c})^2) \qquad (2.5)$$

Further insight into the structure of $\text{Im } A^1_{++}$ in other reactions may be extracted from a more detailed examination of the data on elastic πN, KN and $N\bar{N}$ differential cross sections. Equation (2.2) shows how we can isolate $\text{Im } A^1_{++}$ in πN CEX,

which receives contributions from just rho exchange.
Unfortunately the $\pi^{\pm}p$ difference is so small (approximately
4 mb at $t = 0$ and $P_{lab} = 5.0$ Gev/c), because of the large flip
to non flip ratio of the rho coupling to NN, that further analysis
is very difficult. However, this is not the case in KN and $N\bar{N}$
scattering. For example, if we represent the contribution of a
particular exchange to the full amplitude by its trajectory
label, then

$$A(K^{\mp}p) = P + P' + A_2 \pm \omega \pm \rho$$

Since the omega coupling to NN is mainly non flip, the difference
in this case is appreciable (15 mb at $t = 0$ and $P_{lab} = 5.0$ Gev/c).
Furthermore, if we assume that

(i) the $K^{\pm}p$ forward differential cross sections are
dominated by the non flip amplitude,

(ii) the P, P' and ω have mainly non flip couplings,

(iii) the ρ and A_2 couple mainly to flip amplitudes,

(iv) the contribution $(P+P')$ is predominantly imaginary

at small t, then

$$\frac{d\sigma}{dt}(K^{\pm}p) \approx |P + P'|^2 + |\omega|^2 \mp 2\,\text{Im}(P+P')\text{Im}\omega_{++} \qquad (2.6)$$

and the ω_{++} contribution may be isolated using the combination

$$\Delta\omega_K = \text{Im}\,\omega_{++}\bigg|_{KN} \approx \frac{\frac{d\sigma}{dt}(K^-p) - \frac{d\sigma}{dt}(K^+p)}{\sqrt{8\left[\frac{d\sigma}{dt}(K^-p) - \frac{d\sigma}{dt}(K^+p)\right]}} \qquad (2.7)$$

A similar result follows for $\Delta\omega_N$, the omega contrib-
ution in pp and $p\bar{p}$ scattering. Barger et al[35] have examined
the data in this way and they isolate the crossover zero in $\Delta\omega_{++}$
at $t \sim -0.2$ (Gev/c)^2 in both KN and $N\bar{N}$, with a second zero at

larger $|t|$ consistent with the analysis of Evakajeer et al for the rho in πN. However, the magnitude of $\Delta\omega$ allows one to go further and extract the energy dependence of $\text{Im}\,\omega_{++}$. The results of ref.(35) are reproduced in fig.(2.4) and again show strong shrinkage consistent with $\alpha'_\omega \sim 1$ $(\text{Gev/c})^{-2}$. So both the rho and the omega non flip amplitudes exhibit Regge shrinkage, which is an important conclusion since we know that the cuts are large in these amplitudes.

There is one point where the non flip amplitude may be extracted unambiguously from the data – namely at $t = 0$ from total cross section measurements via the optical theorem. The behaviour of

$$\Delta\sigma(\pi p) = \sigma(\pi^- p) - \sigma(\pi^+ p) \tag{2.8}$$

should give an accurate estimate of $\alpha_\rho(0)$. The data is shown in fig.(2.5). In a Regge model we expect

$$\Delta\sigma(\pi p) \sim \left(P_{lab}\right)^{\alpha_\rho(0)-1} \tag{2.9}$$

If we take the data for $P_{lab} \lesssim 70$ Gev/c (Serpukhov range), the value obtained for the rho intercept is $\alpha_\rho(0) = 0.69 \pm 0.05$, which is in rather serious disagreement with the value $\alpha_\rho(0) = 0.56 \pm 0.02$ obtained from the differential cross section at $t = 0$. However, the recent data from NAL[36] casts doubt on the overall normalisation of the Serpukhov data. A good fit to just the low energy $(P_{lab} \lesssim 20$ Gev/c) plus NAL (50,100,150,200 Gev/c) data can be obtained with $\alpha_\rho(0) = 0.56$.

Finally, it should be noted that $\Delta\sigma$ is an important ingredient in any fit since it fixes both the magnitude and energy dependence of $\text{Im}\,A'_{++}$ $(t = 0)$.

2.3 NEUTRAL PION PHOTOPRODUCTION AND RELATED PROCESSES

Having seen how the data on πN and other reactions fixes the behaviour of the vector mesons ρ and ω, it is useful to look at these exchanges in a completely different context. The reaction $\gamma p \rightarrow \pi^{o} p$ is expected to be dominated by ω exchange, whilst the SU(3) related process $\gamma p \rightarrow \eta^{o} p$ receives the main contribution from ρ exchange.

The t dependence of the differential cross sections for π^{o} photoproduction and πN CEX are remarkably similar, with the former also showing the dip at $t \sim -0.6 \ (\text{Gev/c})^{2}$ and the turnover in the extreme forward direction. Vector Dominance (VDM) provides the link between photoproduction and purely hadronic reactions. VDM represents the photon as an incoherent sum of the vector mesons ρ, ω and ϕ, with the ϕ being completely negligible. (It is estimated[37] that the ϕ contribution is less than 2% of the ω in $\gamma p \rightarrow \pi^{o} p$). The omega couples mainly to spin non flip, and since we automatically pick up one unit of helicity flip at the $\gamma \pi$ vertex, the most important amplitude in neutral pion photoproduction is that due to single flip omega exchange.

The α_{eff} for π^{o} photoproduction is shown in fig.(2.6a) and should be compared with the purely hadronic CEX reaction fig.(2.1). The difference between the two is striking. Whilst the latter is approximately linear out to $t \sim -1.5 \ (\text{Gev/c})^{2}$, the former shows linearity for $0 \leqslant |t| \leqslant 0.3 \ (\text{Gev/c})^{2}$ but has a marked dip followed by a secondary maximum around $t \sim -0.6 \ (\text{Gev/c})^{2}$. This behavior is characteristic of all cut models in which the branch point trajectory takes the form obtained by Mandelstam (equation (1.23)) - see for example fig.(2.2). Good data at higher

energies and particularly at larger values of $|t|$ would be useful
in fixing the shrinkage of $\alpha_{eff}(t)$ in the region past the dip.
As it stands, fig.(2.6a) appears to support a SCRAM type model
with the dip produced by pole-cut interference and the trajectory
past the dip showing about half the shrinkage observed for
$|t| \lesssim 0.3$ $(Gev/c)^2$, where presumably the pole dominates. We shall
see in chapter three, that a strong cut model fits this data very
well. Nevertheless, it is possible that the presence of cuts in
the weaker non flip and double flip amplitudes could postpone
the really strong Regge shrinkage to larger values of $|t|$.

In appendix one, we show the relevant formalism for
the photoinduced reactions in terms of the four helicity amplitudes
A_{-+} , A_{++} , A_{--} , A_{+-} . If only the rho and omega poles contribute
to these amplitudes, then

$$A_{++} = A_{--} \tag{2.10}$$

$$A_{+-} = -A_{-+} \tag{2.11}$$

and the polarised photon asymmetry Σ, is identically equal to
one for all s and t. Unnatural parity exchanges such as B and H
contribute to A_{+-} and A_{-+} with the same sign, whilst cuts
contribute to both parities. So the departure of Σ from unity
measures

(i) the strength of the cuts in A_{+-} and A_{-+}

or   (ii) the strength of the unnatural parity exchanges.
It is difficult to decide which of the two is the most important.

Since unnatural parity exchanges do not couple to
the single flip amplitudes, it is perhaps not surprising that Σ
is significantly different from one only in the region of the dip
in the differential cross section, where A_{++} and A_{--} are small.

As we shall see in chapter three, cuts preserve (2.10) also, but violate (2.11), so any reasonable cut model should reproduce, at least qualitatively, the data on the polarised photon asymmetry.

A much more rigorous test of the amplitude phases is provided by the polarised target asymmetry data, since this depends on the relative phases of the amplitudes. If we assume that (2.10) holds in all models, then near to $t \sim -0.6$ $(Gev/c)^2$ we expect the polarised target asymmetry to be given (approximately) by

$$A \sim Re\ A_{++}\ Im\ (A_{+-} - A_{-+})$$ (2.12)

It is therefore crucial in fixing the phases of the non and double flip amplitudes.

If we allow only ρ, ω, B and H exchanges, then the polarised target asymmetry and the recoil nucleon polarisation are predicted to be equal. This follows from equation (2.10). It has been noted[37] that exchanges in the 2^{--} octet would contribute to A_{++} and A_{--} with opposite sign, thus breaking this equality. No measurement of the recoil nucleon polarisation exists at the present time so the prediction is untested.

The other experimental observables for which data exists are the ratio R of π^o photoproduction from neutrons and protons, and the η photoproduction differential cross section. R fixes the ratio of the isoscalar (ω and H) to isovector (ρ and B) exchanges. SU(3) relates π and η photoproduction and the Clebsch-Gordon coefficients are such that the isovector amplitude is the important one in $\gamma p \rightarrow \eta^o p$. The rho couplings to $N\bar{N}$ mean that it contributes mainly to A_{+-} and A_{-+} in photoproduction. The absence of a dip in η^o photoproduction means that models with EVSZ have great difficulty in fitting

the data[12]. They require either very strong cuts or a large B contribution (or both) to fill in the dip.

In fig.(2.6b) we plot $\alpha_{eff}(t)$ for the ρ^0 reaction. The errors are rather large for any firm conclusion to be drawn. However, α_{eff} does show considerably more structure than is observed in hadronic reactions (compare fig.(2.1)). Furthermore, it is tempting to say that the structure, which we would want to blame on pole-cut interference, occurs before $t \sim -0.6$ (Gev/c)^2. This would then correlate nicely with the dominance of the rho non/double flip amplitudes (i.e. flip at the nucleon vertex) and the absence of a dip at $t \sim -0.6$ (Gev/c)^2 in the differential cross section.

2.4 THE AMPLITUDE PHASES AND THEIR J-PLANE STRUCTURE

In section two of this chapter we saw how the positive polarization in $\pi^-p \rightarrow \pi^0 n$ leads to the conclusion that Re A^1_{++} does not change sign for $|t| \lesssim 0.5$ (Gev/c)^2. Now the absorption model in which the elastic amplitude is mainly imaginary at $t = 0$, predicts that both real and imaginary parts of the input pole amplitude are absorbed approximately equally at small $|t|$. Thus, if we have the crossover zero in Im A^1_{++} , we are forced to accept a zero in Re A^1_{++} near to $t \sim -0.2$ (Gev/c)^2 with disast-erous consequences for the polarization. This is true whether the crossover zero is obtained by direct pole-cut interference (SCRAM) or by attempting to use the cuts to "pull in" the NWSZ from $t \sim -0.5$ (Gev/c)^2 to $t \sim -0.2$ (Gev/c)^2. We can conclude that even though the magnitude of Re A^1_{++} is poorly determined by the data, its sign is fixed and is in direct conflict with the absorption model.

The reason for the failure is clearly the wrong phase

in the absorbing amplitude. With a Pomeron having $\alpha_p(0) = 1$, the position of the rho pole and the $\rho \otimes P$ cut coincide at $t = 0$, producing equal absorption in real and imaginary parts. Worden[38] has shown that the solution is to add an extra component besides the $\rho \otimes P$ cut, which contributes with opposite sign in real and imaginary parts at small $|t|$. This means that we require something whose Regge phase gives $Re/Im < 0$ for $|t| \leq 0.5$ $(Gev/c)^2$. In the J-plane therefore, we require a singularity in the region $0 < J < -1$. It is now clear why the Berger-Phillips "five pole fit"[39], in which the $I_t = 1$ amplitude was parameterised as a sum of ρ and ρ' exchanges, predicted the πN CEX polarization correctly. The ρ' trajectory lying half a unit below the rho, is in precisely the correct region of the J-plane to give agreement with the data.

Several modifications of the simple absorption model have been proposed. One of these is, as we shall discuss in the next chapter, to add Regge-Regge cuts. The essential ingredient in all the models is that the non flip amplitude receives significant contributions from the broad J-plane spectrum $0.5 < J < -1$.

The inclusion of lower lying singularities specifically designed to reproduce the 6.0 Gev/c phases, means that the extrapolation to low energy gives problems because the different terms get "out of step" as we go down in energy.[39] This is reflected in the poor agreement of all the new absorption models with the FESR's. As may be anticipated, particularly severe disagreement is observed in the non flip FESR, where the low lying contributions completely overwhelm the rho pole at low energy bringing the crossover zero in towards $t = 0$.

A final point which we have mentioned before is that

all absorption models in which the position of the cut is given
by the Mandelstam formula (1.23) cannot reproduce the strong
shrinkage observed in πN reactions. We shall study this problem
in greater detail in the next section.

2.5 A GENERAL SURVEY OF EFFECTIVE TRAJECTORIES

Fig.(2.1) and fig.(2.4) together with the results of
ref.(33), provide strong evidence for Regge shrinkage consistent
with $\alpha_\rho(t) \sim 0.5 + t$ in both the flip and non flip amplitudes
in πN CEX. Therefore, it is interesting to look at a much wider
set of reactions involving different amplitudes and exchanges,
in an attempt to determine whether this is a universal feature
of all strong interactions. A review of α_{eff}'s was presented
in 1969 by G.C. Fox[28], who came to the conclusion that only
πN CEX exhibits strong shrinkage. Since then however, more
detailed and accurate data over a wider range of s and t has
become available which does not support this statement. We there-
fore present a compilation of α_{eff}'s, some of which we have
calculated from the data as described in appendix two and others
which have been reproduced as they appear in the literature.
Table (2.1) shows the processes considered together with the
possible exchanges and the range of s and t over which the data
extends.

For the class of processes $0^- + \frac{1}{2}^+ \rightarrow 0^- + \frac{1}{2}^+$ which
have only single flip and non flip helicity amplitudes as in the
prototype reaction πN CEX, there is no evidence to suggest that
shrinkage does not persist out to and beyond $t \sim -1.0$ $(Gev/c)^2$.
In the cleanest reactions and those for which data exists over
the widest range of s and t , this conjecture is most strongly
supported.

Such reactions include

$$\pi^- p \to \pi^0 n$$
$$K^- p \to \bar{K}^0 n$$
$$K_L^0 p \to K_S^0 p \qquad (2.13)$$
$$K^- p \to K^0 \Lambda$$
$$\pi^+ p \to K^+ \Sigma^+$$

Until the data from NAL became available recently, the only disturbing reaction was

$$\pi^- p \to \eta^0 n \qquad (2.14)$$

Calculated from the low energy data ($P_{lab} \lesssim 18$ Gev/c), α_{eff} appears to flatten out around $t \sim -0.5$ (Gev/c)^2, which could be interpreted as being due to an $A_2 \boxtimes P$ cut. Several authors[40] have commented on the difficulty of analysing (experimentally) this reaction, since there is the problem of separating the η^0 from the much larger π^0 signal. All the data below 6.0 Gev/c comes essentially from one experiment[41] and is rather poor for $|t| > 0.5$ (Gev/c)^2. Furthermore, an analysis of ρ and A_2 exchange in the reactions

$$\pi^+ p \to \pi^0 \Delta^{++} \qquad (2.15)$$
$$\pi^+ p \to \eta^0 \Delta^{++} \qquad (2.16)$$

supports the view that both the ρ and A_2 exhibit strong Regge shrinkage. In (2.16) the A_2 trajectory is consistent with $\alpha_{A_2}(t) \sim 0.5 + t$.

All of this casts doubt on the reliability of the low energy $\pi^- p \to \eta^0 n$ data. Recents results from Serpukhov and NAL[36] support this view and are in good agreement with the A_2 as obtained from other sources such as (2.16).

Finally we summarise the main features of the experimental

data which are particularly relevant to Regge cut phenomenology.

(i) The 6.0 Gev/c amplitude analysis in πN scattering suggest that we need absorptive corrections which are strong in imaginary parts but weak in real parts.

(ii) Apart from the special case of photoproduction, Regge shrinkage appears to be a universal feature of strong interaction amplitudes. A cut model is needed which does not produce $\alpha_c(t)$ given by (1.23), but instead gives a branch point trajectory which approximates to $\alpha_R(t)$ over the present limited energy range. We attempt to formulate such a model in chapters four and five.

REACTION	FIGURE NO.	EXCHANGE(S)	Max P_{lab} Gev/c	Max t $(Gev/c)^2$
$\pi^- p \to \pi^\circ n$	2.1	ρ	48	1.5
$\pi^- p \to \pi^\circ n$	2.3	ρ	4.83	5.0
$K^\pm p \to K^\pm p$	2.4a	Isolates $Im\ \omega_{++}$	7.2	1.0
$NN \to NN$	2.4b	Isolates $Im\ \omega_{++}$	16	1.4
$\gamma p \to \pi^\circ p$	2.6a	$\omega\ (\rho)$	15	1.4
$\gamma p \to \rho^\circ p$	2.6b	$\rho\ (\omega)$	6.5	1.0
$\pi^- p \to \rho^\circ n$	2.7	A_2	50	1.2
$K^- p \to \bar{K}^\circ n$	2.8	$\rho,\ A_2$	12.3	1.5
$K^+ n \to K^\circ p$	2.9	$\rho,\ A_2$	12.0	0.8
$K_L^\circ p \to K_S^\circ p$	2.10	ω	10	1.6
$\pi^+ p \to \pi^\circ \Delta^{++}$	2.11a	ρ	8	0.8
$\pi^+ p \to \rho^\circ \Delta^{+}$	2.11b	A_2	8	0.8
$\pi^+ p \to K^+ \Sigma^+$	2.12,2.13a	$K^*,\ K^{**}$	14	1.4
$K^- p \to \pi^\circ \Sigma^\circ$	2.13b	$K^*,\ K^{**}$	16	0.9
$\pi^- p \to K^\circ \Lambda$	2.14a	$K^*,\ K^{**}$	15.7	0.9
$K^- p \to \pi^\circ \Lambda$	2.14b	$K^*,\ K^{**}$	14.3	0.9
$\pi^+ p \to \omega \Delta^{++}$	2.15a	Isolates B	7.1	0.9
$\pi^- p \to \rho^\circ n$	2.15b	Isolates π	17.2	0.9
$K^+ p \to K^\circ \Delta^{++}$	2.16	$\rho,\ A_2$	15.7	0.8

TABLE 2.1

Reactions for which the effective trajectory $\alpha_{eff}(t)$ has been calculated together with the relevant exchanges and the range of energy and t over which the data extends.

FIGURE CAPTIONS - CHAPTER TWO

2.1 Effective trajectory for the reaction $\pi^- p \rightarrow \pi^0 n$ [26].

2.2 Effective trajectory for the strong cut model of ref.(27)

for the reaction $\pi^- p \rightarrow \pi^0 n$.

2.3 Effective trajectory at large $|t|$ for the reaction $\pi^- p \rightarrow \pi^0 n$ [29]

2.4 Effective trajectory for the non flip omega exchange amplitude

in a) $K^{\pm} p \rightarrow K^{\pm} p$ and b) $NN \rightarrow NN$ from ref.(35)

2.5 The quantity $\Delta\sigma(\pi N) = \sigma(\pi^- p) - \sigma(\pi^+ p)$ [26]

2.6 Effective trajectory for the reaction

a) $\gamma p \rightarrow \pi^0 p$ from the data of ref.(42).

and b) $\gamma p \rightarrow \eta^0 p$ from the data of ref.(43).

2.7 Effective trajectory for the reaction $\pi^- p \rightarrow \eta^0 n$. The points

marked o were calculated from the data of ref.(41), whilst

those marked $\circ$ are calculated from the Serpukhov and NAL

data [36].

2.8 Effective trajectory for the reaction $K^- p \rightarrow \bar{K}^0 n$ from the data

of ref.(44).

2.9 Effective trajectory for the reaction $K^+ n \rightarrow K^0 p$ from the data

of ref.(45).

2.10 Effective trajectory for the reaction $K_L^0 p \rightarrow K_S^0 p$ [46].

2.11 Effective trajectories for the reactions

a) $\pi^+ p \rightarrow \pi^0 \Delta^{++}$ [47]

and b) $\pi^+ p \rightarrow \eta^0 \Delta^{++}$ [47].

2.12 Effective trajectory for the reaction $\pi^+ p \rightarrow K^+ \Sigma'$ from the data

of ref.(48).

2.13 Effective trajectories for the reactions

a) $\pi^+ p \rightarrow K^+ \Sigma^+$ [6]

and b) $K^- p \rightarrow \pi^- \Sigma^+$ [6].

2.14 Effective trajectories for the reactions

a) $\pi^- p \rightarrow K^0 \Lambda$ [6]

and b) $K^- p \rightarrow \pi^0 \Lambda$ [6].

2.15   a) Effective trajectory for the B exchange contribution

in $\pi^+ p \rightarrow \omega \Delta^{++}$ (49).

b) Effective trajectory for the π exchange contribution

in $\pi^- p \rightarrow \rho^\circ n$ (50).

2.16 Effective trajectory for the reaction $K^+ p \rightarrow K^\circ \Delta^{++}$ from

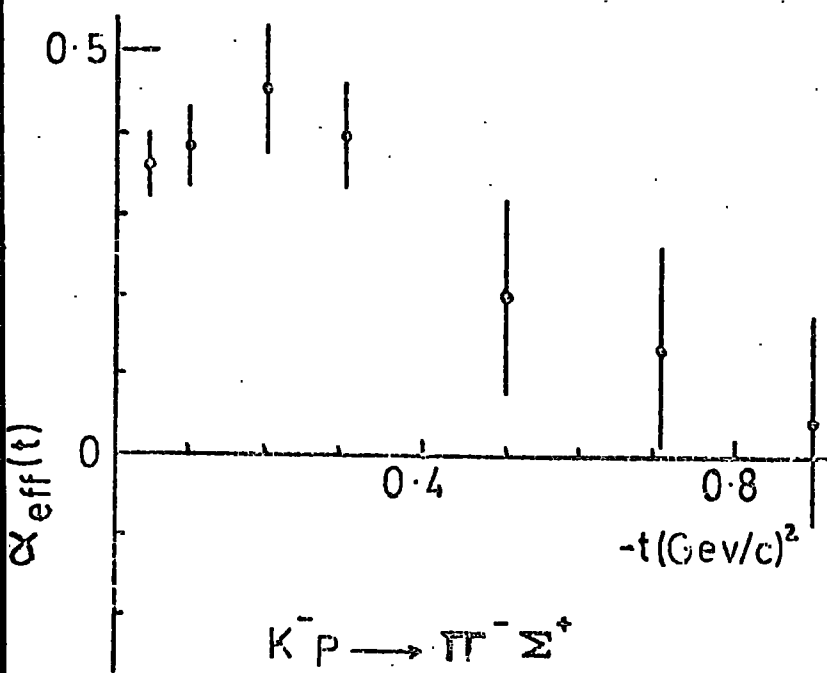J. P. De Brion and C. Lewin (Nuovo Cimento $\underline{19A}$ 225 (1974)).
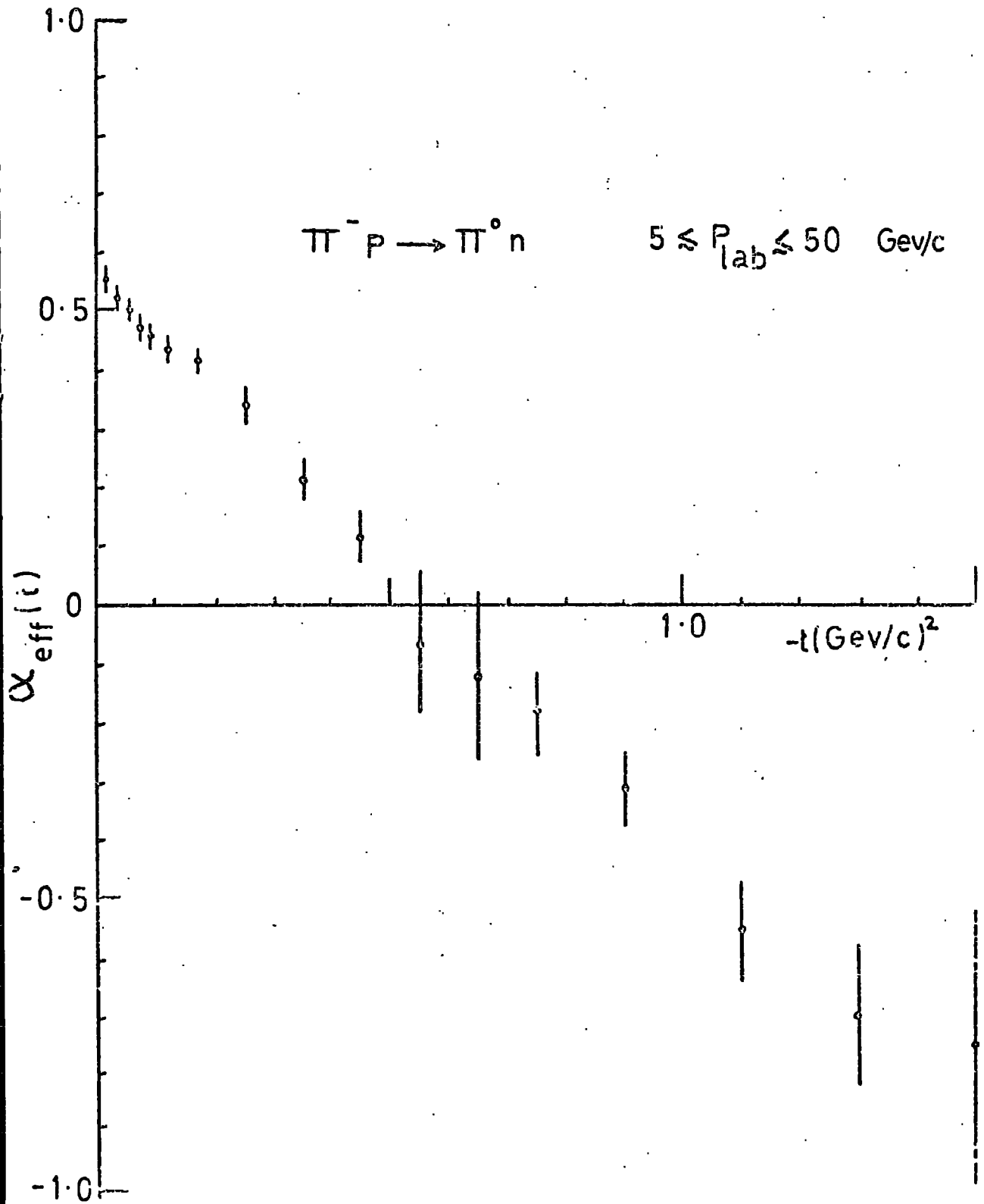
Fig 2·1
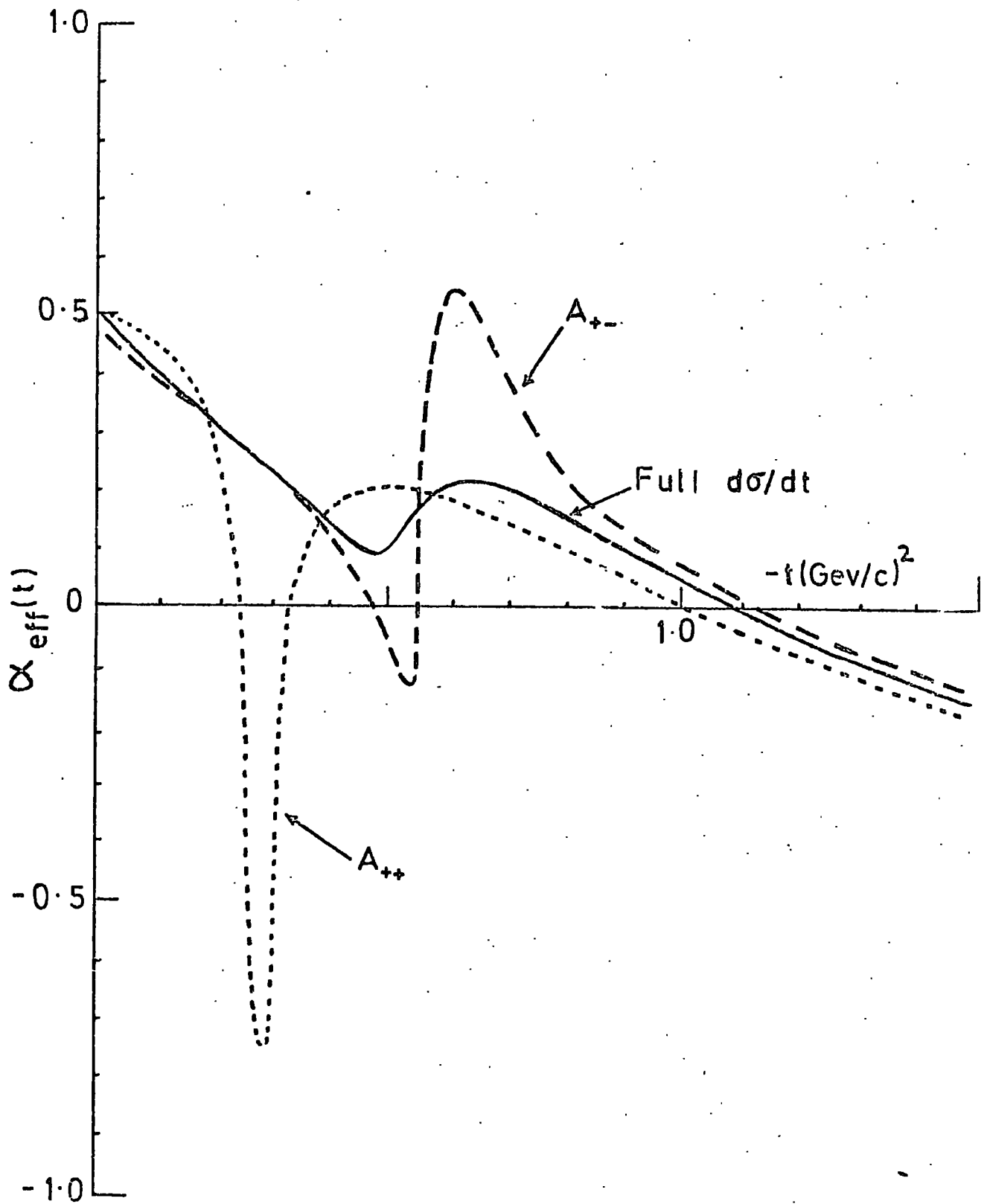
Fig 2·2
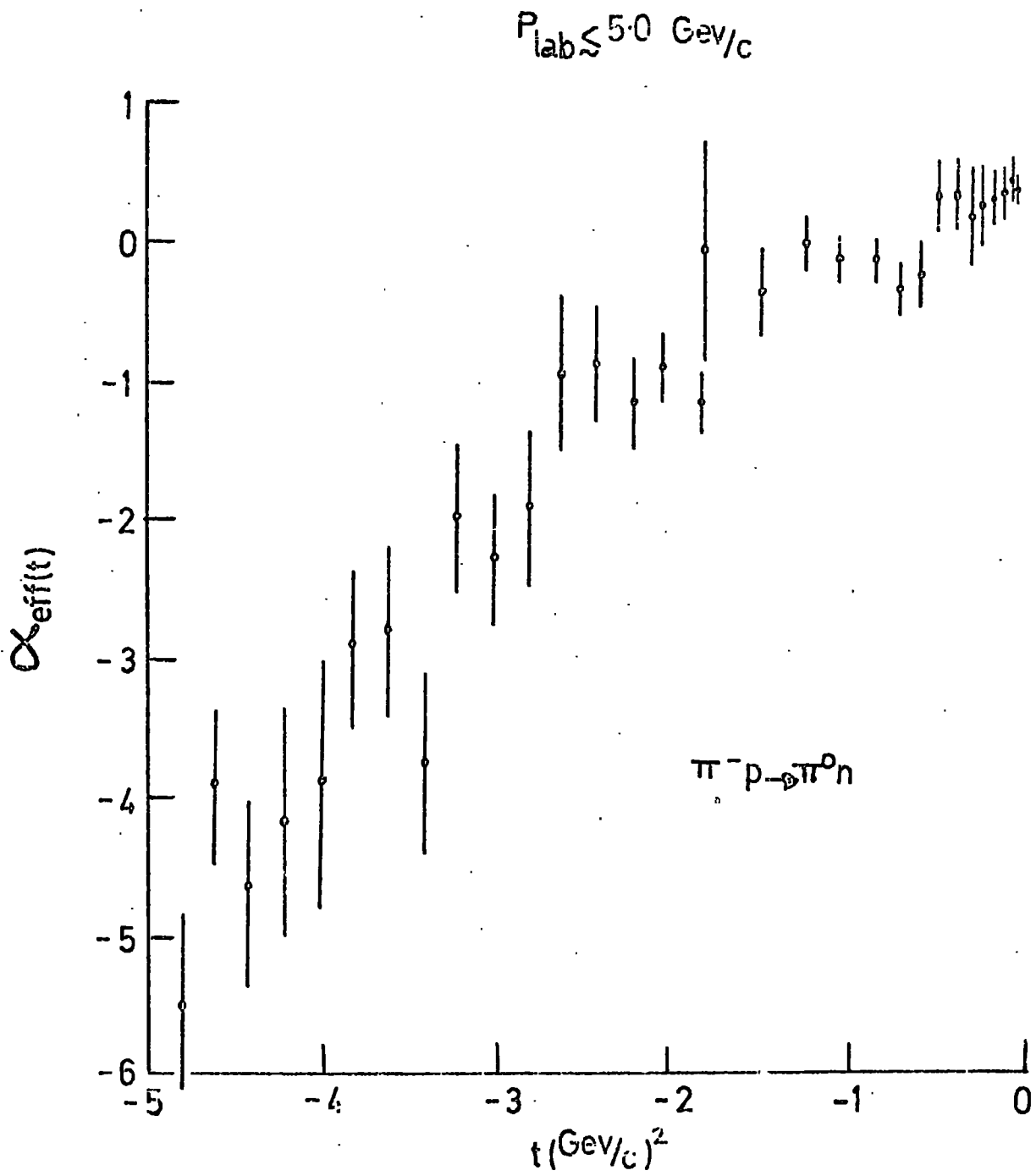
Fig 2·3
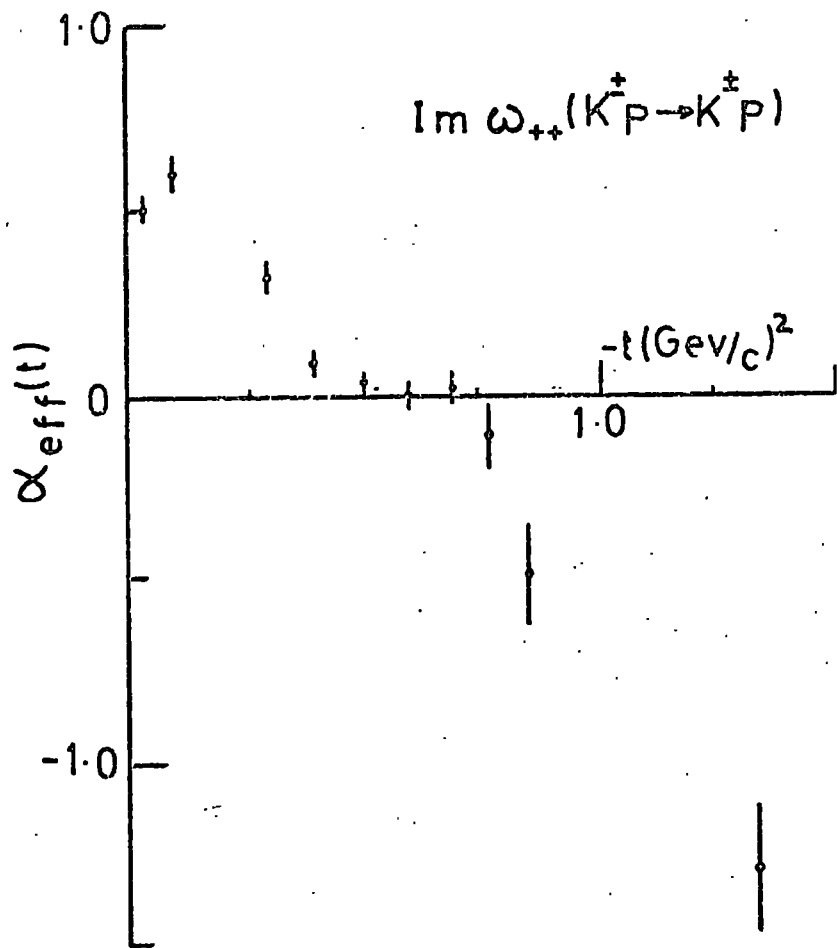
Fig 2.4 a
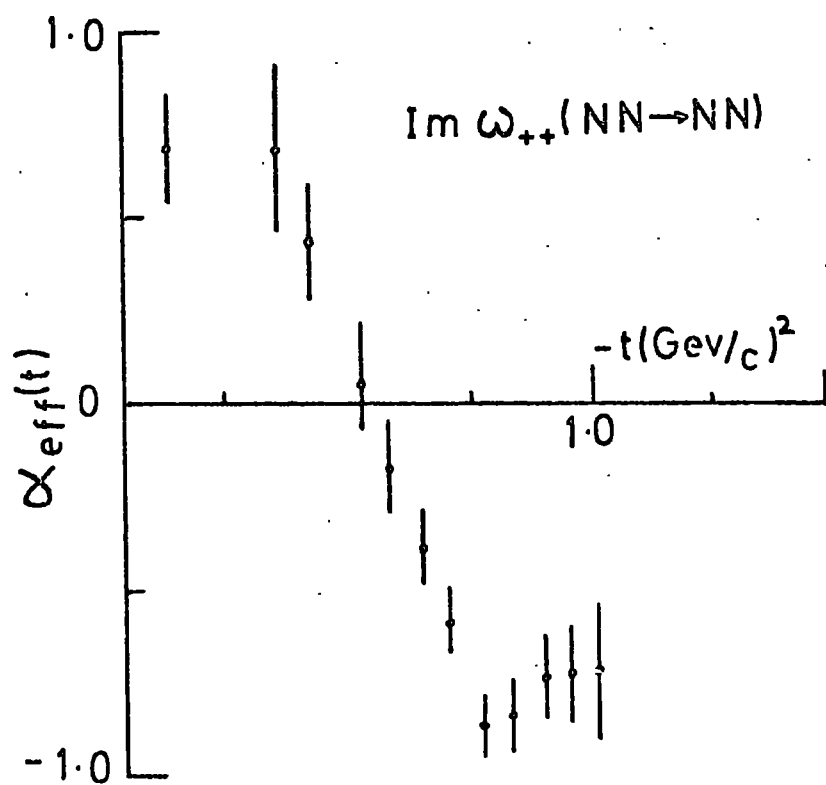
Fig 2.4 b
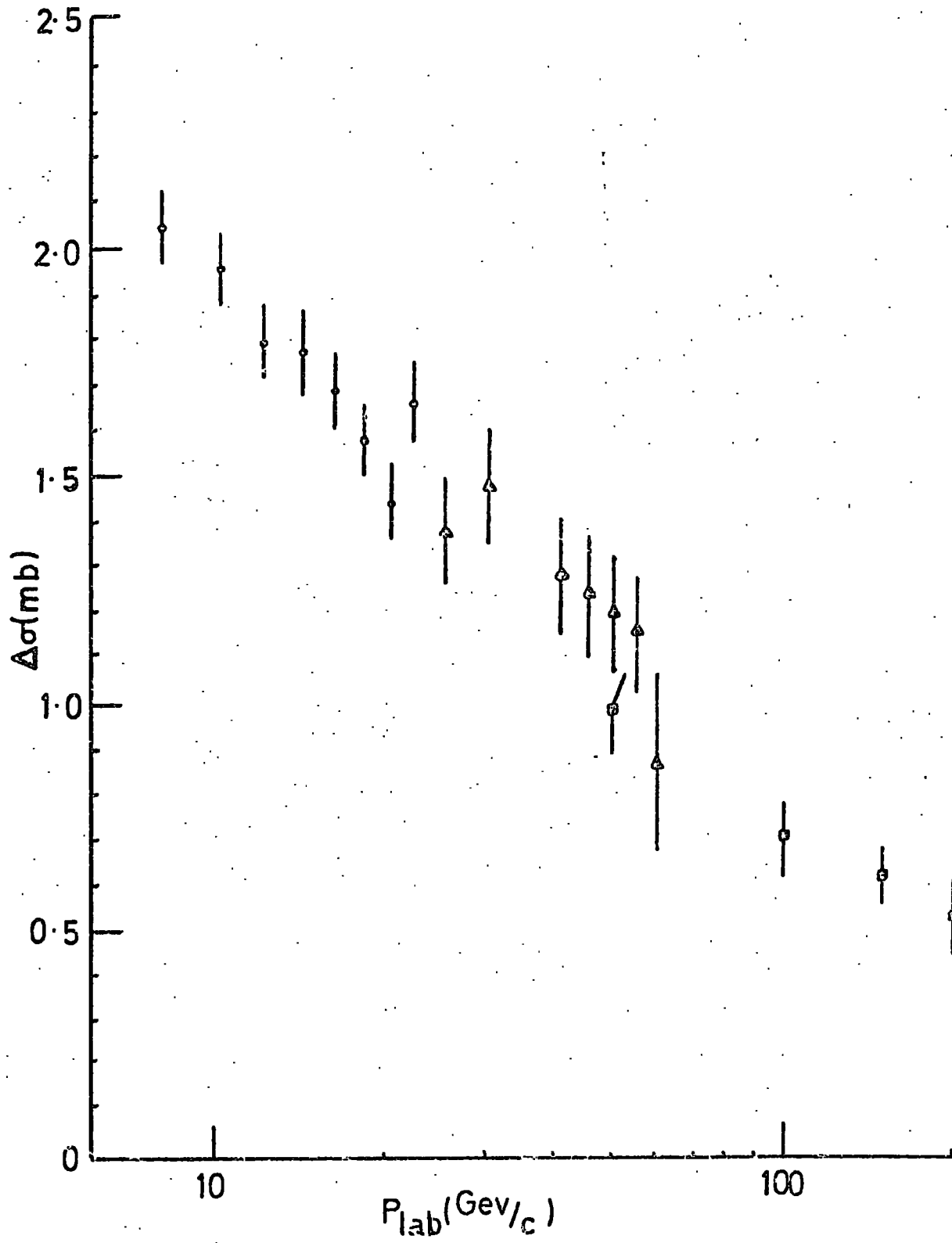
Fig 2·5
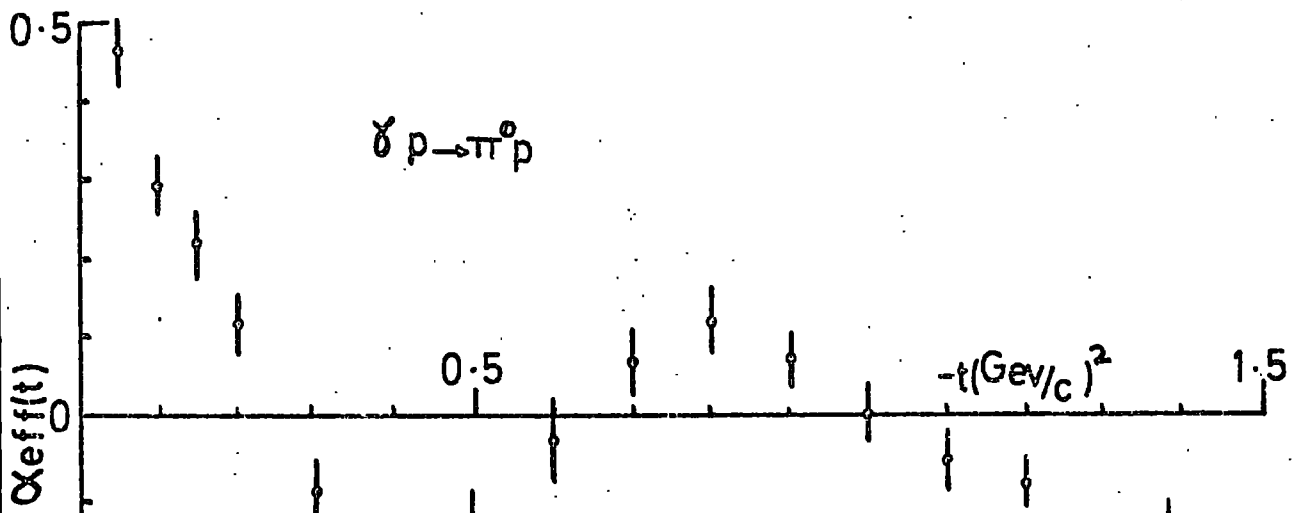
Fig 2·6a
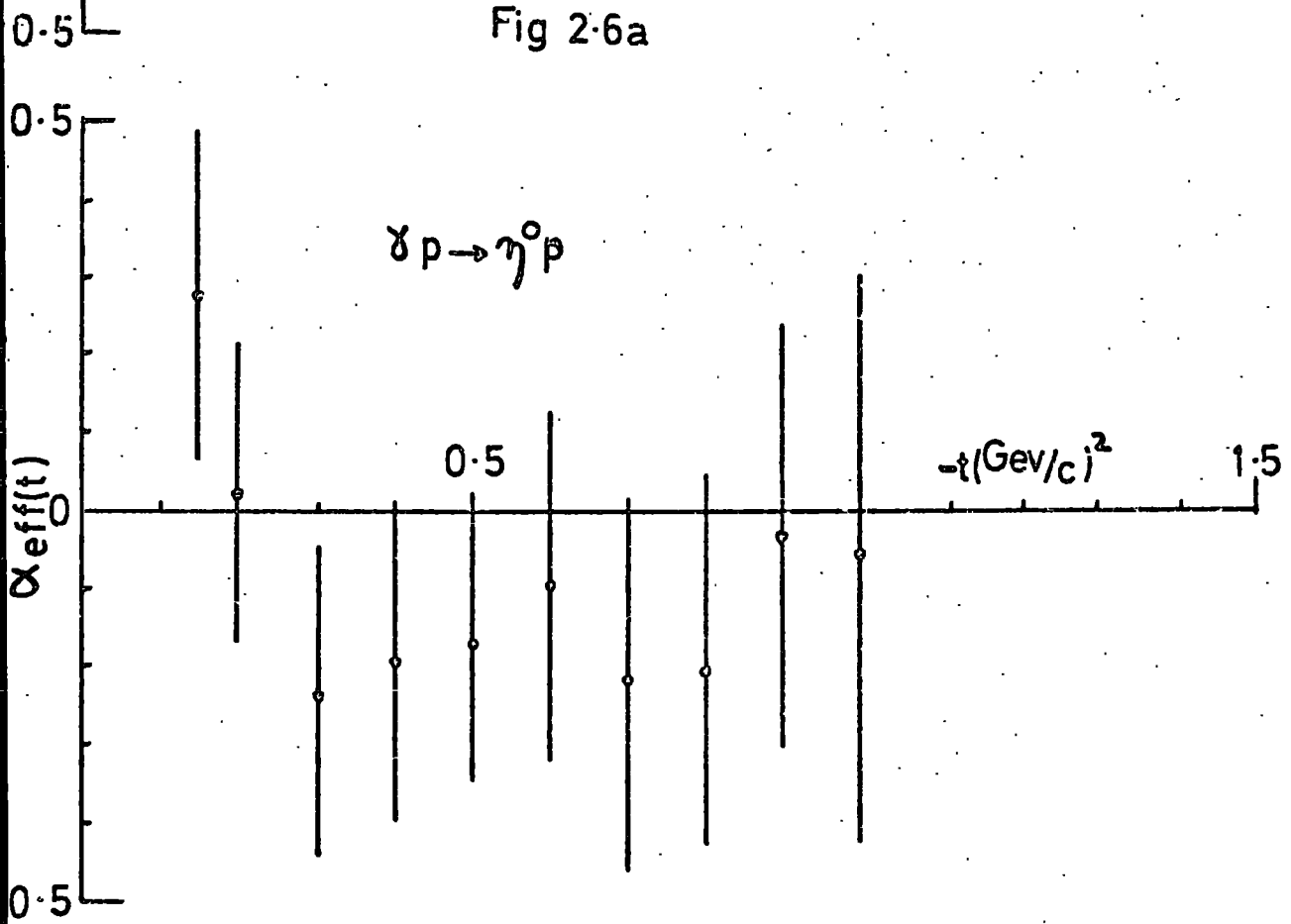
Fig 2·6b
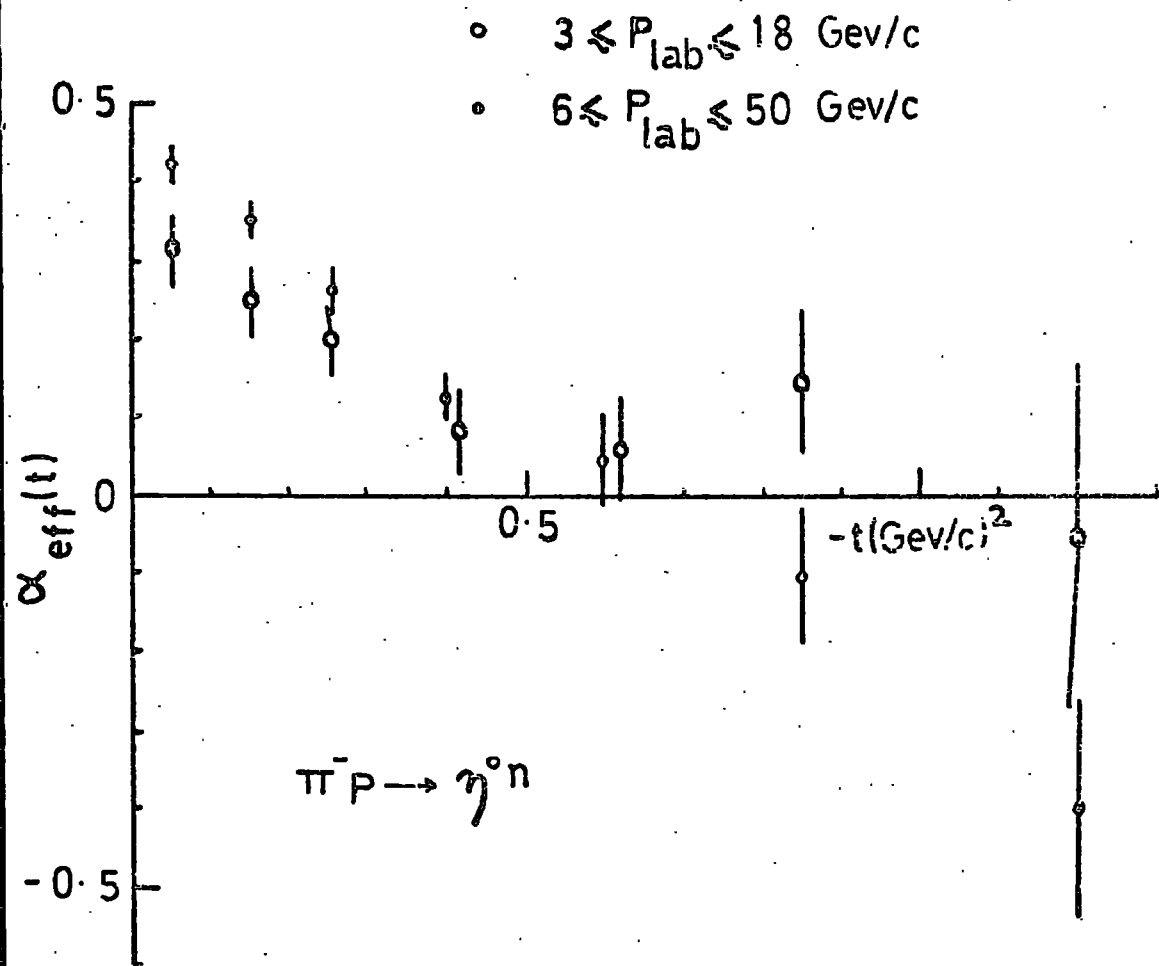
Fig 2·7
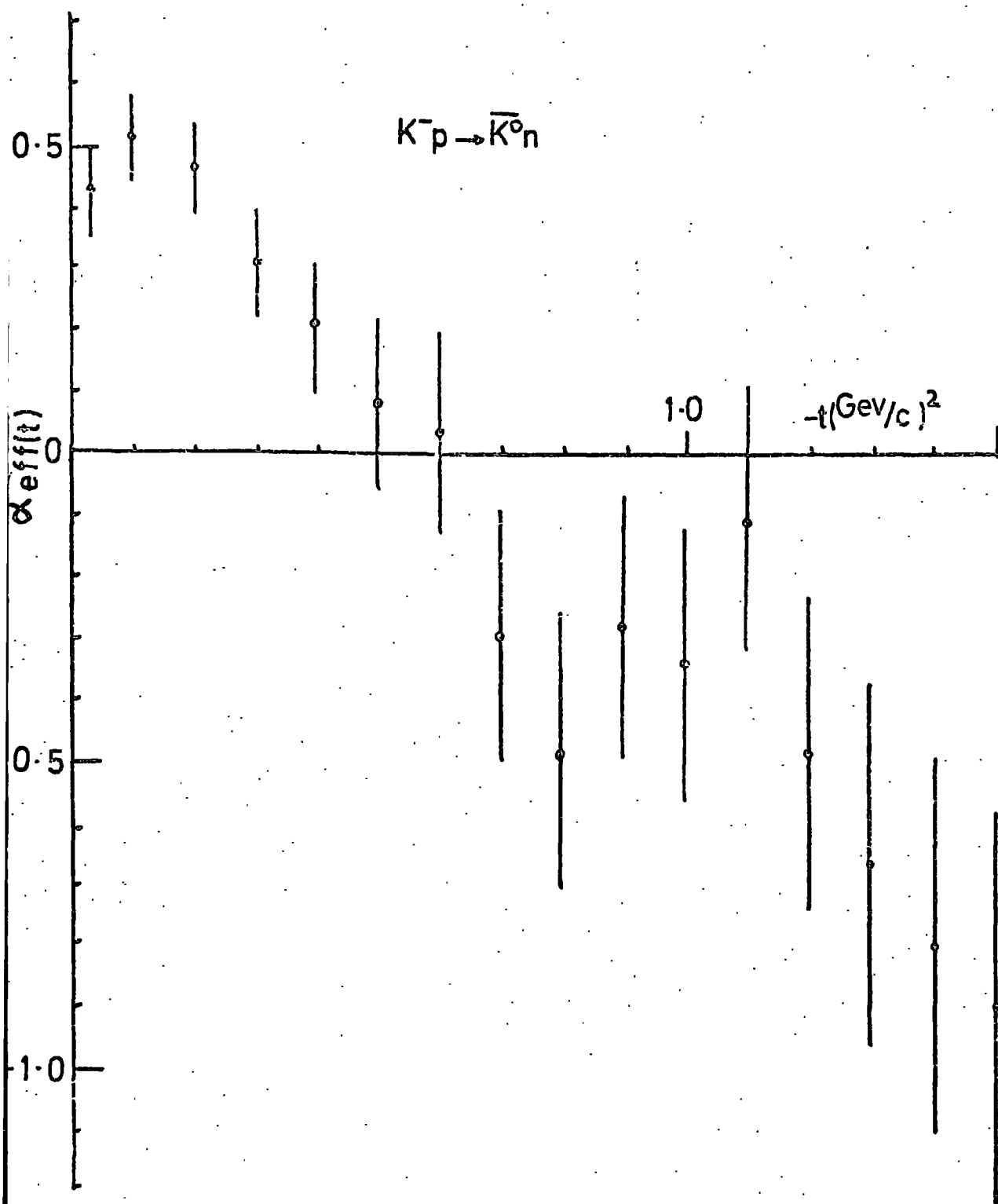
Fig 2·8
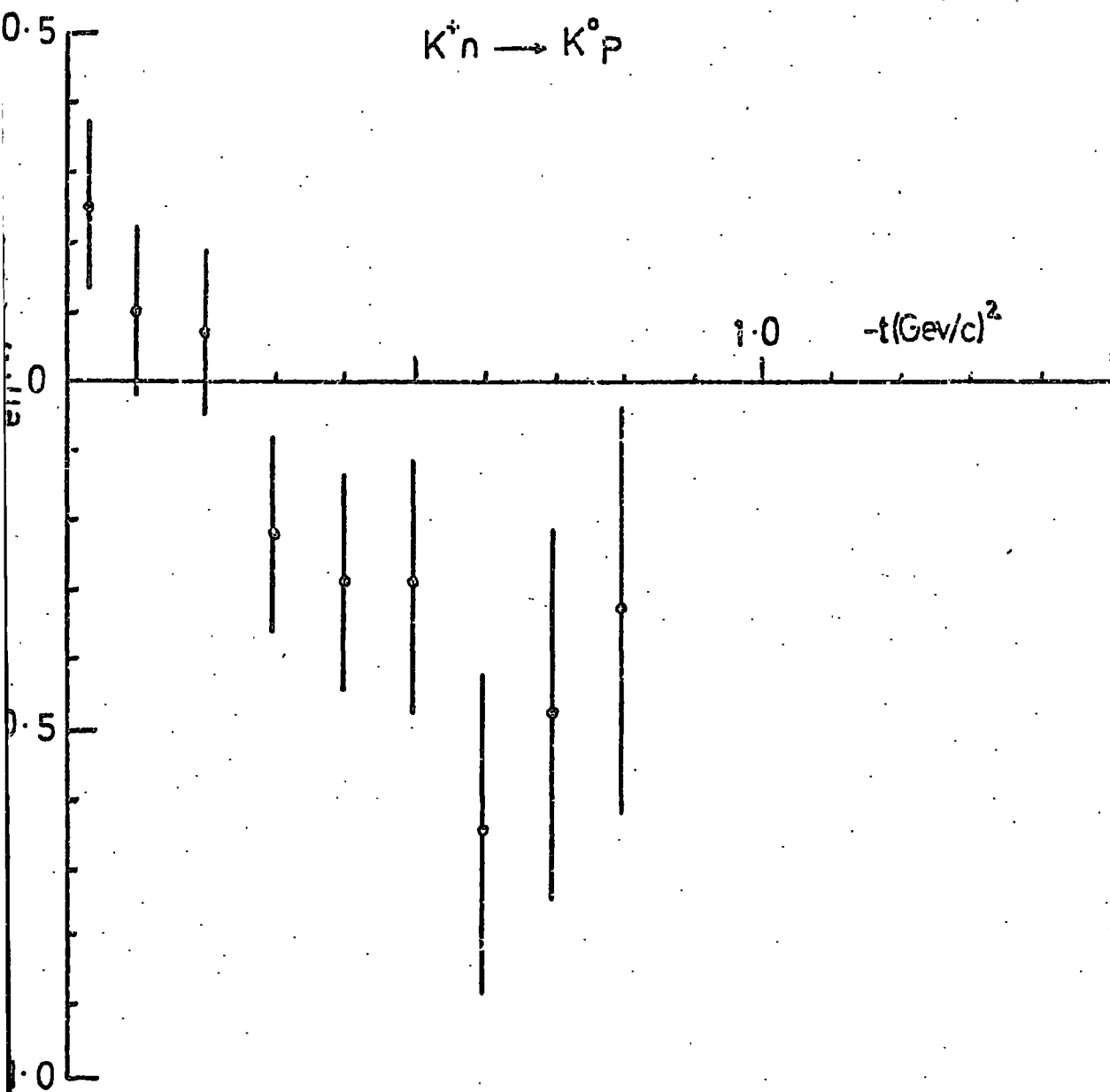
Fig 2·9
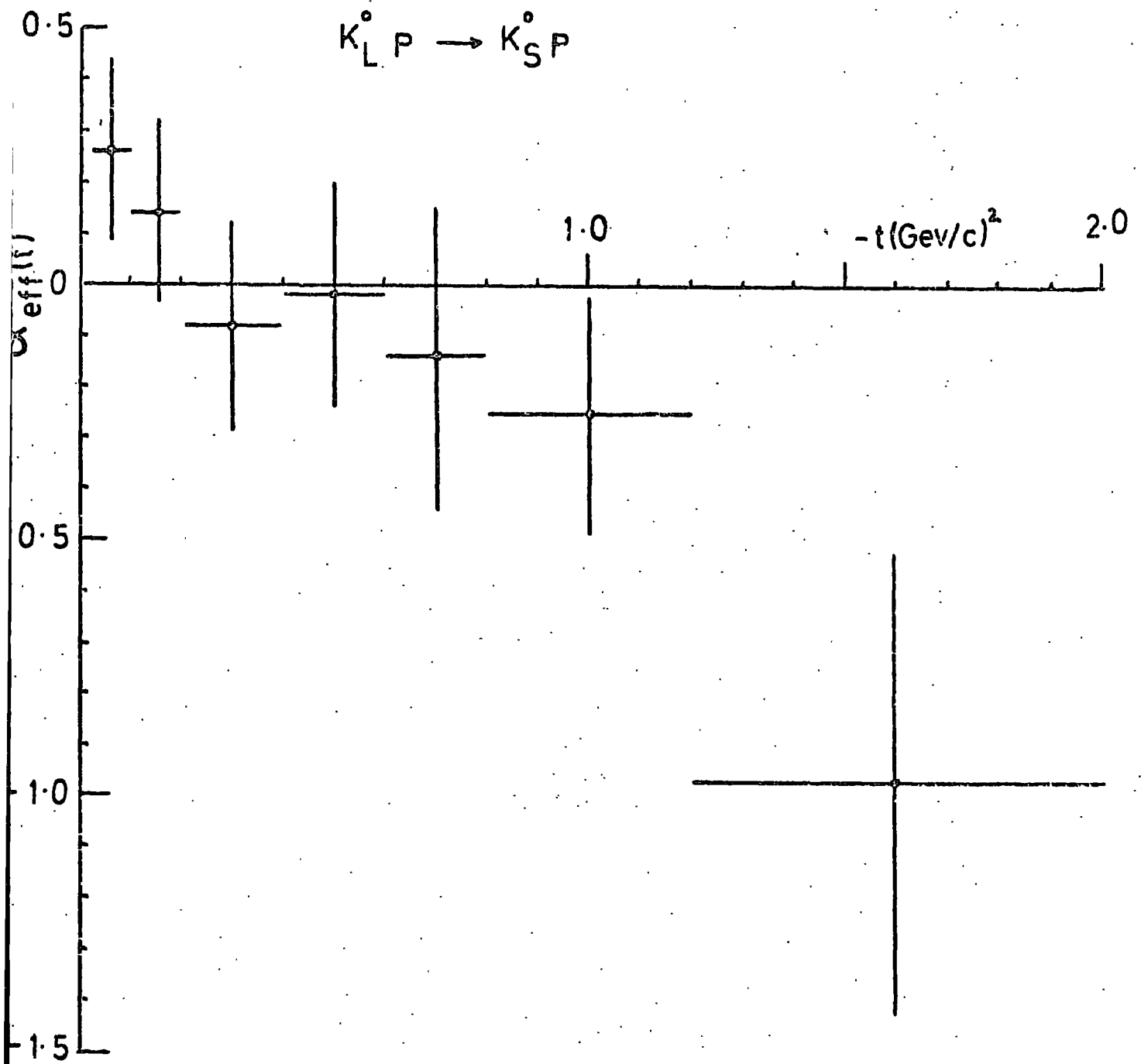
Fig 2·10

$\pi^+ P \longrightarrow \pi^0 \Delta^{++}$

$-t(\text{Gev/c})^2$

Fig 2·11 a

$\pi^+ P \longrightarrow \eta^0 \Delta^{++}$

$-t(\text{Gev/c})^2$

Fig 2·11 b

Fig 2·12

Fig 2·13 a

$\pi^+ p \longrightarrow K^+ \Sigma^+$

Fig 2·13 b

$K^- p \longrightarrow \pi^- \Sigma^+$

Fig 2.14 a

$\pi^- p \longrightarrow K^0 \Lambda$

Fig 2.14 b

$K^- p \longrightarrow \pi^0 \Lambda$

B exchange
in $\pi^+ p \longrightarrow \omega \Delta^{++}$

$-t(Gev/c)^2$

Fig 2·15 a

π exchange
in $\pi^- p \longrightarrow \rho^0 n$
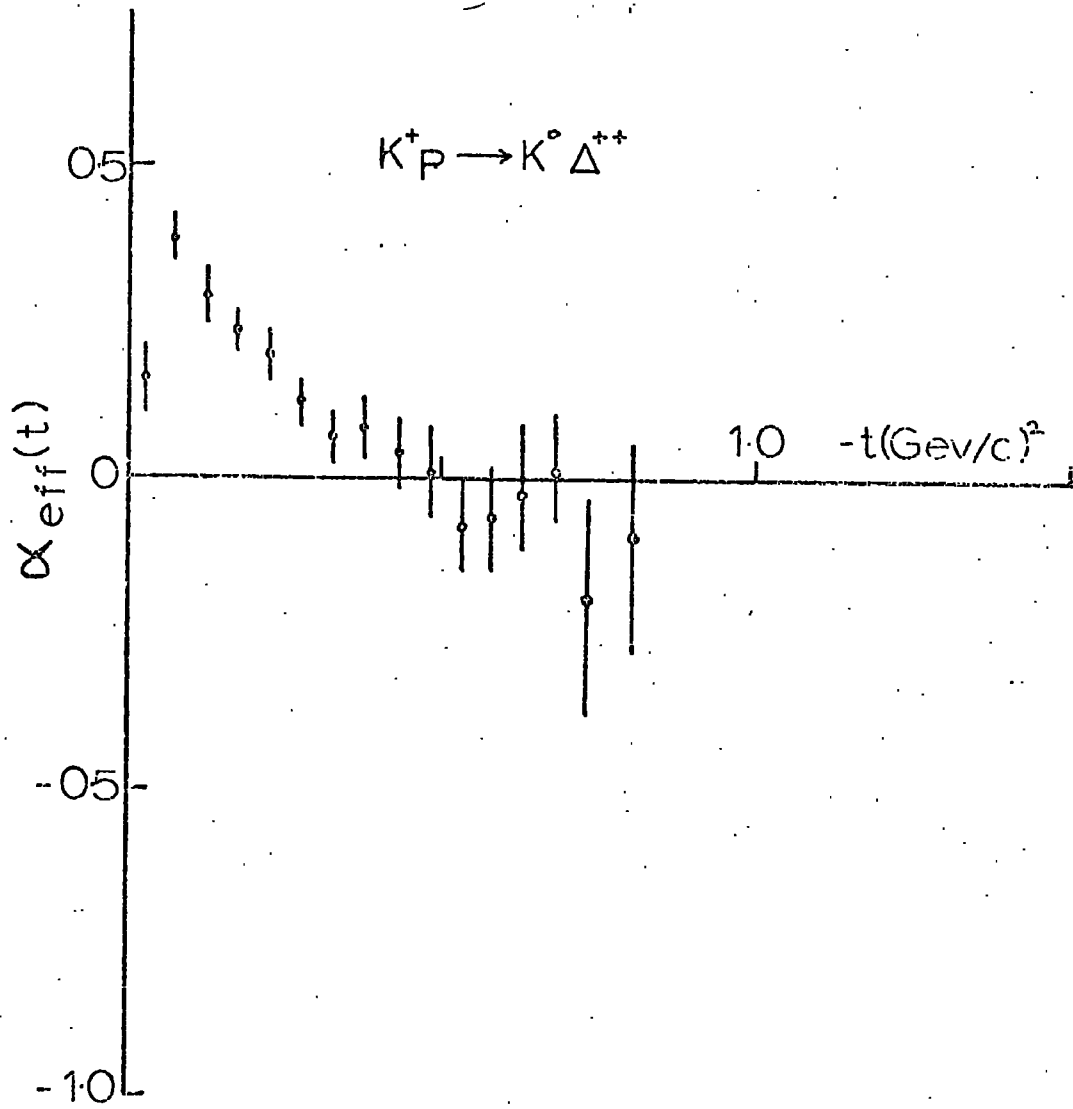
$-t(Gev/c)^2$
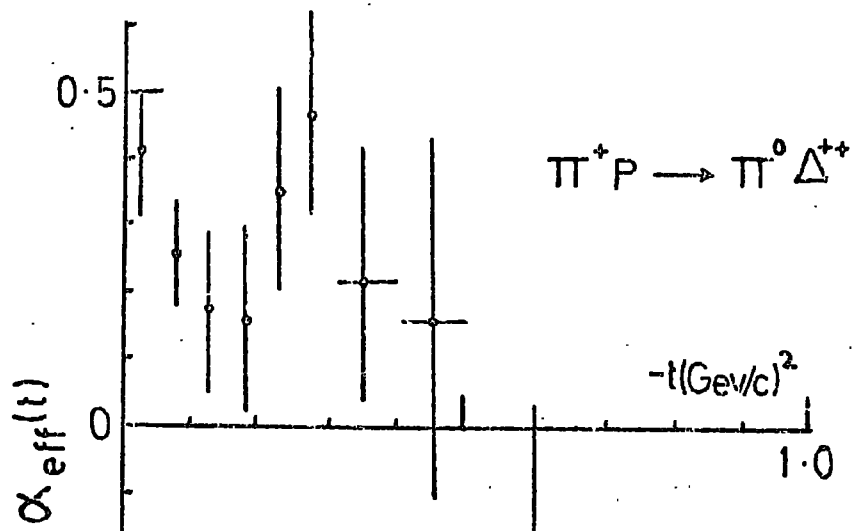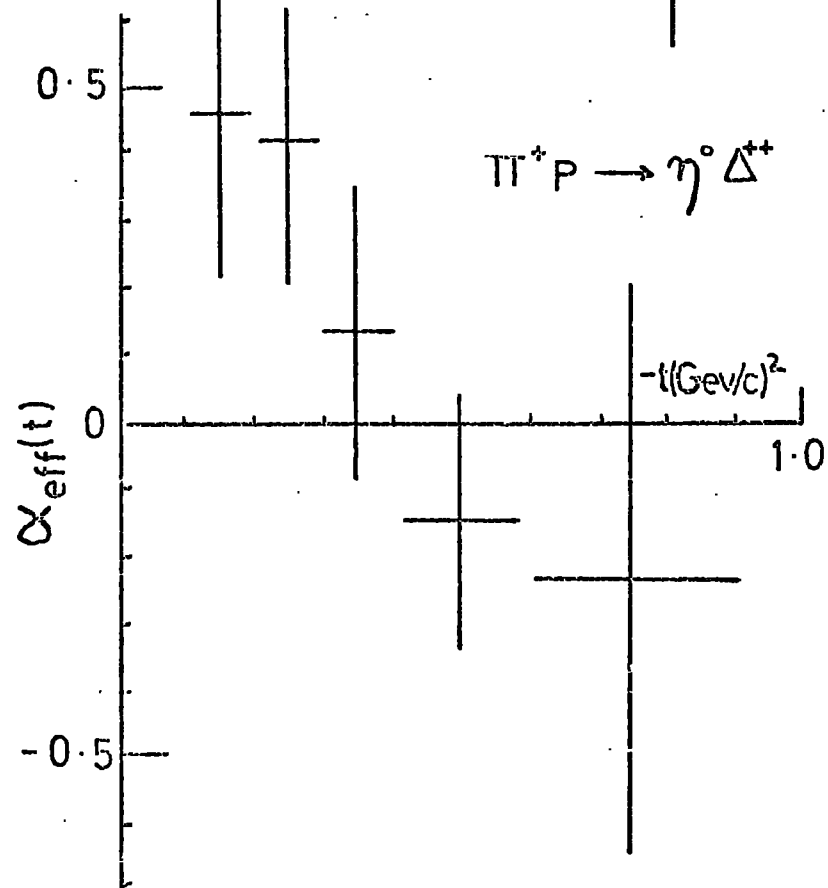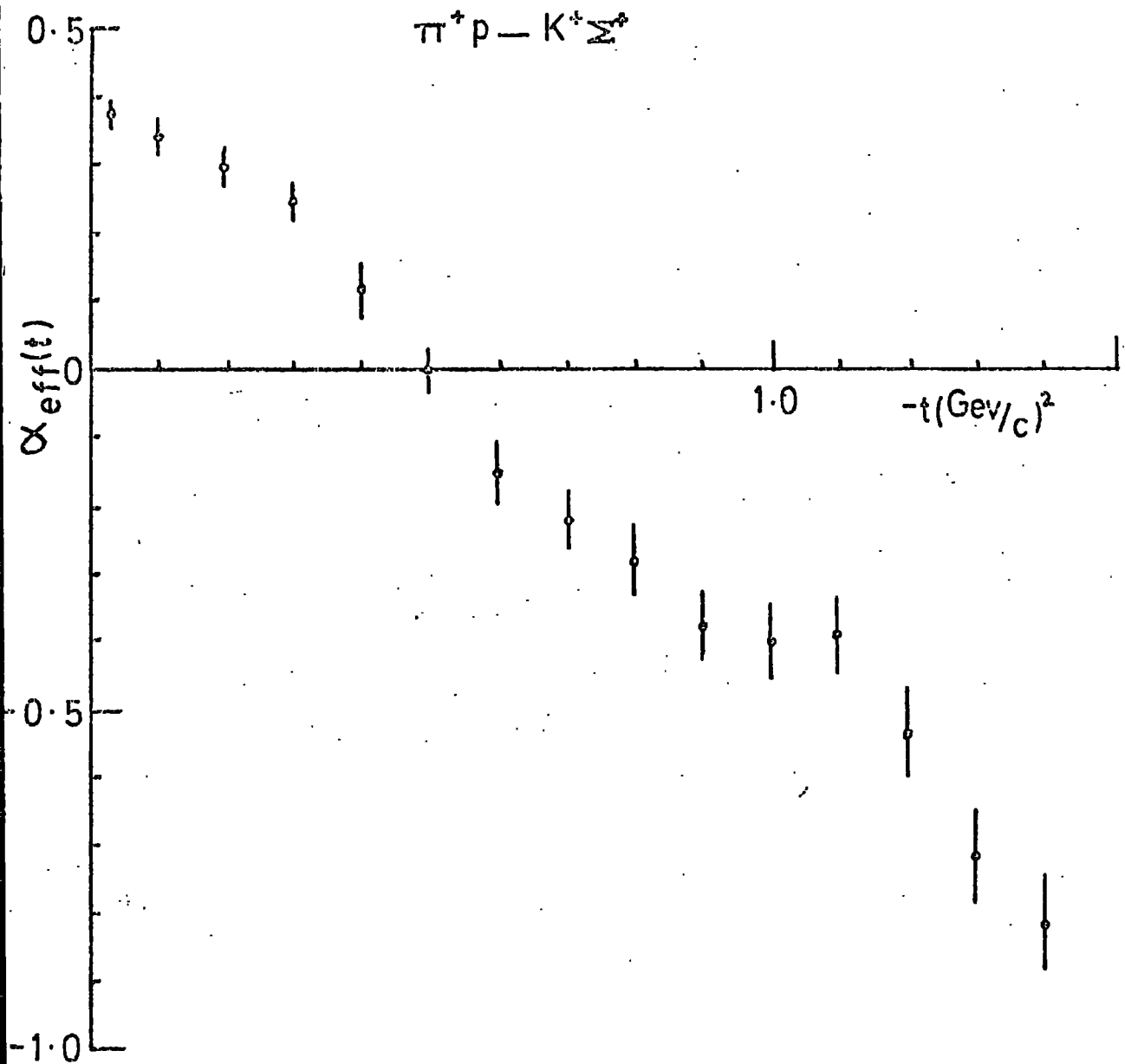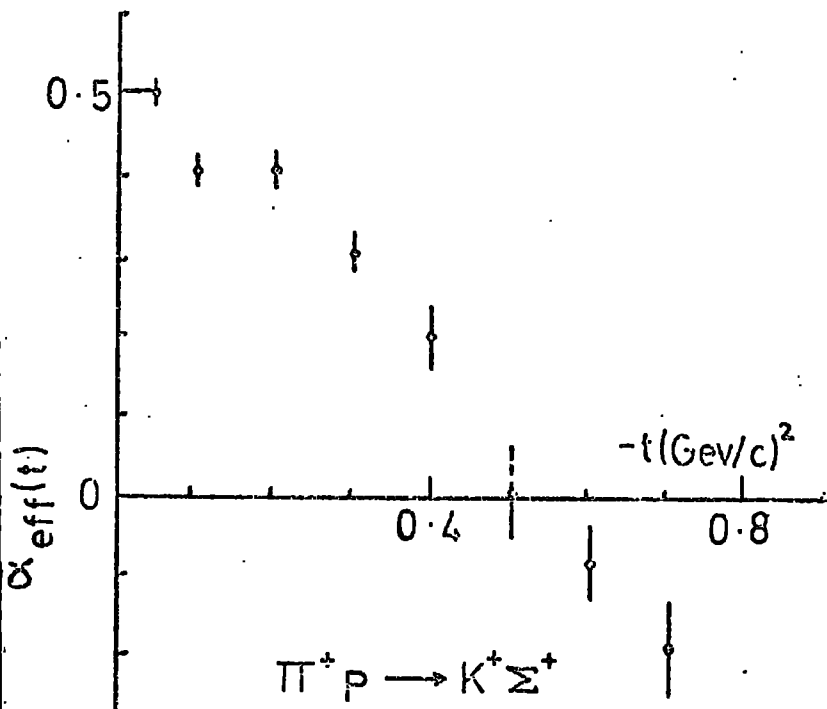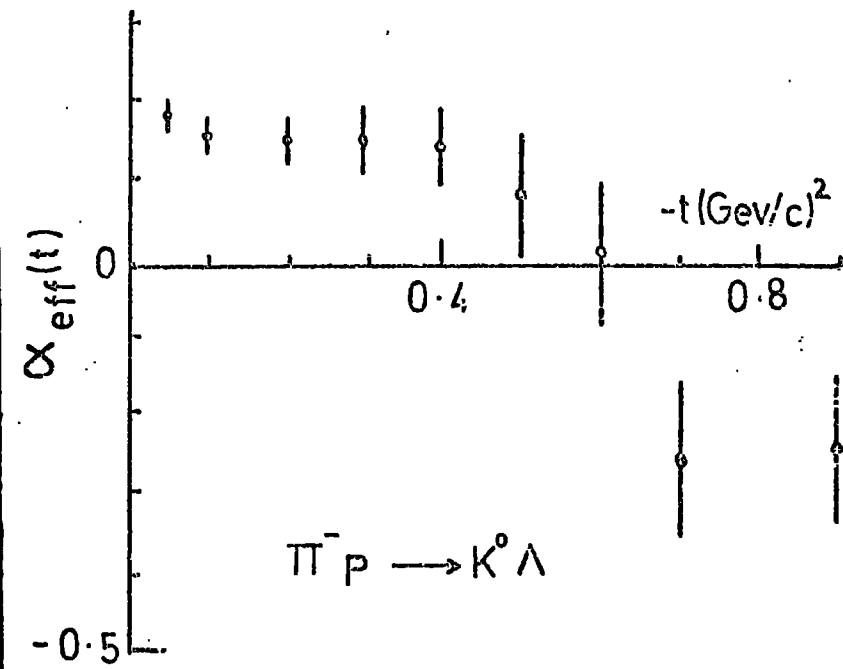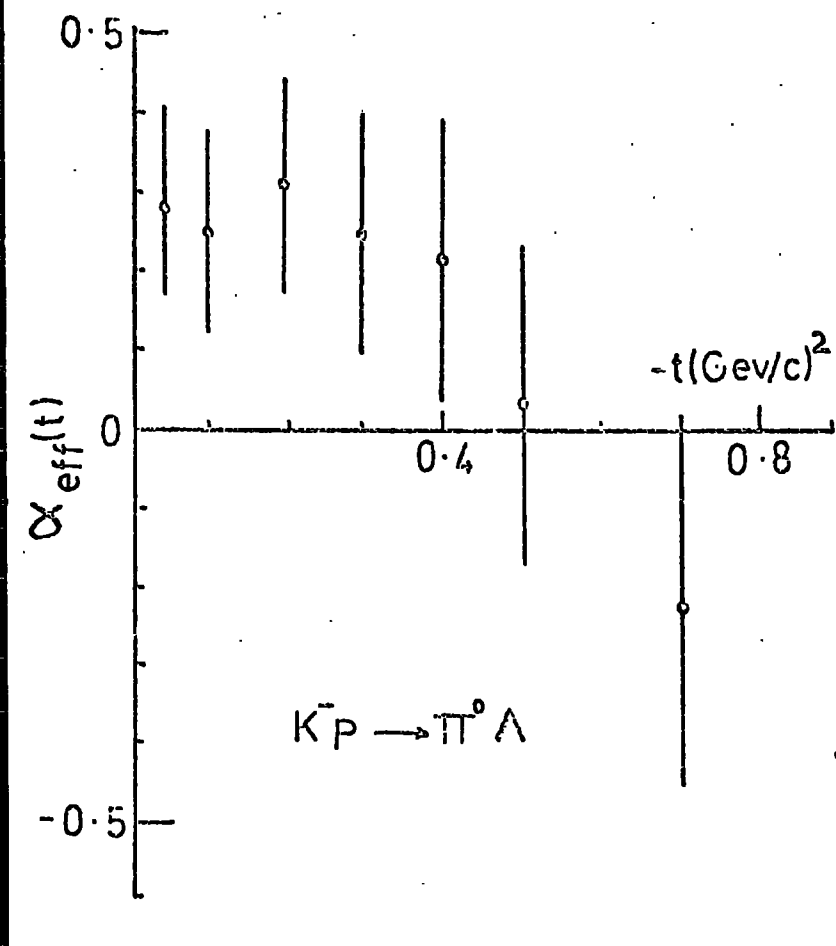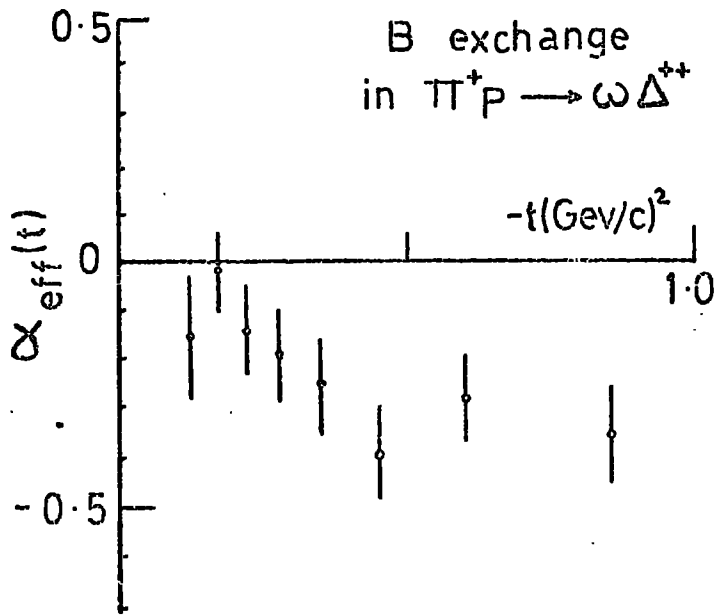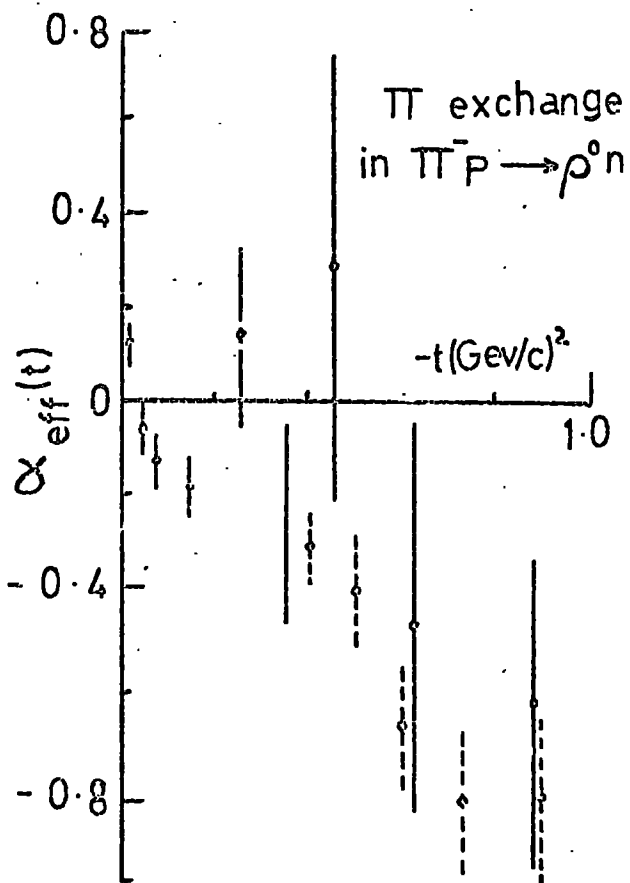
Fig 2·15 b

Fig 2·16

CHAPTER   THREE

3.1 THE EIKONAL MODEL

In chapter one we introduced the absorption model, in which the rescattering corrections to single Regge pole exchange are calculated by multiplying each term of the partial wave expansion by a factor which accounts for elastic scattering. One of the fundamental problems with this approach was that the diagrams had a planar topology. Consequently we could not be sure that we were calculating a true Regge cut, even though the rescattering term had the correct $s^{\alpha_c}(\log(s))^{-1}$ behaviour.

An attractive approach which utilises the close analogy between absorption in nuclear and high energy elementary particle physics, is the eikonal model first proposed by Glauber[51]. Of crucial importance is the composite nature of the scattering particles, which allows them to break up into their constituents, scatter and then subsequently recombine. If we consider deuteron-deuteron scattering, then we can draw the following diagrams.
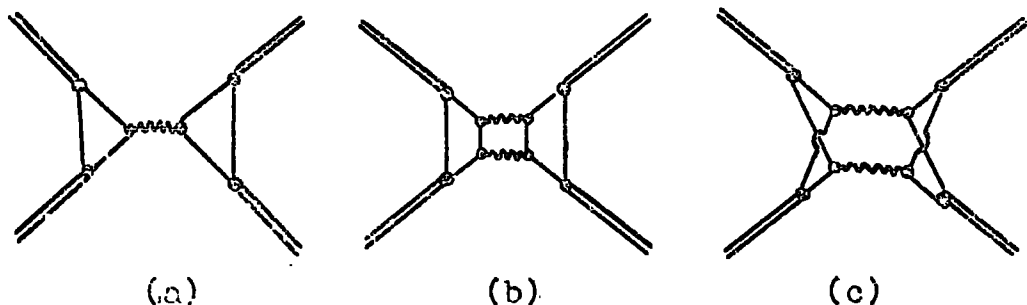

(a)   (b)   (c)

Diagram (a) represents single scattering which in the high energy context is of course the basic Regge pole exchange, whilst (b) and (c) are rescattering terms. At high energy, (c), where each of the constituents of the first particle scatters once off each constituent of the other particle, is much more probable than (b), where the interaction occurs twice between the same pair of particles. This picture is fine for the deuteron

whose binding energy is small ($B.E./m_d \sim 10^{-3}$), but is difficult to reconcile with the highly bound systems which we encounter in strong interactions.

In recent years many papers have appeared in the literature, which seek to justify the eikonal model in high energy scattering [52]. The crucial non-planar structure is obtained as follows. We work within the framework of ϕ^3 theory and ascribe to each Reggeon a two particle form factor vertex. Thus we are lead to consider the sum of diagrams

$$\text{(a)} \quad + \quad \text{(b)} \quad + \quad \text{(c)} \quad + \quad \text{(d)}$$

$$\text{(e)} \quad + \quad \text{(f)}$$
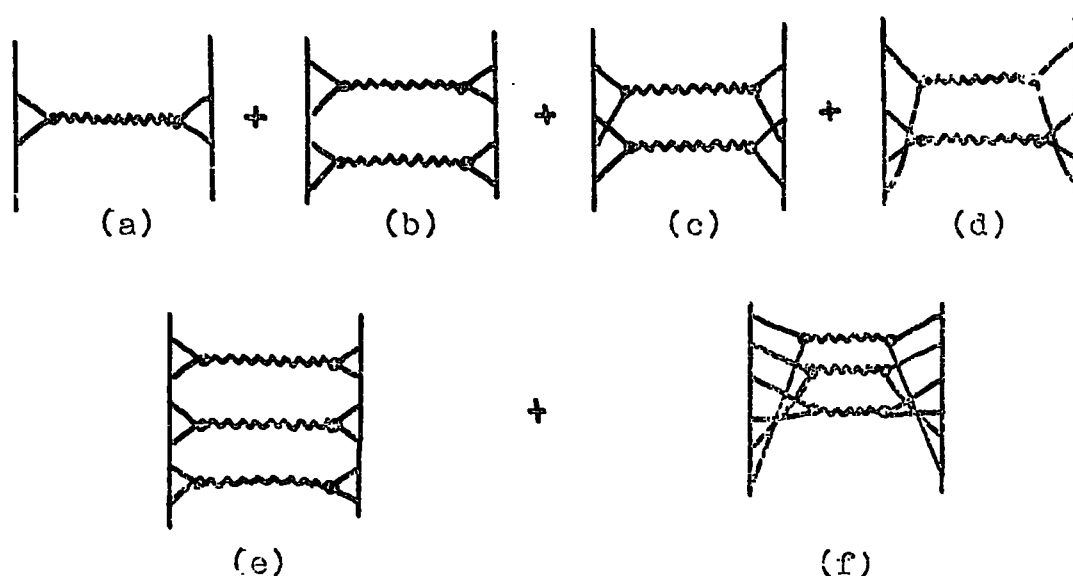
(a) is the usual Regge pole exchange which in the eikonal model plays the role of the "born term", whilst (b) gives the AFS cut with the correct $s^{-3}\log(s)$ behaviour. The graph (d), in which the couplings are nested maximally agrees both in form and (approximate) magnitude[53] with the second term of the eikonal series which we shall develop later. Furthermore, it has the correct topological (double cross) structure to satisfy the Mandelstam criterion for a true Regge cut. The contribution from (c) where the couplings are nested, but not maximally, is one power of $\log(s)$ down on (d). Finally, (d), (f) and the higher order diagrams give expressions which correspond to those obtained

by exponentiation of the basis Regge pole exchange, as in the eikonal series.

Thus in calculating the eikonal series we are summing the contributions from the set of graphs shown above. The structure of these graphs obviates those problems of the absorption model stemming from the non planar nature of the prescription. The addition of a two body form factor vertex ensures a cut-off in momentum transfer, so that most of the incident particles' momenta passes up the sides of the diagram. (The eikonal model in nuclear physics is often called the "straight-line approxim-ation".) This is also a feature of Gribov's Reggeon calculus and of course corresponds very closely to the physical situation at high energy.

A point emphasised by Cardy[54] is that a complete theory should include both s and t-channel unitarity. Therefore we should also consider the t-iterations of the simple pole and cut diagrams as shown below.
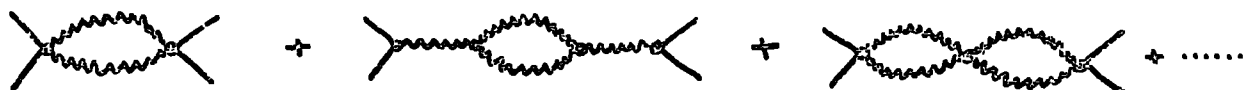
The t-iterations of Regge pole exchange play a vital role in "softening" the nature of the cut discontinuity and also in removing the Gribov-Pomeranchuk fixed pole at $J = -1$. In chapter four we shall investigate further the effects of t-channel unitarity on the phenomenology of Regge cuts.

3.2 THE EIKONAL SERIES[4]

In the eikonal model we have an approximation to the full s-channel partial wave series.

$$A_{H_s}(s,t) = 16\pi \sum_{J=m}^{\infty} (2J+1) A_{H_s}^J(s) \, d_{\mu'\mu}^J(z_s) \qquad (3.1)$$

This equation should be compared with (1.2) which was written for the case of particles without spin. H_s represents the set of s-channel helicity labels and $d_{\mu'\mu}^J(z_s)$ are the usual rotation functions.

In the high energy limit $s \to \infty$, $|t|/s \to 0$ the following replacement is valid

$$d_{\mu'\mu}^J(z_s) \longrightarrow J_N\left((J + \tfrac{1}{2})\theta_s\right) \qquad (3.2)$$

The index of the Bessel function is equal to the net s-channel helicity flip (1.15) and θ_s is the s-channel scattering angle. We now introduce the impact parameter b, defined by

$$J = q_s b - \tfrac{1}{2} \qquad (3.3)$$

In the large s, small $|t|$ limit, $\cos\theta_s \approx t/(2q_s^2)$ so that $\theta_s \approx (-t/q_s^2)^{\frac{1}{2}}$, and in equation (3.2)

$$(J + \tfrac{1}{2})\,\theta_s \longrightarrow b\,\sqrt{-t} \qquad (3.4)$$

Thus we can now replace the summation over J in (3.1) by an integral over impact parameters

$$A_{H_s}(s,t) \approx 16\pi \int_0^{\infty} q_s \, db \, (2q_s b) \, A_{H_s}^J(s) \, J_N(b\sqrt{-t}) \qquad (3.5)$$

The eikonal phase shift $\chi_{H_s}(s,b)$ is defined by

analogy with the normal phase shift $\delta_J(s)$.

$$A^J_{H_s}(s) \equiv \frac{e^{2i\delta_J(s)} - 1}{2i\rho(s)} \longrightarrow \frac{e^{i\chi_{H_s}(s,b)} - 1}{2i\rho(s)} \qquad (3.6)$$

where we have now made the approximation discussed in the last section; that the only effect of the interaction is to alter the phase of the incident particles wave front, with no effect on its direction.

Now remembering that $\rho(s) = 2q_s/\sqrt{s}$ and from Appendix one

$$q_s \xrightarrow[s \to \infty]{} \sqrt{s}/2 \qquad (3.7)$$

we finally end up with

$$A_{H_s}(s,t) \approx 4\pi s \int_0^\infty b\,db\; i\left(1 - e^{i\chi_{H_s}(s,b)}\right) J_N(b\sqrt{-t}) \qquad (3.8)$$

$$= 4\pi s \int_0^\infty b\,db\left[\chi - \frac{i(i\chi)^2}{2!} - \frac{i(i\chi)^3}{3!} - \cdots\right] J_N(b\sqrt{-t}) \qquad (3.9)$$

$$= 4\pi s \int_0^\infty b\,db\left[\chi + \frac{i\chi^2}{2!} - \frac{\chi^3}{3!} + \cdots\right] J_N(b\sqrt{-t})$$

where, for convenience, we have dropped the helicity labels on χ_{H_s}. The crucial step is to identify the first term of this series with the Fourier-Bessel transform of the Regge pole amplitude via the equation

$$\chi_{H_s}(s,b) = \frac{1}{8\pi s} \int_{-\infty}^0 dt\; J_N(b\sqrt{-t}) A_{H_s}(s,t) \qquad (3.10)$$

The Regge pole therefore, acts as the born term in the series and plays the role of the potential in nuclear physics. The second term in (3.9) is the two Reggeon cut and so on.

This formalism allows for an obvious extension to inelastic processes involving quantum number exchange, in which the basic interaction is treated to lowest order but full account is taken of elastic scattering in the initial and final states. Continuing the analogy with nuclear physics to include the Distorted Wave Born Approximation[55], we make the replacement

$$i\left[1 - e^{i\chi_{H_s}(s,b)}\right] \longrightarrow \chi^R_{H_s}(s,b)\, e^{i\chi^{el}_{H_s}(s,b)} \tag{3.11}$$

$$= \chi^R_{H_s} + i\,\chi^{el}_{H_s}\chi^R_{H_s} - \frac{(\chi^{el}_{H_s})^2\,\chi^R_{H_s}}{2!} + \cdots \tag{3.12}$$

where $\chi^r_{H_s}$ is now the Fourier-Bessel transform of the Regge pole which carries the quantum numbers, and the second factor in (3.11) is the elastic S-matrix. If we include the λ introduced by the Michigan group to allow for the possibility of diffractively produced intermediate states (for the "weak cut model" set $\lambda = 1$), the full replacement (3.11) becomes

$$\chi^R_{H_s}\,\exp\left[i\lambda\,\chi^{el}_{H_s}\right] \tag{3.13}$$

and (3.8) is now (dropping helicity labels again)

$$A(s,t) = 4\pi s \int_0^\infty b\,db\left[\chi^R + i\lambda\chi^R\chi^{el} - \chi^R\frac{(\lambda\chi^{el})^2}{2!} + \cdots\right] J_N(b\sqrt{-t}) \tag{3.14}$$

As a simple illustration of the use of these formulae which will prove useful later, we consider the effect of elastic rescattering - given by Pomeron exchange - on the single Regge

pole amplitude. For a helicity amplitude having net helicity flip $N \ (= 0, 1, 2, \text{etc.})$ we parameterise the Regge pole as

$$A_N^R(s,t) = i \left(\frac{s}{s_0} e^{-i\pi/2} \right)^{\alpha(0)} (-t)^{N/2} G_N \, e^{c_N t} \tag{3.15}$$

$$c_N = a_N + \alpha' \left[\ln\left(\frac{s}{s_0}\right) - \frac{i\pi}{2} \right] \tag{3.16}$$

where we have obtained (3.15) from the general expression (1.14) by making the following replacements.

$$\alpha(t) = \alpha(0) + \alpha' t .$$

$$\gamma_{N_2}(t) = \gamma_N(t) = G_N \, e^{a_N t} . \tag{3.17}$$

$$F_{N_0}(\alpha(t)) = 1 \quad , \quad x = 0 .$$

For the signature factor, which provides the Regge phase, we have considered an odd signature Regge pole (e.g. the rho) and made the approximation

$$\frac{1 - e^{-i\pi\alpha}}{\sin \pi\alpha} = \frac{i \, e^{-i\pi\alpha/2}}{\cos \frac{\pi\alpha}{2}} \approx i \, e^{-i\pi\alpha/2} \, e^{bt} \tag{3.18}$$

and we have absorbed the factor e^{bt} into the residue function. Equation (3.15) with $s_0 = 1 \ (\text{Gev/c})^2$ represents a typical Regge parameterisation which we shall use repeatedly throughout this work.

For simplicity, we take elastic scattering to be given by spin non flip Pomeron exchange.

$$A^{el}(s,t) = i \, \sigma_T s \, e^{c_P t} \tag{3.19}$$

$$c_P = a_P + \alpha_P' \left[\ln\left(\frac{s}{s_0}\right) - i\pi/2 \right] \tag{3.20}$$

$$\alpha_P(t) = 1 + \alpha_P' t \tag{3.21}$$

The corresponding eikonal phases χ^R and χ^{el} are easily obtained by substituting (3.15) and (3.19) into (3.10) and performing the integration with the aid of the relationship[56]

$$\int_{-\infty}^{0} e^{ct} (-t)^{N/2+m} J_N(b\sqrt{-t}) \, dt = \left(\frac{b}{2}\right)^N \left(-\frac{\partial}{\partial c}\right)^m \frac{e^{-b^2/4c}}{c^{N+1}} \tag{3.22}$$

The result is

$$\chi^R(s,b) = \frac{i\left(se^{-i\pi/2}\right)^{\alpha(0)}}{8\pi s} G_N \left(\frac{b}{2}\right)^N \frac{e^{-b^2/4c_N}}{c_N^{N+1}} \tag{3.23}$$

$$\chi^{el}(s,b) = \frac{i\sigma_T}{8\pi} \frac{e^{-b^2/4c_P}}{c_P} \tag{3.24}$$

We now have to evaluate the series (3.14). To do this let us consider just the second term, which is the Reggeon-Pomeron cut. (The first term gives us back the Regge pole (3.15).)

$$A_N^{(2)}(s,t) = \frac{i\left(se^{-i\pi/2}\right)^{\alpha(0)}}{2} G_N \left(-\frac{\lambda\sigma_T}{8\pi c_P}\right) \times$$

$$\times \int_0^\infty b \, db \left(\frac{b}{2}\right)^N J_N(b\sqrt{-t}) \frac{\exp\left[-\frac{b^2}{4}\left(\frac{1}{c_P}+\frac{1}{c_N}\right)\right]}{c_N^{N+1}} \tag{3.25}$$

To perform the integration we use the inverse of (3.22).

$$\int_0^\infty b \, db \, e^{-b^2/4c} (b^2)^{\frac{N}{2}+m} J_N(b\sqrt{-t}) = (-t)^{N/2} \left(4c^2\frac{\partial}{\partial c}\right)^m (2c)^{N+1} e^{ct} \tag{3.26}$$

Then if we define $\chi = c_P / (c_P + c_N)$, not to be confused with the eikonal phase shifts, we find

$$A_N^{(2)}(s,t) = i\left(se^{-i\pi/2}\right)^{\alpha(0)} G_N (-t)^{N/2} \left(\frac{-\lambda\sigma_T}{8\pi c_P}\right) \times \tag{3.27}$$

$$\times \, \chi^{N+1} e^{c_N \chi_N t}$$

To generalise the notation to include the higher order terms in the eikonal series, we replace X by

$$\chi_n = \frac{c_P}{(n-1)\, c_P + c_N} \tag{3.28}$$

The full series of cuts $R \boxtimes P^{n-1}$ is then simply

$$A_N(s,t) = i\left(s\, e^{-i\pi/2}\right)^{\alpha(0)} G_N(-t)^{N/2} \sum_{n=1}^{\infty} \left(\frac{-\lambda \sigma_T}{8\pi c_P}\right)^{n-1} \frac{\chi_n^{N+1}}{(n-1)!}\, e^{c_N \chi_n t} \tag{3.29}$$

As expected, the first term gives us back the Regge pole and the whole sum represents the set of Reggeon–Pomeron cuts.

$$R + R \boxtimes P + R \boxtimes P \boxtimes P + \ldots\ldots \tag{3.30}$$

Thus by taking a Pomeron which is purely imaginary at $t = 0$ (3.19), we have ended up with a two particle cut which has the opposite sign to, and therefore interferes destructively with, the input Regge pole. In fact by truncating (3.29) at $n = 2$ we reproduce the absorption model result. The eikonal method however, allows us to calculate multi–Pomeron and multi–Reggeon cuts.

For typical values of the Regge parameters the series converges rapidly, (for example 5% accuracy requires only the first four or five terms to be computed) and the main contribution is from the first two terms. Closer examination of the second term reveals that as $s \to \infty$ its energy dependence is $s^{\alpha_c}(\log(s))^{-1}$ and the cut trajectory $\alpha_c(t)$ is

$$\alpha_c(t) \xrightarrow[s \to \infty]{} \alpha(0) + \frac{\alpha'\, \alpha'_P}{\alpha' + \alpha'_P}\, t$$

as in the Mandelstam result. Also, the exponential t dependence of the cut is less than that of the pole, allowing the pole–cut

interference mechanism to occur.

3.3 THE NEW ABSORPTION MODELS

All of the old absorption models[19,20] fail to reproduce
the phases of the rho amplitudes in πN CEX as revealed by the
6.0 Gev/c amplitude analysis. We have seen that one contributing
factor is an inadequate description of the elastic amplitude
used to generate the absorptive effects. Experimentally[31]

$$\left[\frac{Re\ A^{o}_{++}}{Im\ A^{o}_{++}} \right]_{t\ =\ 0} \approx\ 20\ \%\ \ \text{at 6.0 Gev/c}$$

Therefore the representation of elastic scattering by a Pomeron
with intercept one is clearly insufficient, at least at 6.0 Gev/c.

Several ways of changing the phase of the absorptive
corrections have been proposed[22,23] and Worden has shown that
all owe their success to the introduction of lower lying J-plane
contributions. To avoid using ad hoc prescriptions to introduce
the required phase modifications and to retain contact with
Regge phenomenology, we prefer to describe the I_t= 0 exchange
amplitude as a sum of Pomeron (P) and P'. Then, in addition to
the $\rho \boxtimes$ P cuts with the usual intercept $\alpha_c(0) \sim 0.5$, there will
also be $\rho \boxtimes$ P' cuts. These will considerably alter the phase of
the total cut contribution since their intercept will be

$$\alpha_{\rho P'}(0)\ =\ \alpha_\rho(0)\ +\ \alpha_{P'}(0)\ -\ 1\ \approx\ 0$$

Collins and Swetman[27] have demonstrated that the
result of using such a prescription is a distinct improvement
in the phase of the I_t= 1 amplitudes. In particular their fit
gives a positive polarization in the region $0 \lesssim |t| \lesssim 0.5$ (Gev/c)^2
consistent with the data. In the next section we shall briefly
describe this model in order to be able to generalise the eikonal
formalism to include $R \boxtimes$ P' cuts, and to extend the model to

include neutral pion photoproduction and related processes.

However we should first mention a recent paper by Worden
[57] in which he uses the Gribov Reggeon calculus to establish
symmetry relationships between the different Regge-Regge cuts
which may contribute to a given process. In the Reggeon calculus
(discussed in greater detail in the next chapter) the two Reggeon
cut is produced by a diagram of the type shown below
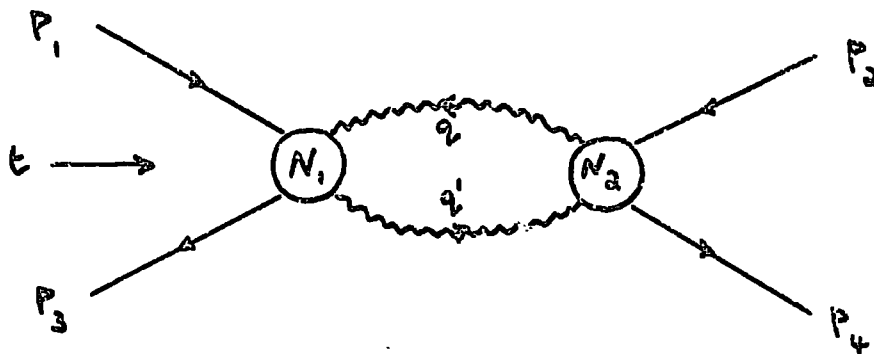
The N's are Gribov vertices, which are the residues of the
fixed poles in the appropriate Reggeon-particle scattering
amplitudes. The Gribov vertices vanish if these amplitudes do
not have a third d.s.f.[4]. This is an analogous statement to the
Finkelstein selection rule[58] which says that Regge-Regge cuts
can only be present if there exists a planar s-u duality
diagram (i.e. both the s and u channel non exotic). If we make
the following assumptions:

(i) SU(3) symmetry is exact for the Regge residues,

(ii) Strong EXD holds for $\rho - A_2$ and $P' - \omega$,

then it is possible to derive symmetry relationships between the
Gribov vertices.

e.g. $N_{\rho\pi \to \rho'\pi} (q,q') = - N_{A_2\pi \to \omega\pi} (q,q')$

These in turn imply corresponding relationships between the
Regge-Regge cuts, and predict a cancellation between the $P' \boxtimes \rho$
cut in πN CEX and the $\omega \boxtimes A_2$ cut.

A useful way of representing the internal symmetry properties of Regge-Regge cuts[59] is to use an extension of the technique proposed by Harari and Rosner[60] for Regge poles. If we have a pair of EXD Regge poles such as $\rho - A_2$ or $P' - \omega$, these add to give an amplitude with a rotating phase and subtract to give one which is purely real. The duality diagrams corresponding to these two possibilities for the relevant case of meson-baryon scattering are shown below.

(a)   (b)
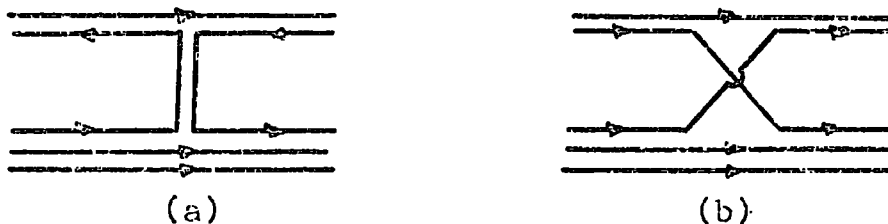
(a) represents the rotating case whilst (b) is the real combination. To obtain a Regge-Regge cut we combine (a) and (b) with the addition of an extra twist of a pair of internal lines on both the upper and lower halves of the diagram. The result is shown below where we take the explicit example of πN CEX.

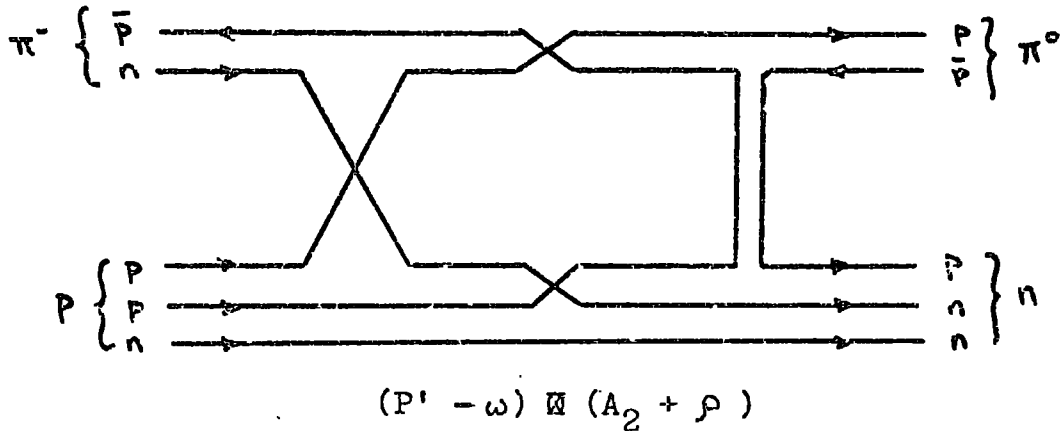$$(P' + \omega) \boxtimes (A_2 - \rho)$$
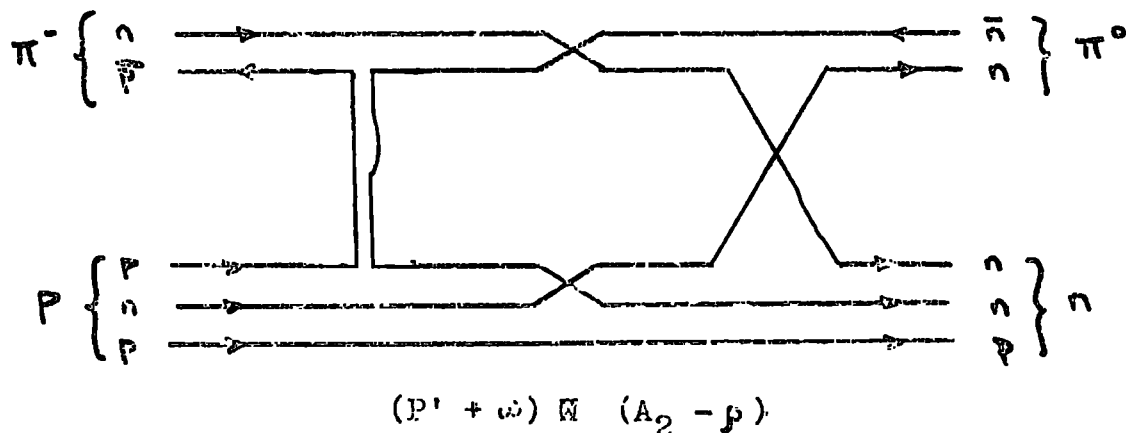
If we label the quark lines and remember that

$$\pi^o = \frac{1}{2} (\bar{p}p - \bar{n}n)$$

we see that the diagram corresponds to the case in which we have the $n\bar{n}$ component of the π^o. From this we must subtract

the diagram below.

$$(P' - \omega) \boxtimes (A_2 + \rho)$$

Therefore we have

$$(P' - \omega) \boxtimes (A_2 + \rho) - (P' + \omega) \boxtimes (A_2 - \rho)$$
$$= 2 (P' \boxtimes \rho - \omega \boxtimes A_2) \tag{3.30}$$

and if we assume exact EXD of the residues and trajectories we
arrive at Worden's conclusion - that the odd signature Regge-
Regge cuts in πN CEX cancel. Girardi et al[61] take this approach
one stage further by adopting an explicit model for the Pomeron
(in a duality diagram sense) and using this to examine the
properties of $R \boxtimes P \boxtimes R$ cuts. If we accept that the cancellation
in (3.30) is exact, then these cuts are expected to provide the
main correction to the simple $\rho + \rho \boxtimes P$ cut model of πN CEX.
However, the cancellation (3.30) only occurs if EXD holds. We
shall indicate later why this may not be such a good approxima-
tion and why the $\omega \boxtimes A_2$ cut may be small.

3.4 REGGE-REGGE CUTS IN πN SCATTERING

Collins and Swetman take for the $I_t = 0$ amplitudes of
appendix one the following sum of P and P'.

$$A_{++}^0(s,t) = i\sigma_T s \, e^{c_p t} + E_0 \, e^{c_{p'} t} \, \alpha_{p'}(t) \times$$
$$\times \left(s/s_0 \, e^{-i\pi/2} \right)^{\alpha_{p'}(0)} \tag{3.31}$$

$$A_{+-}^0(s,t) = \frac{\sqrt{-t}}{2m} \left[i C_0 \, s \, e^{d_p t} + F_c \, e^{d_{p'} t} \, \alpha_{p'}(t) \times \right.$$
$$\left. \times \left(s/s_0 \, e^{-i\pi/2} \right)^{\alpha_{p'}(0)} \right] \tag{3.32}$$

Where

$$c_p = a_p + \alpha_p' (\ln(s/s_0) - i\pi/2) \qquad\qquad (3.33)$$

$$c_{p'} = a_{p'} + \alpha_{p'}' (\ln(s/s_0) - i\pi/2)$$

with similar definitions for d_p and $d_{p'}$.

Now, Berger and Phillips[39] (BP) have proposed a model of πN scattering in which the $I_t = 0$ amplitudes involve the sum of $P + P' + P''$ exchanges, and are in good agreement with both the FESR constraints and the 6.0 Gev/c amplitude analysis. To facilitate the fitting procedure, Collins and Swetman treated the BP amplitudes as "data" to which they fitted the parameterisations (3.31) and (3.32). This can be done in two possible ways:

(i) We can treat the equations above as simply providing a functional representation of the $I_t = 0$ amplitude which allows the integrals involved in the eikonal prescription to be done analytically. We call this the "effective pole representation".

(ii) Alternatively we can consider (3.31) and (3.32) as the input Regge pole terms to the eikonal series (3.9) which generates the full set of multiparticle cuts

$$P + P \boxtimes P + P \boxtimes P \boxtimes P + \ldots + P' + P' \boxtimes P + P' \boxtimes P \boxtimes P + \ldots$$

Both methods were tried by Collins and Swetman and found to give approximately the same results. However, we are interested in using the $I_t = 0$ amplitude to calculate absorptive corrections to the pole in the $I_t = 1$ amplitude. For this purpose, (i) is definitely superior since with this method we do not need to evaluate the full eikonal series, just the first two terms, with a corresponding saving in computer time. We shall describe the "effective pole method" and use it when we extend the model to

photoproduction.

We proceed by substituting (3.31) and (3.32) into (3.10) to calculate the eikonal phase shifts. In an obvious notation these are

$$\chi_{++}^{0}(s,b) = \chi_{++}^{P}(s,b) + \chi_{++}^{P'}(s,b) \tag{3.34}$$

$$\chi_{+-}^{0}(s,b) = \chi_{+-}^{P}(s,b) + \chi_{+-}^{P'}(s,b) \tag{3.35}$$

For the rho pole amplitudes, the best parameterisation was found to be in terms of the invarient amplitudes A' and B corresponding to t-channel helicity non flip and helicity flip respectively. At high energy they are related to the usual s-channel helicity amplitudes of Appendix one by

$$A_{++}^{\rho}(s,t) = 2m A'(s,t) - \frac{st}{4m^2} B(s,t) \tag{3.36}$$

$$A_{+-}^{\rho}(s,t) = \frac{\sqrt{-t}}{2m} (2mA'(s,t) - sB(s,t)) \tag{3.37}$$

For the amplitudes A' and B Collins and Swetman take the typical Regge form

$$2m A'(s,t) = i \left(s/s_0 \, e^{-i\pi/2} \right)^{\alpha(0)} A_0 \, e^{c_1 t} \tag{3.38}$$

$$s \, B(s,t) = i \left(s/s_0 \, e^{-i\pi/2} \right)^{\alpha(0)} B_0 \, e^{c_2 t} \tag{3.39}$$

$$c_i = a_i + \alpha' \left[\ln(s/s_0) - i\pi/2 \right] \tag{3.40}$$

Equations (3.36) and (3.37) have eikonal phases χ_{++}^{P} and χ_{+-}^{P} defined as usual through (3.10). To calculate the cuts we now take

$$\chi_{++}'(s,b) = \chi_{++}^{P}(s,b) + i\lambda_{++} \chi_{++}^{P}(s,b) \chi_{++}^{0}(s,b)$$
$$+ i\lambda_{+-} \chi_{+-}^{P}(s,b) \chi_{+-}^{0}(s,b) \tag{3.41}$$

$$\chi'_{+-}(s,b) = \chi^{p}_{+-}(s,b) + i\lambda_{+-}\chi^{p}_{+-}(s,b)\chi^{o}_{++}(s,b)$$

$$+ i\lambda_{+-}\chi^{p}_{++}(s,b)\chi^{o}_{+-}(s,b) \qquad (3.42)$$

In practice the last term in each of these equations is small and can safely be ignored. The first term is of course the pole, whilst the second term corresponds to the $\rho\boxtimes P$ and $\rho\boxtimes P'$ cuts, or in the effective pole representation to the sum of cuts

$$\rho\boxtimes P + \rho\boxtimes P\boxtimes P + \ldots + \rho\boxtimes P' + \rho\boxtimes P\boxtimes P' + \ldots \qquad (3.43)$$

We shall describe the model presented by Collins and Swetman in which the rho adopts the "fixed pole mechanism". In this case there are no nonsense wrong signature zeros in the rho residue and the input pole amplitudes are exactly those given in (3.38) and (3.39). This model is undoubtably the most successful in fitting the data. Also tested was a "sense choosing" model in which a factor $\alpha(t)$ was introduced into (3.39), and a "nonsense choosing" model which also incorporates one $\alpha(t)$ in (3.38).

To calculate cuts we proceed as outlined in equations (3.15) to (3.29) for the simple case of just $\rho\boxtimes P$, except that in the effective pole representation of the elastic amplitude we need only consider the first two terms in the eikonal series. The eikonal phase shifts are

$$\chi^{P}_{++}(s,b) = \frac{i\sigma_{T}}{8\pi}\frac{e^{-b^{2}/4c_{P}}}{c_{P}} \qquad (3.44)$$

$$\chi^{P'}_{++}(s,b) = \frac{E_{o}(s/s_{o}e^{-i\pi/2})^{\alpha_{P'}(s)}}{8\pi s}\alpha_{P'}(o) \times$$

$$\times\left[1 + \frac{\alpha'_{P'}}{\alpha_{P'}(o)}\frac{\partial}{\partial c_{P'}}\right]\frac{e^{-b^{2}/4c_{P'}}}{c_{P'}} \qquad (3.45)$$

which are then incorporated into (3.34).

We do not need (3.35) for the reasons already mentioned. The extra differentation $\partial/\partial c_{p'}$ in the P' eikonal is a result of the $\alpha_{p'}(t)$ in the pole (no compensation mechanism) and arises through equation (3.22)

We now write for the full amplitude

$$A_{++}(s,t) = A_{++}^{P}(s,t) + A_{++}^{PP}(s,t) + A_{++}^{PP'}(s,t) \qquad (3.46)$$

$$A_{+-}(s,t) = A_{+-}^{P}(s,t) + A_{+-}^{PP}(s,t) + A_{+-}^{PP'}(s,t) \qquad (3.47)$$

Where the individual terms are obtained by taking the Fourier-Bessel inverse of (3.41) and (3.42) using (3.26). We consider the $\mathcal{P}\boxtimes P$ and the $\mathcal{P}\boxtimes P'$ cuts separately.

(i) $\mathcal{P}\boxtimes P$ cuts

These are calculated in exactly the same way as in section two except that we now have two terms corresponding to the A' and B parts of each helicity amplitude. In the flip amplitude, both enter on the same footing so that the cut is merely the sum of two similar terms. However, in the non flip case the B part contains the extra t factor which requires a differentiation $\partial/\partial c_2$ in the cut (from (3.22)). Thus by direct analogy to (3.29) we can write

$$A_{++}^{PP}(s,t) = i\left(s/s_0\, e^{-i\pi/2}\right)^{\alpha(0)}\left(-\frac{\lambda_{++}\,\sigma_T}{8\pi}\right)\times$$
$$\times\left[A_0\,\frac{\gamma_{P_1}e^{c_1\chi_{P_1}t}}{c_p} - \frac{B_0}{\mathcal{Z}_m^2}\frac{\partial}{\partial c_2}\frac{\chi_{P_2}e^{c_2\chi_{P_2}t}}{c_p}\right] \qquad (3.48)$$

$$A_{+-}^{PP}(s,t) = i\left(s/s_0\, e^{-i\pi/2}\right)^{\alpha(0)}\left(-\frac{\lambda_{+-}\,\sigma_T}{8\pi}\right)\times$$
$$\times\left[A_0\,\chi_{P_1}^2\,\frac{e^{c_1\chi_{P_1}t}}{c_p} - B_0\,\chi_{P_2}^2\,\frac{e^{c_2\chi_{P_2}t}}{c_p}\right] \qquad (3.49)$$

Where we have defined

$$\chi_{pi} = \frac{c_p}{c_p + c_i} \qquad (\text{ } i = 1,2) \qquad (3.50)$$

Note the extra differentiation in (3.48) and the fact that we have used only the second term of (3.29), not the full series.

(ii) $\rho \boxtimes P'$ cuts

We define, as in the P case

$$\chi_{p'i} = \frac{c_{p'}}{c_{p'} + c_i} \qquad (\text{ } i = 1,2) \qquad (3.51)$$

Then examination of the eikonal phases (3.44) and (3.45) reveals that to go from P to P' , we must

(a) make the replacement

$$\left(\frac{-\sigma_\tau}{8\pi}\right) \rightarrow \frac{i\,\epsilon_o\,\left(\frac{s}{s_o}\,e^{-i\pi/3}\right)^{\alpha_{p'}(o)}}{8\pi S} \qquad (3.52)$$

(b) introduce the differentiation cuased by the no compensation factor $\alpha_{p'}(t)$. That is we make the replacement

$$\frac{\chi_{pi}^{N+1}\,e^{c_i\chi_{pi}t}}{c_p} \longrightarrow \alpha_{p'}(o)\left(1 + \frac{\alpha'_{p'}}{\alpha_{p'}(o)}\frac{\partial}{\partial c_{p'}}\right)\frac{\chi_{p'i}^{N+1}\,e^{c_i\chi_{p'i}t}}{c_{p'}} \qquad (3.53)$$

where $N = 1,0$. The following formulae are useful

$$\frac{\partial}{\partial c_{p'}}\left(\chi_{p'i}^{N+1}\right) = \frac{(N+1)c_i}{c_{p'}^2}\chi_{p'i}^{N+2} \qquad (3.54)$$

$$\frac{\partial}{\partial c_{p'}}\left(e^{c_i\chi_{p'i}t}\right) = \frac{c_i^2 t}{c_{p'}^2}\chi_{p'i}^2\,e^{c_i\chi_{p'i}t}$$

$$\frac{\partial}{\partial c_{p'}}\left(\chi_{p'i}^{N+1}\,e^{c_i\chi_{p'i}t}\right) = \frac{e^{c_i\chi_{p'i}t}}{c_{p'}}\chi_{p'i}^{N+1}\left[\frac{c_i^2 t}{c_{p'}^2}\chi_{p'i}^2 + \frac{(N+1)c_i}{c_{p'}^2}\chi_{p'i} - \frac{i}{c_{p'}}\right]$$

Since, in (3.53), we need $\left(1 + \frac{\alpha'_{p'}}{\alpha_{p'}(o)}\frac{\partial}{\partial c_{p'}}\right)$, it is convenient to define

$$F_{p'i}^{(N)} = 1 + \frac{\alpha'_{p'}}{\alpha_{p'}(o)}\left[\frac{c_i^2 t}{c_{p'}^2}\chi_{p'i}^2 + \frac{(N+1)c_i}{c_{p'}^2}\chi_{p'i} - \frac{1}{c_{p'}}\right] \qquad (3.55)$$

Using this notation, the $\rho \otimes P'$ cuts are

$$A_{++}^{\rho P'}(s,t) = i\left(s/s_0\, e^{-i\pi/2}\right)^{\alpha(0)} \left[\frac{i E_0 \lambda_{++}\left(s/s_0\, e^{-i\pi/2}\right)^{\alpha_{p'}(0)}}{8\pi s} \right] \alpha_{p'}(0) \times$$

$$\times \left[A_0 \frac{e^{c_1 \chi_{p'_1} t}}{c_{p'}} \chi_{p'_1} F_{p'_1}^{(0)} - \frac{B_0}{4m^2} \frac{\partial}{\partial c_2} \frac{e^{c_2 \chi_{p'_2} t}}{c_{p'}} \chi_{p'_2} F_{p'_2}^{(0)} \right] \quad (3.56)$$

$$A_{+-}^{\rho P'}(s,t) = i\left(s/s_0\, e^{-i\pi/2}\right)^{\alpha(0)} \left[\frac{i E_0 \lambda_{+-}\left(s/s_0\, e^{-i\pi/2}\right)^{\alpha_{p'}(0)}}{8\pi s} \right] \alpha_{p'}(0) \times$$

$$\times \left[A_0 \chi_{p'_1}^2 \frac{e^{c_1 \chi_{p'_1} t}}{c_{p'_1}} F_{p'_1}^{(1)} - B_0 \chi_{p'_2}^2 \frac{e^{c_2 \chi_{p'_2} t}}{c_{p'}} F_{p'_2}^{(1)} \right] \quad (3.57)$$

Finally the full amplitude is obtained by combining all the relevant amplitudes in (3.46) and (3.47).

If the rho chooses sense or nonsense the formulae are further complicated by the $\alpha_\rho(t)$ factors which require extra differentiations similar to (3.54). However, since Collins and Swetman concluded that the fixed pole coupling mechanism was the the most successful in describing the data, we shall proceed no further along these lines. Much of this formalism will carry over into the photoproduction case to be disscussed in the next section.

A useful preliminary step to a full data fitting programme, is to actually fit the BP $I_t = 1$ amplitudes with the parameterisation above. The reasoning behind this is that the BP amplitudes satisfy the FESR constraint and also the detailed phase information available at 6.0 Gev/c from the amplitude analysis. Since the experimental phase sensitive data (polarizations) is very scarce and has such large errors, it carries very little weight in the fit. It is very easy therefore, to get reasonable agreement with the differential cross section data from a completely spurious

phase structure. Fitting the BP amplitudes avoids such false minima in χ^2 by ensuring that the parameters are in approximately the correct region before going on to fit the actual data. Rapid convergence is usually obtained in this way.

Briefly, the results of the fit are:

(i) All the CEX data are well represented in this model including the polarization, crossover zero and the dip in the differential cross section.

(ii) Problems occur in the elastic polarizations because of the poor description of Re A^1_{+-} at $t \sim -0.5$ $(Gev/c)^2$. In chapter two we described how the data forces a double zero in Re A^1_{+-} at this point, whilst the fit has only a single zero. More seriously $|A^1_{+-}|$ is too small at large $|t|$ so that the mirror symmetry is badly broken.

Thus the conclusion is that the BP description of the elastic amplitudes fails to give a completely satisfactory fit to all the πN data. The analysis of Kelly[21] indicates a slightly different structure for the $I_t = 0$ amplitudes — in particular a zero in Re A^0_{++} at $t \sim -0.85$ $(Gev/c)^2$. A fit to these instead of the BP amplitudes failed to improve the elastic polarizations, even though it generated (through the cuts) a different phase phase structure in the $I_t = 1$ contribution. This is an indication of the sensitivity of the cuts to the shape of the absorbing amplitude. However, the model is still a distinct improvement over the old absorption model without the Regge-Regge cuts.

3.5 REGGE-REGGE CUTS IN PHOTOPRODUCTION

Encouraged by the successes obtained in πN scattering
by including Regge-Regge cuts to correct the deficiencies of the
old absorption model, we decided to extend the approach to describe
π^o photoproduction and the other SU(3) related processes. The
rich amplitude structure in photo-induced reactions makes this
a severe test of the cut phases.

A recent analysis by Chadwick et al[62] has shown that
both the strength and shape of the diffractive amplitude in
$\gamma p \rightarrow \gamma p$ and $\gamma p \rightarrow \rho^o p$, are very much the same as in $\pi N \rightarrow \pi N$
when scaled by Vector Dominance. So, replacing π by γ at the meson
vertex appears to have little effect on the $I_t = 0$ exchange.
We therefore take for the elastic amplitude the form given in
equation (3.31), with the parameters fixed by the fit of Collins
and Swetman to πN scattering (Table (3.1)). Using this amplitude
to calculate the cuts makes the model highly constrained in that
the relative phase of pole and cut is completely fixed, and the
only freedom is in the Regge pole parameters and the overall
strength of absorption through the usual λ factors.

In the previous section we indicated that it was useful
to fit the BP amplitudes directly before going on to fit the
actual data. Worden[63] has produced a model of π and η photo-
production which describes most of the data and is also consistent
with the FESR's. However, the absorptive corrections are freely
parameterised and the model also includes the lower lying B and
H trajectories, so it is difficult to decide just how good the
model really is. Nevertheless, the phases of the amplitudes
should be reasonably accurate. We therefore used Worden's amplitudes
in a similar way to the BP amplitudes in πN to obtain approx-
imately the correct phase structure before fitting the experimental
data.

Our model[64] is then one in which we include the two highest lying exchanges ρ and ω. In the notation of Appendix one we parameterise the poles as

$$A^R_{\mu'\mu}(s,t) = i\,(-t)^{(N+x)/2}\,\left(s/s_0\,e^{-i\pi/2}\right)^{\alpha_R(0)}\,G^R_{\mu'\mu}\,e^{c^R_{\mu'\mu}t} \tag{3.58}$$

where $R = \{\rho,\omega\}$, and as usual

$$c^R_{\mu'\mu} = a^R_{\mu'\mu} + \alpha'_R\left[\ln(s/s_0) - i\pi/2\right] \tag{3.59}$$

The trajectories are linear functions of t, with the intercepts constrained so that they extrapolate through the physical particles. In Table (3.2) we define the Regge couplings along with the values of N and x for the different helicity states. S_0 is again taken to be 1 (Gev/c)^2.

The cut formalism is much simpler than in the last section because we have only one term in (3.58) instead of the two in πN because of the A' and B parameterisation. If we again write for the full amplitude

$$A_{\mu'\mu}(s,t) = \sum_{R=\rho,\omega} A^R_{\mu'\mu}(s,t) + A^{PR}_{\mu'\mu}(s,t) + A^{P'R}_{\mu'\mu}(s,t) \tag{3.60}$$

then the cuts are calculated in exactly the same way as before.

(i) $\underline{x = 0 \text{ amplitudes}}$ ($N = 0, 1, 2$)

(a) R ⊠ P cuts

$$A^{PR}_{\mu'\mu}(s,t) = i\,\left(s/s_0\,e^{-i\pi/2}\right)^{\alpha_R(0)}\,G_{\mu'\mu}\,(-t)^{N/2}\,\times$$
$$\times\,\left(-\frac{\lambda^R_{\mu'\mu}\,\sigma_T}{8\pi}\right)\chi^{N+1}_{PR}\,\frac{e^{c_R\chi_{PR}t}}{c_P} \tag{3.61}$$

For convenience we have dropped the helicity labels on $c^R_{\mu'\mu}$, and defined

$$X_{PR} = \frac{c_P}{c_R + c_P} \qquad (3.62)$$

(b) R ⊠ P' cuts

If we make the replacements outlined in (3.52) and (3.53), then

$$A^R_{\mu'\mu}(s,t) = i\left(s/s_0 \, e^{-i\pi/2}\right)^{\alpha_R(0)} G^R_{\mu'\mu} \, (-t)^{N/2} \times$$

$$\times \left[\frac{i \lambda^R_{\mu'\mu} E_0 \left(s/s_0 \, e^{-i\pi/2}\right)^{\alpha_{P'}(0)}}{8\pi s} \right] \alpha_{P'}(0) X^{N+1}_{P'R} \, F^{(N)}_{P'R} \, \frac{e^{c_R X_{PR} t}}{c_{P'}} \qquad (3.63)$$

where $F^{(N)}_{P'R}$ is defined in (3.55) and

$$X_{P'R} = \frac{c_{P'}}{c_R + c_{P'}} \qquad (3.64)$$

(ii) x = 2 amplitudes (N = 0)

Comparing (3.22) and (3.58) we see that the N = 0, x = 2 cuts can be obtained by substituting N = 0 in (3.60) and (3.63) and differentiating with respect to c_R. (We actually take $-\frac{\partial}{\partial c_R}$ to bring down the factor (-t) in (3.58).) In fact

$$-\frac{\partial}{\partial c_R}\left(X_{PR} \, \frac{e^{c_R X_{PR} t}}{c_P}\right) = -\frac{e^{c_R X_{PR} t}}{c_P}\left[X^3_{PR} \, t - \frac{X^2_{PR}}{c_P}\right] \qquad (3.65)$$

which gives

(a) R ⊠ P cuts

$$A^{RP}_{-+}(s,t) = i\left(s/s_0 \, e^{-i\pi/2}\right)^{\alpha_R(0)} G^R_{-+} \left(-\frac{\lambda^R_{-+} \, \sigma_T}{8\pi}\right) \times$$

$$\times \frac{e^{c_R X_{PR} t}}{c_P} \left[\frac{X^2_{PR}}{c_P} - X^3_{PR} \, t\right] \qquad (3.66)$$

(Note: In reference (63), equation (11), which details the replacement needed to obtain (3.65) from (3.60), a minus sign has been omitted.)

(b) R ⊗ P' cuts

Here the differentiation $-\dfrac{\partial}{\partial c_R}$ is more complicated. Using a result similar to (3.65) for the P' case, we find

$$A^{P'R}_{\mu'\mu}(s,t) = i\left(s/s_0\, e^{-i\pi/2}\right)^{\alpha_R(0)}\, G^{R}_{-\alpha}\,\times$$

$$\times \left[\frac{i\lambda^{R}_{-+}\epsilon_0\left(s/s_0\, e^{-i\pi/2}\right)^{\alpha_{P'}(0)}}{8\pi s}\right]^{\alpha_{P'}(0)}\,\times \quad (3.67)$$

$$\times\ \frac{e^{c_R\chi_{P'R}t}}{c_{P'}}\left\{\left[\frac{\chi_{P'R}}{c_{P'}} - \chi^3_{P'R}\,t\right]F^{(0)}_{P'R} - \chi_{P'R}\,\bar{F}^{(0)}_{P'R}\right\}$$

Where

$$\bar{F}^{(0)}_{P'R} \equiv \frac{\partial}{\partial c_R}\left[F^{(0)}_{P'R}\right]$$

$$= \frac{\alpha'_{P'}}{\alpha_{P'}(0)}\left(\frac{2c_R t}{c^2_{P'}}\chi^3_{P'R} + \frac{\chi^4_{P'R}}{c^2_{P'}}\right) \quad (3.68)$$

Thus equations (3.61),(3.63),(3.66),(3.67) form our prescription for the Regge cuts and the full amplitude is given by (3.60). If we place the same interpretation on the elastic amplitude as before (effective pole representation), these equations correspond to the series of exchanges (fig.(3.1))

$$R + R \otimes P + R \otimes P \otimes P + \ldots$$
$$+ R \otimes P' + R \otimes P' \otimes P + \ldots \quad (3.69)$$

We again checked that if we use the parameters for the elastic amplitude obtained from the second method of fitting the $I_t = 0$ amplitudes (see section (3.4)) and evaluate the full eikonal series to give (3.69), very similar results are obtained but they take very much longer to compute. Therefore, we adopt the effective pole method for practical purposes, and by first fitting Worden's amplitudes rapid convergence was achieved when

the experimental data was inserted.

3.6 RESULTS AND DISCUSSION

We display the results of the fit to the available π^{o} and η^{o} photoproduction data[65] in figs.(3.2) - (3.6) and table (3.3). The agreement with the data is excellent. Particularly encouraging is the good description of the polarised target asymmetry, as this provides the most severe test of the non flip and double flip amplitude phases. As we discussed in chapter two, if $A_{++} = A_{--}$ and $A_{+-} = -A_{-+}$, then $\Sigma = 1$ identically. Looking at table (3.2), we see that the poles certainly satisfy this, whilst (3.61) and (3.66) show how the cuts do not. The violation occurs in the non flip and double flip amplitudes and the deviation of Σ from unity measures the strength of this violation. It is of course important at $t = 0$ and t -0.5 $(Gev/c)^2$ and is less significant at large t ; Fig.(3.3) reflects this general trend. In our model, the unnatural parity components in the cuts replace the B and H exchanges used by Worden.

The ratios of vector to tensor couplings at the nucleon vertex which we obtain are

$$\frac{G_V^\rho}{G_T^\rho} \approx 0.2 \qquad\qquad \frac{G_V^\omega}{G_T^\omega} \approx 0.9$$

The rho is therefore in good agreement with typical values obtained in fits to πN scattering. The large value of the omega flip coupling is essential in our model to obtain good agreement with the neutron/proton ratio of fig.(3.5). Worden includes, in addition to the B, the H meson (which is the isoscalar member of the 1^{+-} octet) with a large flip coupling with respect to the B. He is therefore able to preserve the small non flip omega coupling predicted by Vector Dominance[66]. To compare the Regge prediction with VDM however, we must first extrapolate from the photon

to the vector meson mass m_ω^2 and then down the Regge trajectory to the scattering region $t \lesssim 0$, so our value of 0.9 is by no means incompatible with VDM.

In fig.(3.7) we compare our amplitudes with those obtained by Worden, and also show the effect of including the $R \boxtimes P'$ cuts. It is clear that this is mostly in the real parts as expected, and in fact is crucial in order to obtain a good description of the polarised target asymmetry (fig.(3.4)).

In fig.(3.8) we give the predictions for the polarised target and polarised photon asymmetries in η photoproduction, and for the ratio of η photoproduction from neutrons and protons.

We also attempted to fit the data using a model with nonsense wrong signature zeros. The basic problem with such a model is that it predicts a dip at $t \sim -0.5$ $(Gev/c)^2$ in the differential cross section (dominated by rho exchange), contrary to the data. Even allowing $\lambda > 1$ and a substantial B contribution we are still unable to fill in the dip completely. Of course, as the B exchange dies away with energy, the dip is expected to deepen.

Finally, we return to Worden's argument[57] that, provided the π and B are exchange degenerate, our $\rho \boxtimes P'$ and $\omega \boxtimes P'$ cuts could be cancelled by $A_2 \boxtimes \omega$ and $P' \boxtimes \omega$ respectively. As fig.(3.9) shows, our neglect of the latter pair of cuts is equivalent to assuming a small coupling for the B - thus breaking exchange degeneracy. A similar argument explains why we might expect the $\rho \boxtimes P'$ cut to be much larger than the $\omega \boxtimes A_2$ in πN CEX.

It appears that the inclusion of the P' in order to

obtain a better description of the elastic amplitude can solve many of the problems of the old absorption models. The only worrying feature of this and in fact all the current absorption models, concerns the energy dependence of the cuts. This is revealed in two ways:

(i) As we extrapolate to low energies the cut begins to dominate the pole (their relative strength at 6.0 Gev/c is fixed by the amplitude analysis) causing severe disagreement with the FESR's (see chapter two).

(ii) At high energies the cuts calculated in the absorption/eikonal model predict too little shrinkage at large $|t|$ in hadronic reactions. This is apparent from figs.(2.1) and (2.2) for the particular case of π N CEX. In fig.(3.10) we plot $\alpha_{eff}(t)$ for the model of π^o photoproduction which we have just described and compare it with the "data" of fig.(2.6a). The model reproduces all the features of the data and we are lead to conclude that a strong cut model in which the cut trajectory takes the Mandelstam form (1.23) together with Regge-Regge cuts to produce the correct phase structure, is completely consistent with all aspects of the photoproduction data.

It is this puzzling fact that photoproduction is similar to purely hadronic reactions in all respects except its energy dependence and that the absorption model produces cuts which have the correct energy dependence in photoproduction but not in hadronic reactions, that we shall attempt to investigate further in the final two chapters.

	Pomeron		P'
σ_T	19.92(mb)/0.3893	E_0	-43.31(mb)/0.3893
a_P	2.02	$a_{P'}$	0.23
α_P^r	0.49	$\alpha_{P'}^r$	1.10
$\alpha_P(0)$	1.0 (fixed)	$\alpha_{P'}(0)$	0.55

TABLE 3.1

Parameters for the $I_t = 0$ non flip N amplitude from reference (27)

μ'	μ	N	x	$G^\omega_{\mu'\mu}$	$G^\rho_{\mu'\mu}$
+	+	1	0	$g_{\rho\omega\pi}\, g_{\gamma\rho}\, G^\omega_V$	$g_{\rho\omega\pi}\, g_{\gamma\omega}\, G^\rho_V$
−	−	1	0	$g_{\rho\omega\pi}\, g_{\gamma\rho}\, G^\omega_V$	$g_{\rho\omega\pi}\, g_{\gamma\omega}\, G^\rho_V$
−	+	0	2	$-g_{\rho\omega\pi}\, g_{\gamma\rho}\, G^\omega_T / 2m$	$-g_{\rho\omega\pi}\, g_{\gamma\omega}\, G^\rho_T / 2m$
+	−	2	0	$g_{\rho\omega\pi}\, g_{\gamma\rho}\, G^\omega_T / 2m$	$g_{\rho\omega\pi}\, g_{\gamma\omega}\, G^\rho_T / 2m$

TABLE 3.2

The couplings for Reggeon R exchanged in $\gamma p \rightarrow \pi^0 p$ from reference (12).

The decay width $\omega \rightarrow \gamma\pi^0$ gives $g^2_{\omega\pi\gamma}/4\pi = 0.038$ and the meson couplings were then fixed by the Vector Dominance relations $g_{\omega\pi\gamma} = g_{\rho\omega\pi}\, g_{\gamma\rho}$ and $g_{\gamma\rho} = 3 g_{\gamma\omega} = 0.06$.

M is the nucleon mass.

Parameter	ρ	ω
α'	0.80	1.00
G_V	2.19	15.56
G_T	10.07	20.02
a_{++}	4.42	1.07
a_{+-}	0.02	1.61
λ_{-+}	2.88	1.51
λ_{++}	2.93	2.39
λ_{+-}	2.70	1.65

TABLE 3.3

The final values of the parameters obtained in the fit to the data of reference (65). The trajectory intercepts were constrained so that the trajectories extrapolated through the physical particles.

Also we set $a_{-+} = a_{+-}$ and $\lambda_{-+} = \lambda_{+-}$ for both the rho and the omega.

A final $\chi^2/$ data point of 1.07 was achieved for 111 data points.

FIGURE CAPTIONS - CHAPTER THREE

3.1 The sum of poles and cuts represented by equation (3.60).

3.2 Fit to the differential cross section for $\gamma p \rightarrow \pi^\circ p$.

3.3 Fit to the polarised photon asymmetry for $\gamma p \rightarrow \pi^\circ p$ (solid line). The dashed curve is the model of ref.(63).

3.4 Fit to the polarised target asymmetry for $\gamma p \rightarrow \pi^\circ p$ (solid line). The dashed curve is the model of ref.(63).

3.5 Fit to the neutron/proton ratio (R) for π° photoproduction. (solid line). The dashed curve is the model of ref.(63).

3.6 Fit to the differential cross section for $\gamma p \rightarrow \eta^\circ p$.

3.7 The π° photoproduction amplitudes at 6.0 Gev/c

    (a) Non flip amplitude.

    (b) Single flip amplitude.

    (c) Double flip amplitude.

In each case the solid and dotted curves show the result of our fit with and without the R ⊠ P' cuts respectively. The dashed curve is the model of ref.(63).

3.8 Predictions for various quantities in $\gamma p \rightarrow \eta^\circ p$.

    (a) The ratio $(\gamma n \rightarrow \eta^\circ n)/(\gamma p \rightarrow \eta^\circ p)$

    (b) Polarised target asymmetry.

    (c) Polarised photon asymmetry.

3.9 Pairs of Regge-Regge cuts which may cancel each other if $\pi - B$ exchange degeneracy holds, according to the arguments of ref.(57).

3.10 Effective trajectory calculated from the model of π° photoproduction presented in section (3.5) compared with the "data" of fig.(2.6a).

Fig 3·1

$\gamma p \rightarrow \pi^{\circ} p$

6 Gev/c

9 Gev/c

12 Gev/c

15 Gev/c

$d\sigma/dt \left[\mu b/(Gev/c)^2 \right]$

$-t (Gev/c)^2$
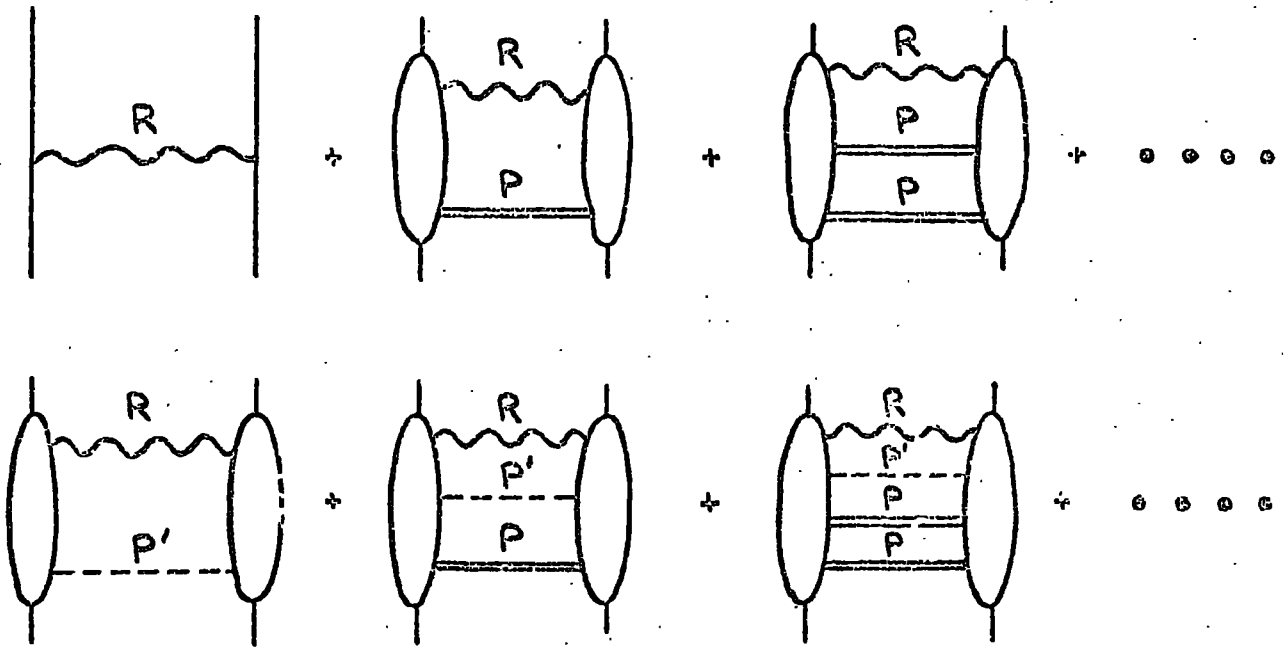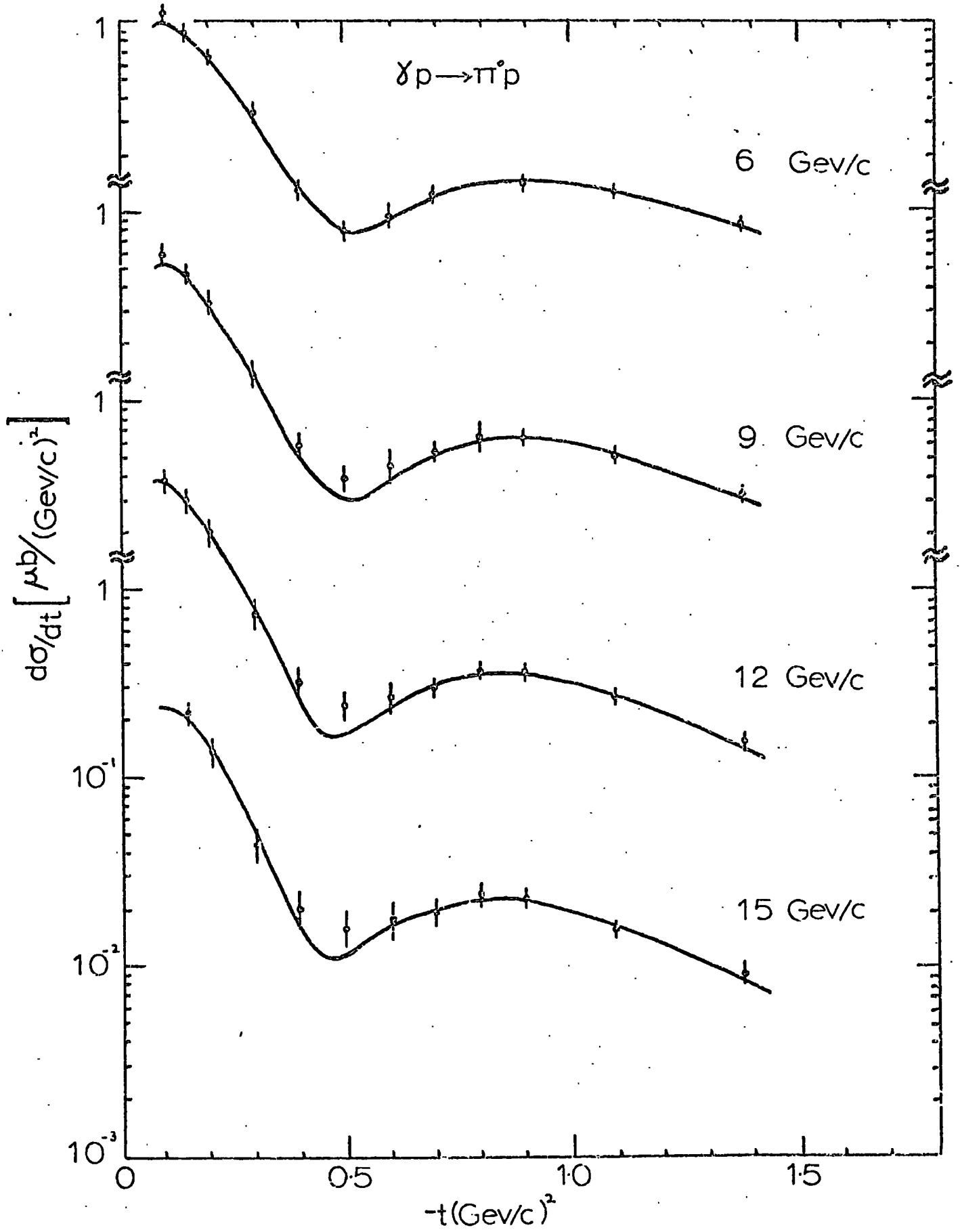
Fig 3.2
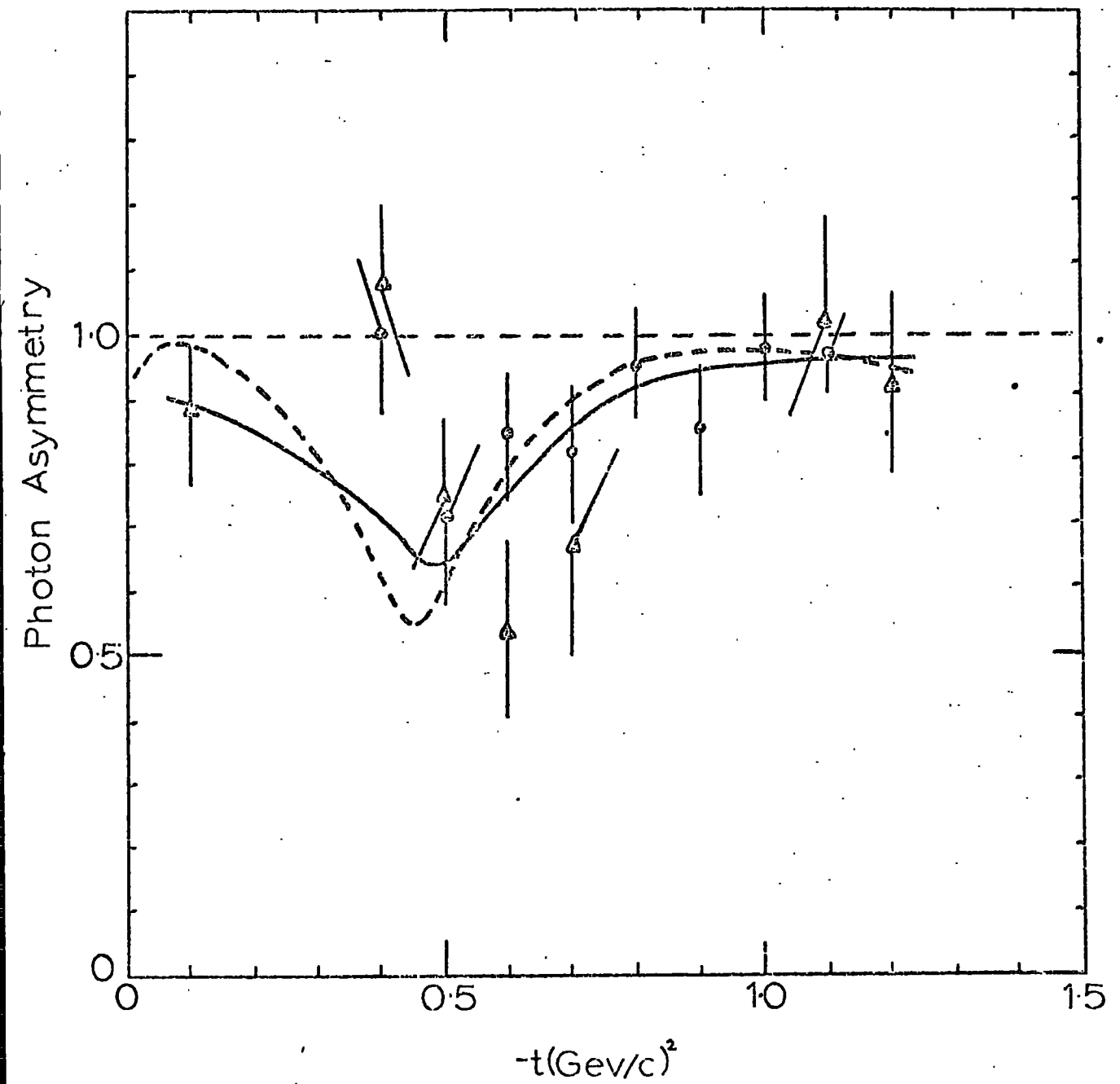
Fig 3·3
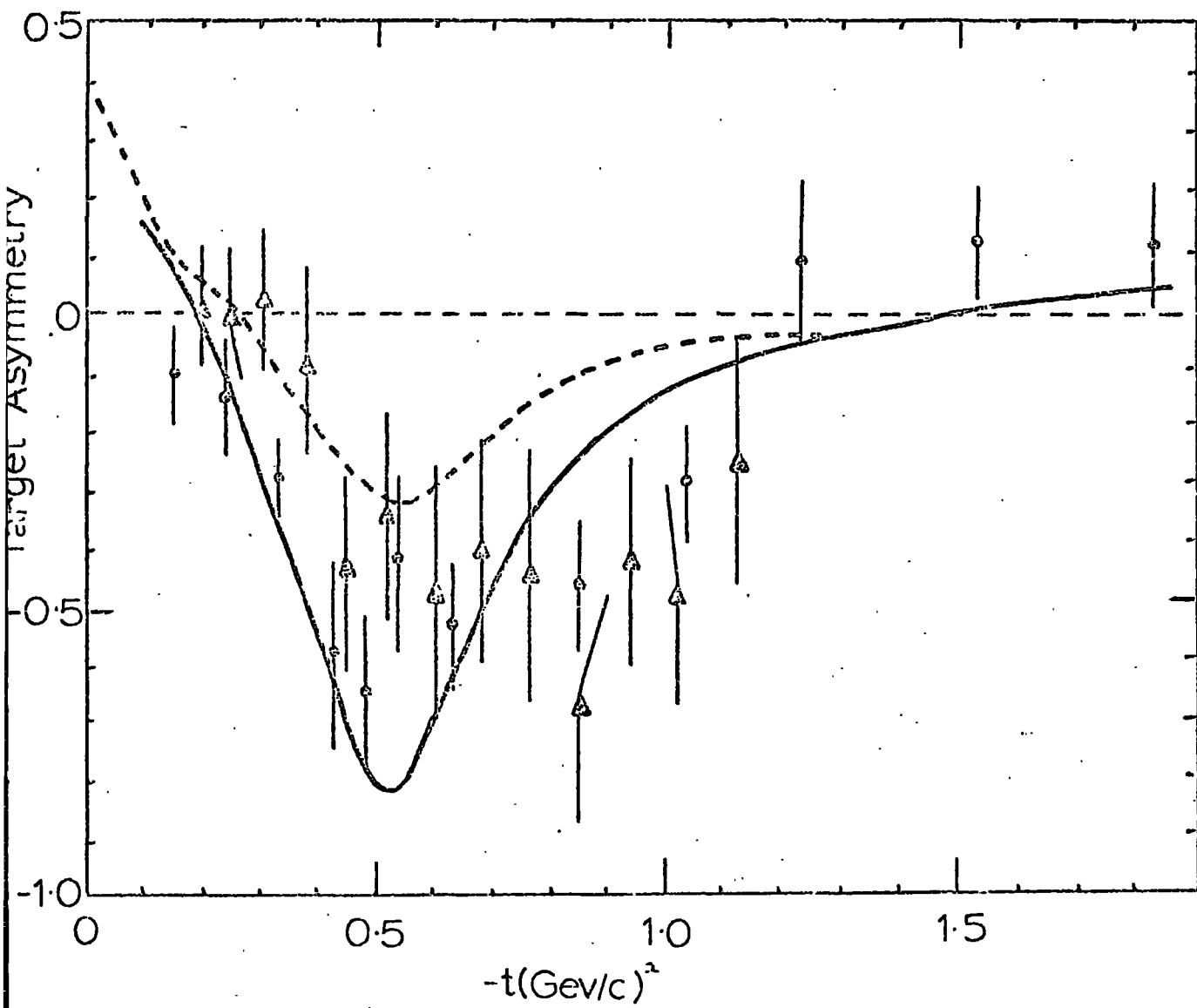
Fig   3·4
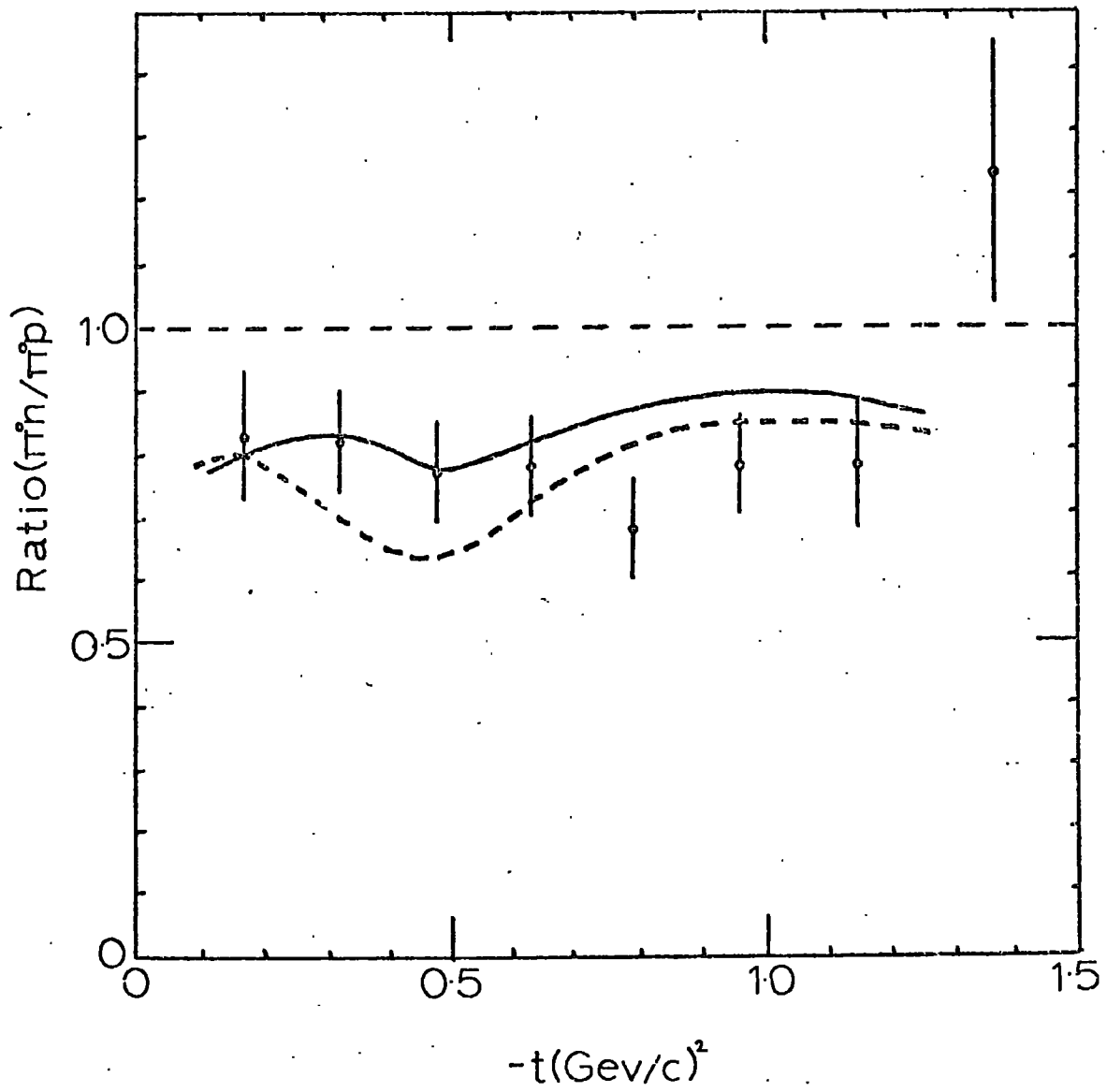
Fig   3·5
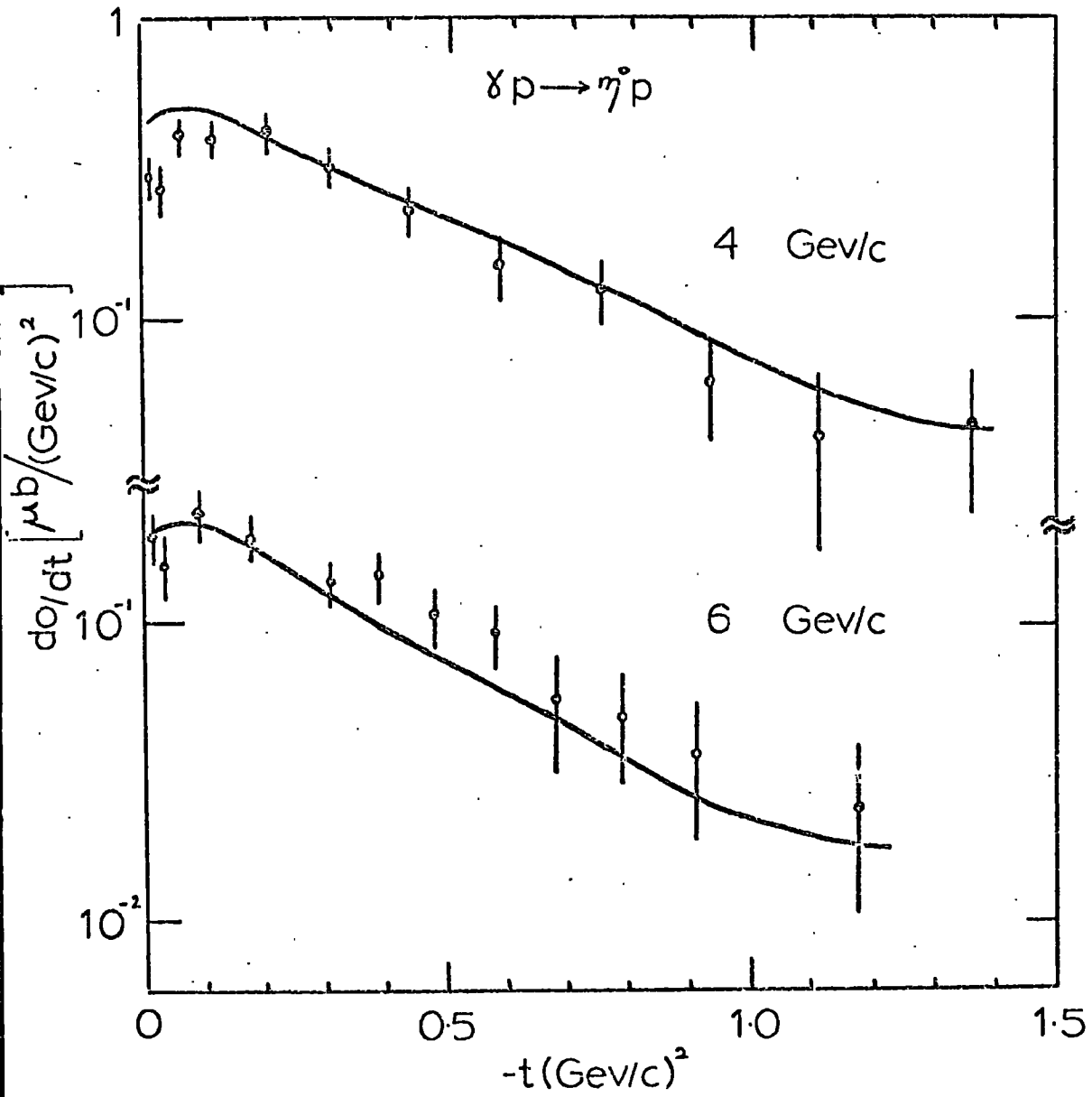
Fig 3·6
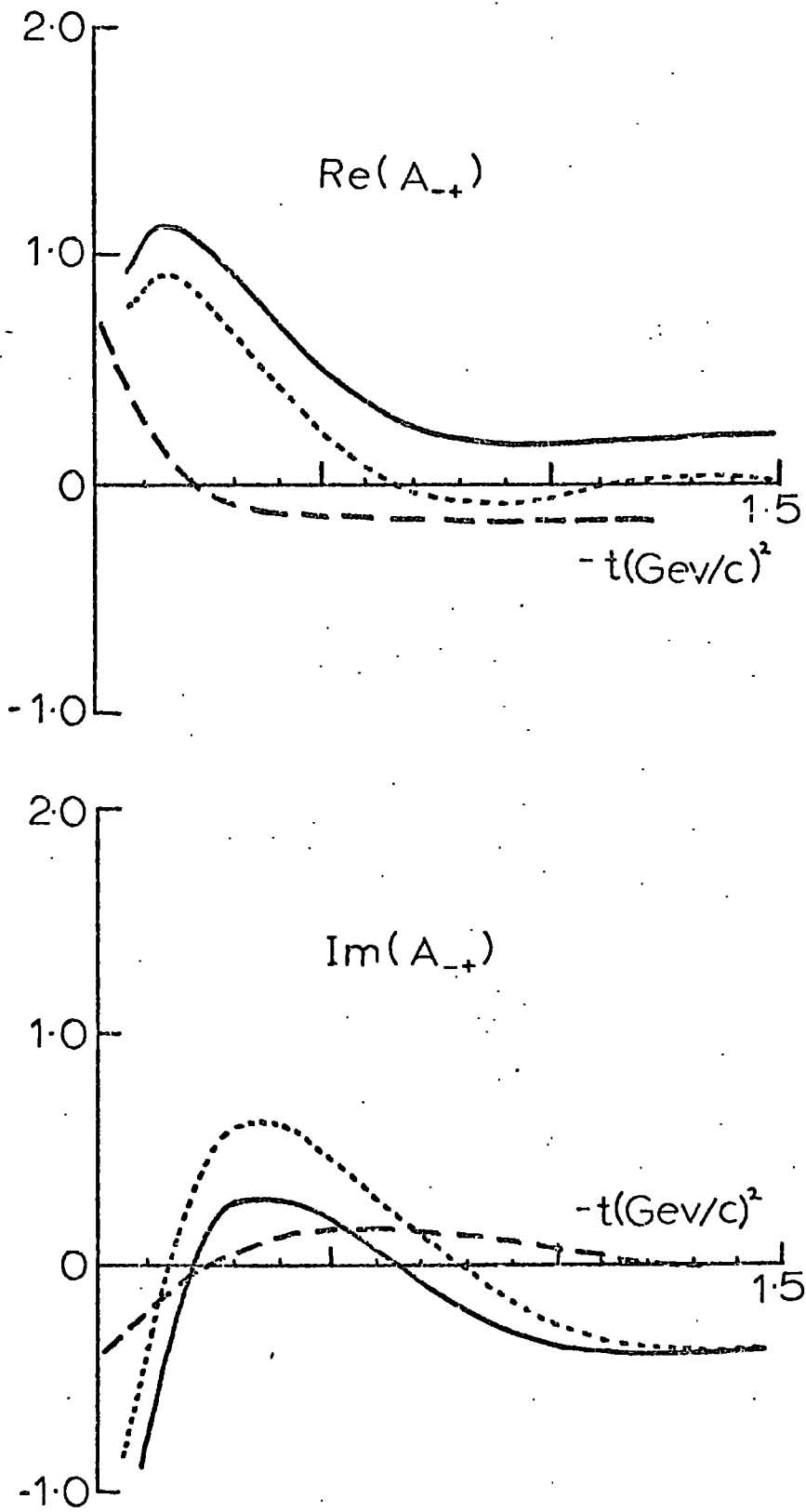
Fig 3·7 a
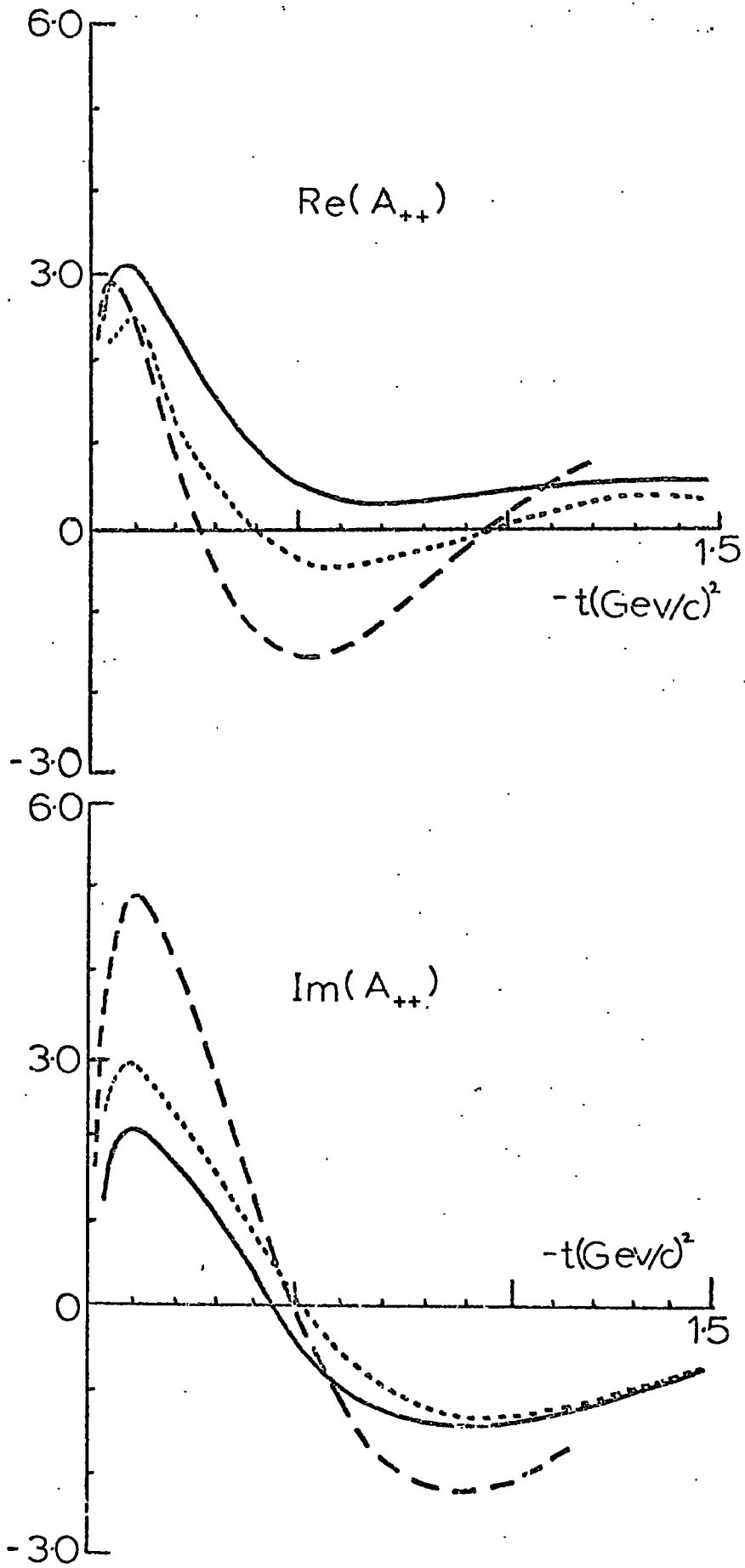
Fig   3.7 b
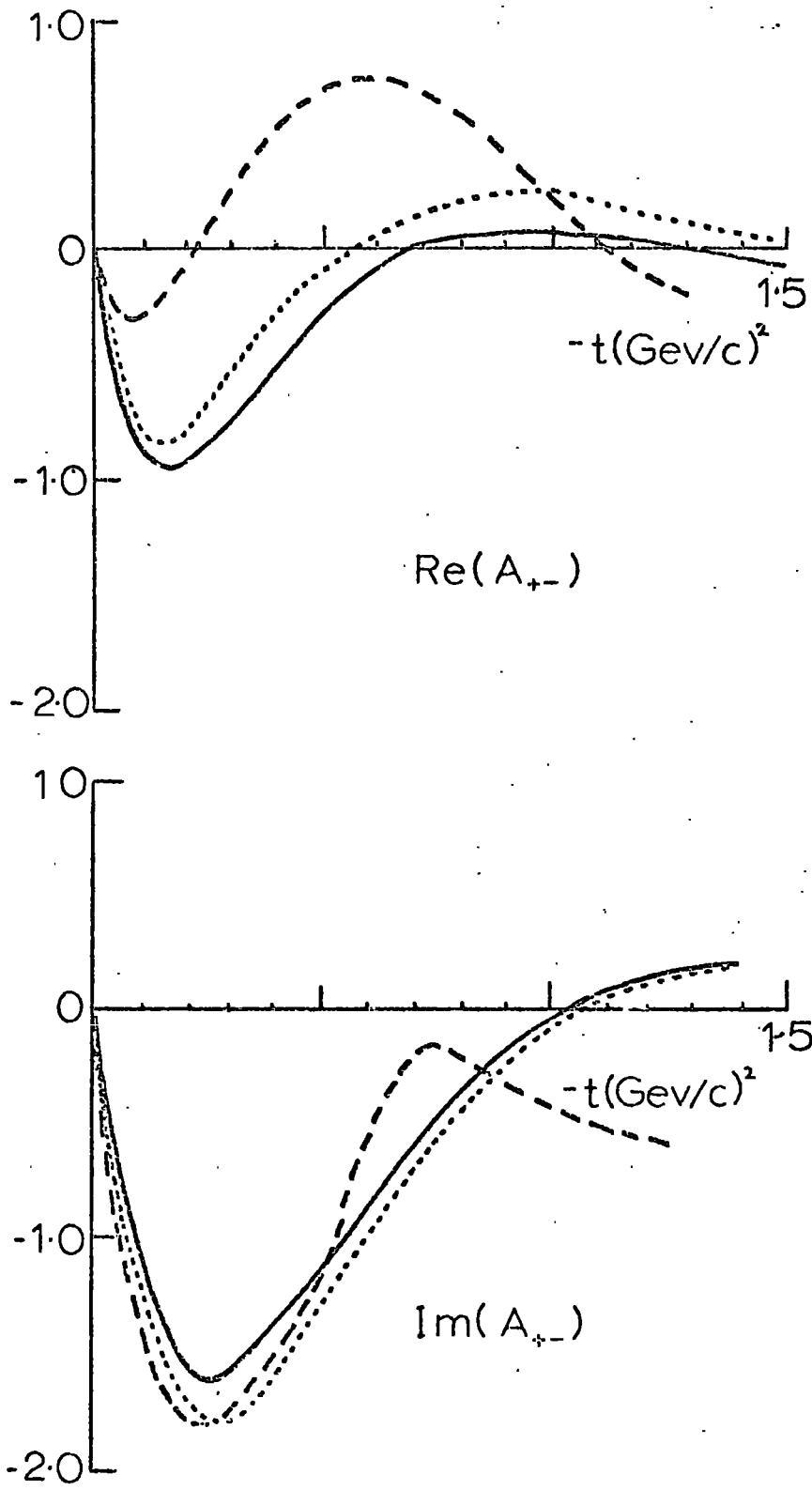
Fig 3.7c
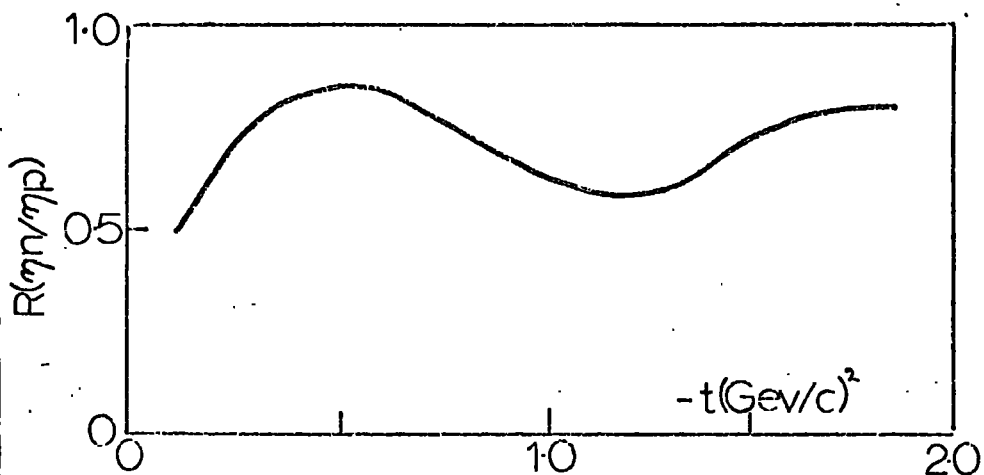
Fig 3.8 a
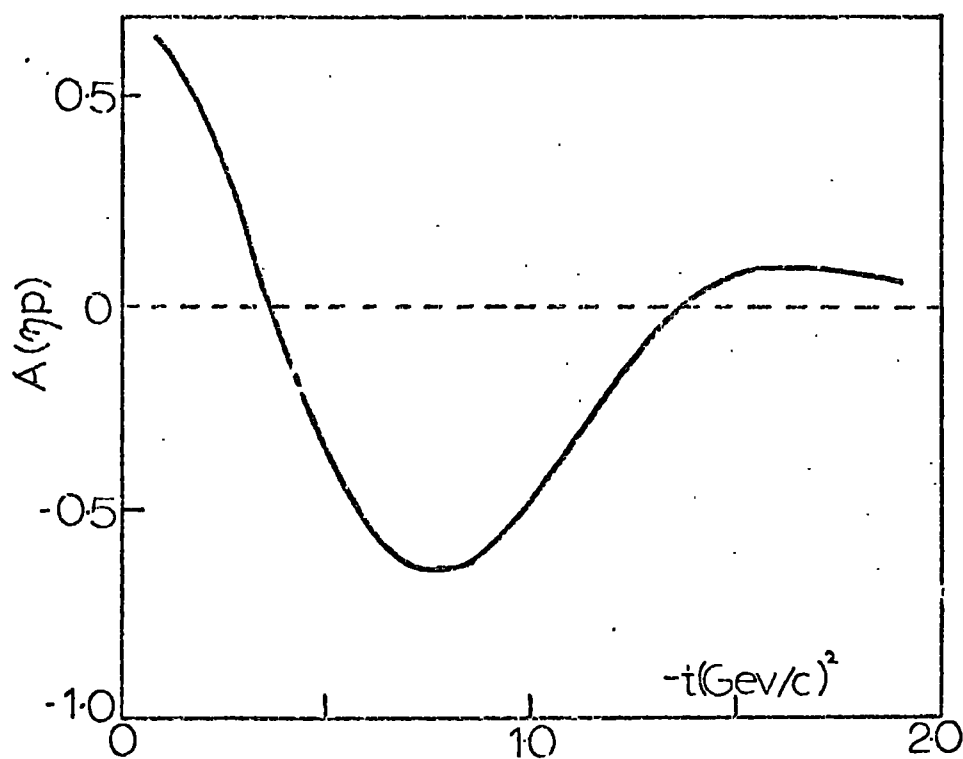
Fig 3.8 b
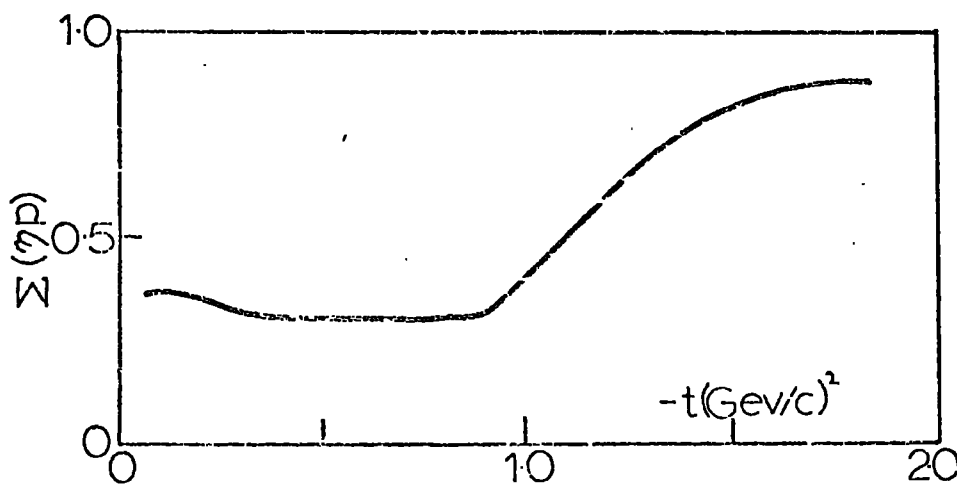
Fig 3.8 c
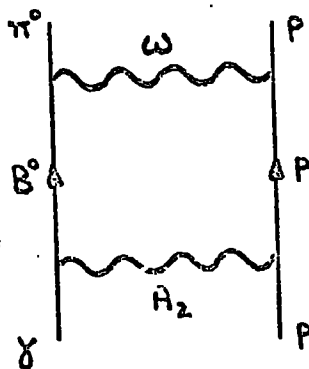
Fig 3·9

Fig 3·10

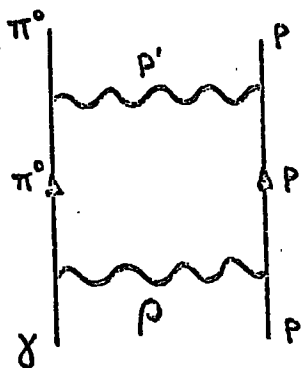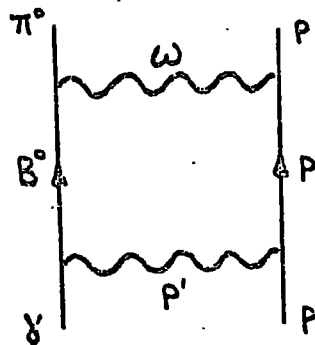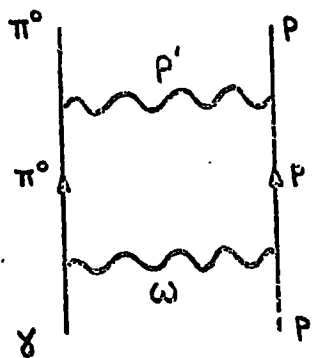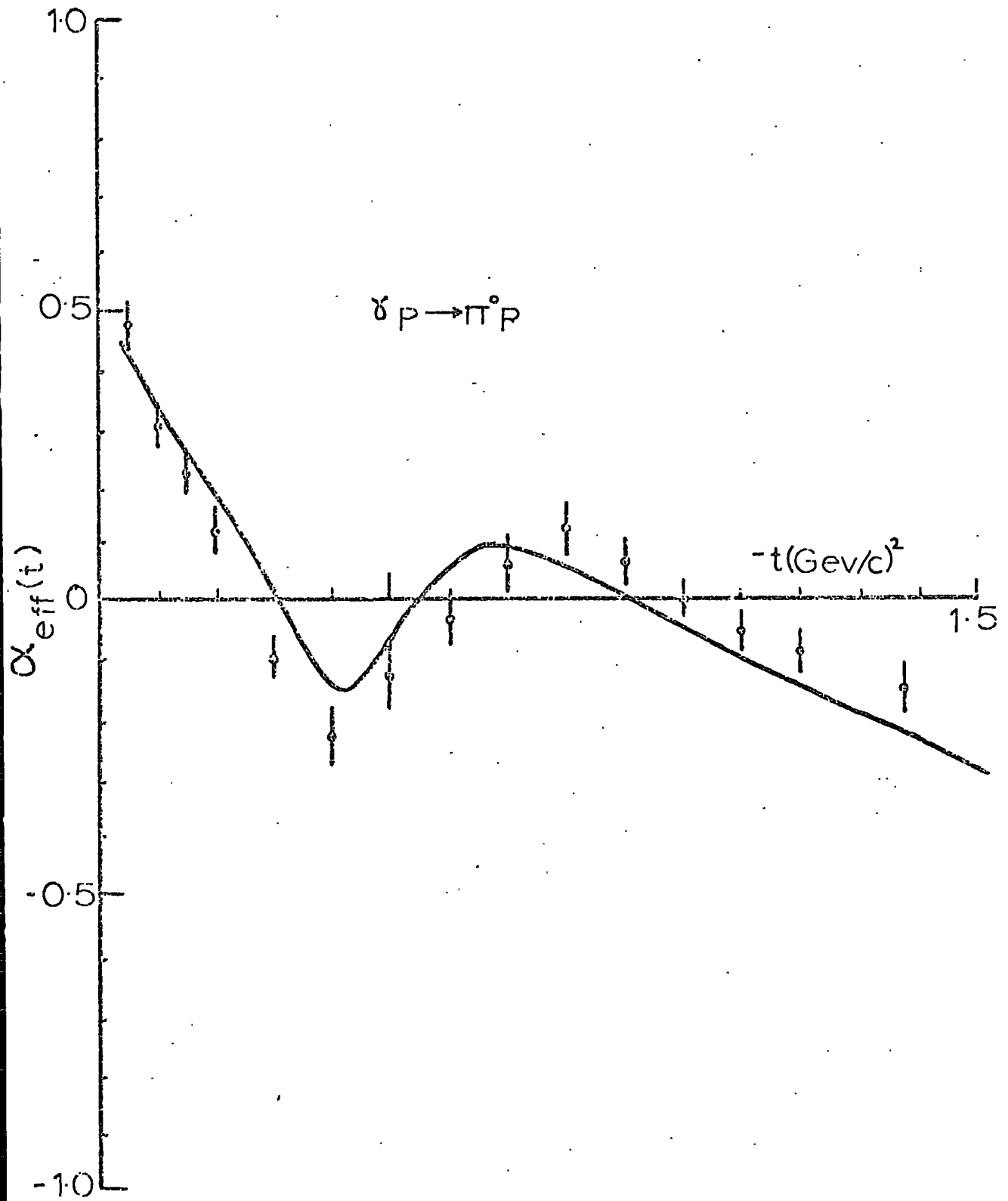CHAPTER   FOUR

4.1 INTRODUCTION

In chapter three we applied the eikonal formalism to the good, phase sensitive data which exists in π N CEX and neutral pion photoproduction. The model was able to describe the phases of the amplitudes very successfully (the one doubt being Re A_{+-} in the CEX reaction) over a limited energy range. However, as higher energy data has become available a serious inconsistency has emerged between the shrinkage predicted by the model at large $|t|$ and that which is present in the data (see figs.(2.1) and (2.2)). We clearly need a modification of the eikonal model in which the cut trajectory approximates to that of the pole over a finite range of s and t.

It is of course well known that the eikonal model satisfies full s-channel unitarity, and in section (3.1) we indicated how the usual Regge pole exchange, when suitably iterated, gives us the eikonal series. Thus the results of chapter three are consistent with unitarity in the direct channel. However, the complete theory must also satisfy unitarity in the crossed (t or u) channel. The importance of t-channel unitarity for Regge cuts is emphasised by the role they play in removing the difficulties presented by the Gribov-Pomeranchuk fixed pole at $J = -1$. Furthermore, Gribov et al[67] have shown how unitarity helps to fix the discontinuities across the Regge cuts in the t-channel partial wave amplitudes.

Several authors have discussed the effect of t-channel unitarity on the simple absorption model and one way of doing this is to use the K-matrix formalism. Typically the absorption model has

$$A(s,t) \sim \beta(t) \, s^{\alpha(t)} - \beta_c(t) \, \frac{s^{\alpha_c(t)}}{\ln s} \tag{4.1}$$

For simplicity we neglect the signature factor and assume that $\beta, \beta_c, \alpha, \alpha_c$ are real functions of t. The first term of (4.1) is the Regge pole and the second term is the (destructive) two particle cut with $\alpha_c(t)$ typically given by (1.23). To exhibit the J-plane structure of (4.1) we take the Mellin transform (partial wave projection) of this equation.

$$A(J,t) = \int_{s_0}^{\infty} ds \, s^{-J-1} \, A(s,t) \tag{4.2}$$

The inverse is

$$A(s,t) = \frac{1}{2\pi i} \int_{-i\infty+\gamma}^{i\infty+\gamma} dJ \, s^{J} \, A(J,t) \tag{4.3}$$

In (4.2), s_0 is the threshold for the amplitude $A(s,t)$ and in (4.3), γ is to the right of all the singularities in the J-plane.

The absorption model therefore gives

$$A(J,t) = \frac{\beta(t)}{(J-\alpha)} + \beta_c(t) \, \ln(J-\alpha_c) \tag{4.4}$$

Mukherji and Desai[68] impose t-channel unitarity by demanding that the full amplitude $\tilde{A}(J,t)$ satisfy

$$\tilde{A}(J,t) = \frac{A(J,t)}{1 - i\rho \, A(J,t)} \tag{4.5}$$

where

$$\rho = \left(\frac{t - 4m^2}{4m^2}\right)^{1/2}$$

By making suitable assumptions about the nature of the cut trajectory (they take a fixed cut corresponding to $\alpha_P' = 0$ in

(1.23)) and the relative strength of pole and cut, they find that uniterisation through the K-matrix formalism (4.5) has the following effects.

(i) It produces a pair of complex conjugate poles $\alpha_{\pm}(t) = \alpha_R \pm i\alpha_x$ which lie on the physical sheet for $t < 0$.

(ii) The discontinuity across the cut is sharply peaked around $J = \alpha_R$, and furthermore vanishes at the jip of the cut $J = \alpha_c$.

$$\text{Disc } \tilde{A}(J,t) \sim \pi \frac{\beta_c (J - \alpha_c)^2}{(J - \alpha_R)^2}$$

Compare this with the hard cut equation (4.4). (Note that for a fixed cut $\alpha_c = \alpha(0)$ for all t.)

This simple analysis indicates that t-channel unitarity could provide important modifications to the usual Regge cut parameterations such as (4.1). In particular, the peaking of the cut discontinuity at the position of the pole, may change the energy dependence of the cuts in precisely the way we require in order to describe the strong shrinkage observed in the data.

One model which satisfied full multiparticle t-channel unitarity is the Reggeon calculus developed by Gribov and others. In recent years this has been examined in great detail, particular attention being paid to the nature of the Pomeron and its couplings to itself, other Reggeons and the external particles. The calculus evolved from an earlier technique proposed by Gribov for calculating diagrams involving Reggeons in a similar way to Feynman graphs containing elementary particles.

4.2 GRIBOV'S REGGEON DIAGRAM TECHNIQUE[69,70]

To illustrate the methods which can be used to calculate arbitrarily complicated Reggeon digrams, we consider the case of the two Reggeon cut given by the diagram shown below.
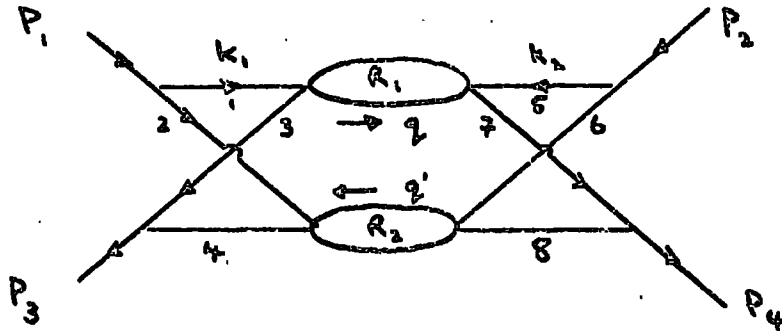
The Feynman rules give

$$A(s,t) = i \lambda^2 \int d^4q \, d^4k_1 \, d^4k_2 \; \frac{R_1(q,k_1,k_2) \, R_2(q',P_1-k_1,P_2-k_2)}{\prod_{m=1}^{8} d_m}$$

(4.6)

where the d's are propagators corresponding to the (eight) internal lines.

$$d_1 = k_1^2 - m^2 + i\varepsilon \qquad \text{etc.}$$

If R_1 and R_2 are taken to be the usual Regge pole amplitudes, then the complete diagram gives the two Reggeon cut. To evaluate the diagram, Gribov et al use the Sudakov technique of writing the internal momenta in terms of their components in the plane of p_1 and p_2 and those perpendicular to this plane. They then assume that the Regge amplitudes give important contributions when

(i) the energy variables $s_1 = (k_1 + k_2)^2$ and $s_2 = (p_1 + p_2 - k_1 - k_2)^2$ are large, and

(ii) the momentum transfers such as $(q - q')^2$ are small (i.e. $\ll s$).

After making the Sommerfeld-Watson transform, they obtain

$$F_{\mathbf{J}}(t) = \int \frac{d^2 q_\perp}{(2\pi)^2} \frac{\gamma(q^2, q'^2) N^2(t, q^2, q'^2)}{(J + 1 - \alpha(q^2) - \alpha(q'^2))} \qquad (4.7)$$
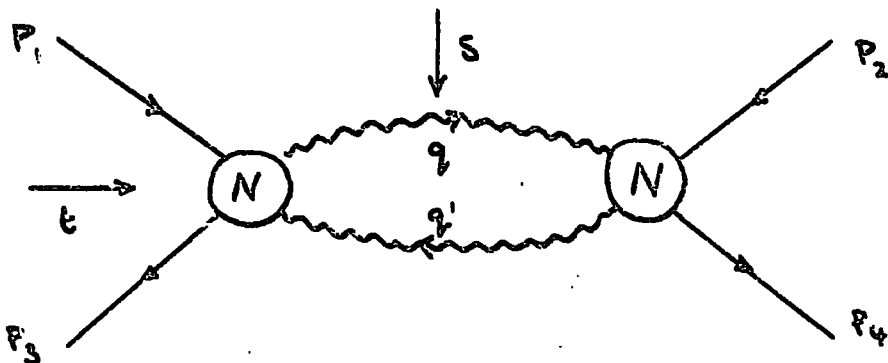
where

$$\Delta = q' - q \qquad \Delta^2 = t$$

$$\gamma(q^2, q'^2) = \frac{\cos\left[\frac{\pi}{2}(\alpha(q^2) + \alpha(q'^2))\right]}{\sin\left[\frac{\pi}{2}\alpha(q^2)\right] \sin\left[\frac{\pi}{2}\alpha(q'^2)\right]}$$

and $q_\perp$ is perpendicular to p_1 and p_2.

We can represent equation (4.7) by the diagram below.

N is then the residue of the fixed pole at $J = \alpha(q^2) + \alpha(q'^2) - 1$ in the Reggeon-particle scattering amplitude. It is essential that the Reggeon-particle couplings have the non planar structure in order that N has both left and right hand singularities. If there is no cross (i.e. only s or u singularities) then $N \rightarrow 0$ and the diagram does not give a cut.

The trajectory of the branch point obtained from this diagram (and also the n-Reggeon exchange diagram) agrees with the Mandelstam result (1.23). One consequence of this for multi-Pomeron exchanges is that provided $\alpha_P(0) = 0$, the Pomeron pole and its cuts accumulate at $t = 0$, $J = 1$. The same is true of a normal Regge pole and the cuts formed by the exchange of the Reggeon with n Pomerons, except that in this case the critical point is $t = 0$, $J = \alpha_R(0)$. It is therefore important to con-

sider, at least at small $|t|$, what effect the pole has on the branch points, and indeed what effect the branch points have on each other. Gribcv et al (69, 71) argue that because of this coincidence of pole and cuts at $t = 0$, the main contribution to a n-Reggeon production process comes from the "pole-enhanced graphs". For example

is dominated by

is dominated by

(a)   (b)
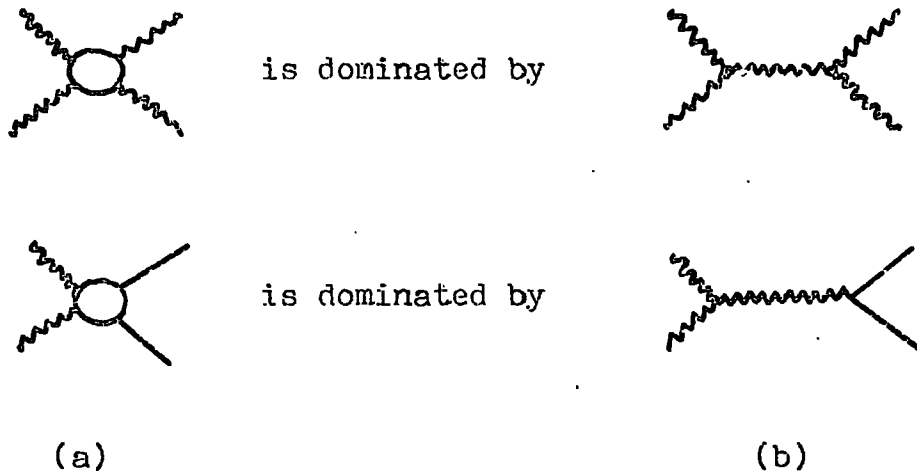
In this chapter we shall represent external particles by solid lines and Reggeons by wavy lines.

This means that to all graphs of the type (a), we expect that there exists one of the type (b) in which the bubble is replaced by the pole. We can therefore draw a pole-enhanced diagram for the two-Reggeon cut considered earlier.

$\longrightarrow$
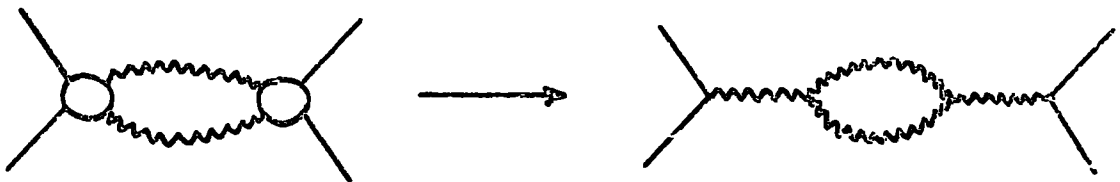
The approximation in which we consider only pole-enhanced graphc is then one in which we are neglecting cuts in the Reggeon-particle production amplitudes.

4.3 THE REGGEON CALCULUS

Most of the work on the Reggeon calculus has been motivated by an investigation into the nature of the Pomeron, and in particular into the structure of its couplings to itself and other particles. In recent years there have been several problems connected with the self-consistency of a moving Pomeron pole with intercept $\alpha_p(0) = 1$. S-channel unitarity has been used extensively to derive the so called "decoupling theorems" which require various Pomeron couplings to vanish (72). The most important of these is the vanishing of the triple pomeron coupling $\Gamma(t, t_1, t_2)$ when the Pomeron legs are at zero momentum transfer.

$$\Gamma(0, 0, 0) = 0$$

One way of obtaining this result is to consider the inclusive process

$$a + b \longrightarrow c + \times$$

in the triple Regge region $s \to \infty$, $s/m^2 \to \infty$, $m^2 \to \infty$. If we use the generalised optical theorem, the leading contribution to the total cross section is provided by the diagram
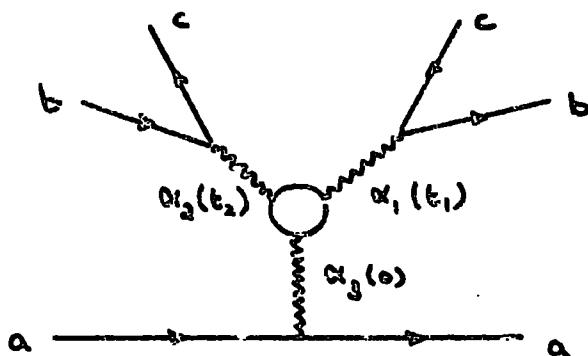
If b has vacuum quantum numbers the graph is controlled by the triple pomeron vertex $\Gamma(0, t_1, t_2)$. When integrated over the

appropriate region of phase space, the result violates the Froissart bound unless either $\alpha_p(0) < 1$ or $\Gamma(0, 0, 0) = 0$. Thus if we wish to preserve the Pomeron intercept at unity, the triple Pomeron coupling must vanish. We shall see that this zero also has a t-channel origin in the Reggeon calculus.

The Reggeon calculus [73] starts with the assumption which is open to question, that the Pomeron is a pole with intercept one. It is treated as a non-relativistic particle having momentum $\underline{k}$ and energy $w = j-1$. The bare propagator is then

$$D_0(w, \underline{k}) = (w + \underline{k}^2)^{-1} \tag{4.8}$$

so that

$$\underline{k}^2 = - t \tag{4.9}$$

Here we assume for simplicity that $\underline{k}^2$ is scaled so that the Pomeron trajectory is

$$\alpha_p(t) = 1 + t$$

The bare triple Pomeron vertex is "ir" and all vertices are assumed to be analytic in w. The general interaction can then be written as a perturbation series expansion in terms of a Reggeon field operator ψ.

$$H_{int} = ir\left[\psi^\dagger \psi^\dagger \psi + \psi \psi \psi^\dagger\right] + \Lambda \psi^\dagger \psi^\dagger \psi \psi + \Lambda_1 \left[\psi^\dagger \psi^\dagger \psi^\dagger \psi + \psi \psi \psi \psi^\dagger\right] + \cdots$$

The renormalised propagator is

$$D(w, \underline{k}) = (w + \underline{k}^2 - \sum\nolimits_c(w, \underline{k}^2))^{-1} \tag{4.10}$$

where $$\sum\nolimits_c(w, \underline{k}) = \sum(w, \underline{k}) - \sum(0,0) \tag{4.11}$$

Equation (4.11) ensures that (4.10), which is the Dyson equation for D, gives the Pomeron pole at $w = 0$, $\underline{k} = 0$.

Gribov and Migdal discuss the "weak coupling solution" to the calculus, in which D differs only slightly from its bare value D_0. That is

$$\sum_c (w, \underline{k}) \ll w + \underline{k}^2 \qquad \text{for} \qquad w \sim \underline{k}^2 \to 0 \qquad (4.12)$$

In this limit they show that the unitarity relation which defines $\sum_c$, reduces to a series expansion in the vertex function Γ_n for the transition of one Reggeon into n Reggeons.

This series only converges provided the triple Pomeron vertex coupling Γ_2 satisfies

$$(\Gamma_2)^2 \ll w \qquad\qquad w \sim \underline{k}^2 \to 0$$

and Gribov and Migdal argue that this constraint on Γ_2 is a result of the instability of the Pomeron — that at $t = 0$ it can decay into an arbitrary number of Pomerons. They propose the general form

$$\Gamma_2(w, \underline{k}; \sigma, \underline{q}) = a w + b \underline{k}^2 + c \underline{q}^2 + \ldots \ldots \qquad (4.13)$$

So the Pomeron is said to be quasistable at $w = \underline{k}^2 = 0$.

Equation (4.13) describes the general triple Pomeron vertex shown below.
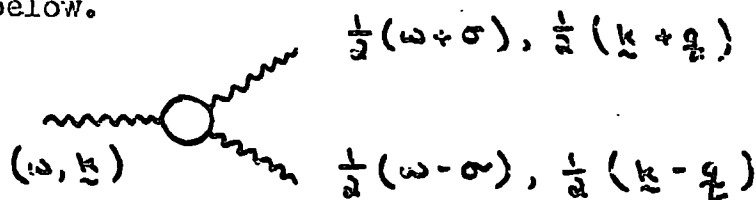
We shall call this the "Gribov vertex" at which the energy, w, is conserved. The inclusive vertex has the extra constraints $w = \underline{k}^2$

and $\sigma = \underline{k}.\underline{q}$ (which ensures that all the Reggeons lie on the appropriate spin shell). Thus

$$\left[\Gamma_a(\omega,\underline{k};\sigma,\underline{q})\right]_{\substack{\omega=\underline{k}^2\\ \sigma=\underline{k}\cdot\underline{q}}} = g_{PPP}\left(\underline{k}^2,(\tfrac{1}{2}(\underline{k}+\underline{q}))^2,(\tfrac{1}{2}(\underline{k}-\underline{q}))^2\right) \quad (4.14)$$
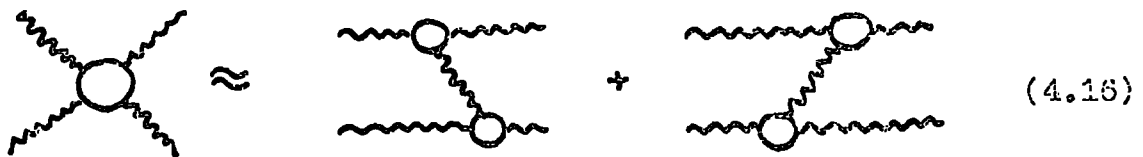
It follows that the inclusive and Gribov vertices coincide at $\underline{k} = \underline{q} = 0$, where in fact they both vanish.

In the Reggeon calculus the triple Pomeron vertex (and all the other relevant amplitudes) satisfies an integral equation which we show in diagrammatic form below. The explicit form of this equation is given in refs.(70) and (74).

$$(4.15)$$

Cardy and White[74] have examined the structure of this equation in which the Kernal contains terms such as

$$(4.16)$$

The presence of the full triple Pomeron vertex in (4.16) means that all the potentially singular contributions to K are softened and so cannot individually be responsible for the vanishing of Γ_2 (4.15). One point of view (first proposed by Gribov et al) is that the zero appears in the full equation (4.15) as a result of cancellations amongst the various terms in the iteration of K. This is only feasible if the terms alternate in sign and is therefore related to the sign of the two Pomeron cut.

The two Pomeron production amplitude and also the

Pomeron-Pomeron scattering amplitude, satisfy similar equations involving K. This suggests that they too have zeros of the same form as Γ_2. For example

$$\tag{4.17}$$

Now, by the process of enhancement discussed earlier, we might expect that the full two Pomeron production amplitude near $t = 0$, $J = 1$, will be dominated by the Pomeron pole.

$$\tag{4.18}$$

So that

$$A_{pole}(w, \underline{k} ; \sigma, \underline{q}) \approx \Gamma_2(w, \underline{k} ; \sigma, \underline{q}) \frac{1}{(w + \underline{k}^2)} B(\underline{k}^2) \tag{4.19}$$

Where A_{pole} is the pole enhanced part of the full amplitude and $B(\underline{k}^2)$ is the usual residue function. Consequently, we expect the leading contribution to the two Pomeron cut (near $t = 0$) to be given by the completely enhanced graph.

$$\tag{4.20}$$

The crosses on the internal lines indicate that these Reggeons satisfy the mass shell constraint.

Gribov et al have written down the general form of the partial wave amplitude. They find[67]

$$\equiv F(J,t) = \frac{A(J,t)}{B(J,t) - \ln(J - \alpha_c(t))} \qquad (4.21)$$

$$\equiv \frac{A(J,t)}{D(J,t)}$$

where A and B are real functions close to $J = \alpha_c(t)$, and $\alpha_c(t)$ is the usual two Pomeron branch point with $\alpha_p(0) = 1$. Now since the pole and cut collide at $t = 0$, $J = 1$, we expect that the Pomeron pole will appear in the partial wave amplitude. It can also be shown that the two Pomeron production amplitude and the Pomeron-Pomeron scattering amplitude take the form

$$\sim \frac{A^{\frac{1}{2}}}{D} \qquad (4.22)$$
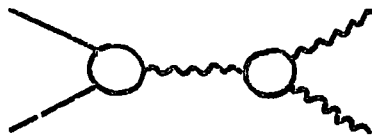
$$\sim \frac{1}{D} \qquad (4.23)$$

If the Pomeron pole in (4.21) were to appear as a pole in A then (4.22) would have a square root branch point, thus violating the Mandelstam representation. It is therefore usually assumed that the pole is generated by a zero in D.

$$D(\alpha(t), t) = 0 \qquad (4.24)$$

Bronzan[75] has shown that in order that the two Pomeron cut contribute to the total cross section with opposite sign to the pole (in agreement with the Mandelstam result and experiment), then $B(J,t)$ must be singular at $t = 0$, $J = 1$. The simplest solution to (4.24) which also satisfies this constraint is that both A and B share a double pole Z_0^{-2} which passes through $J = 1$
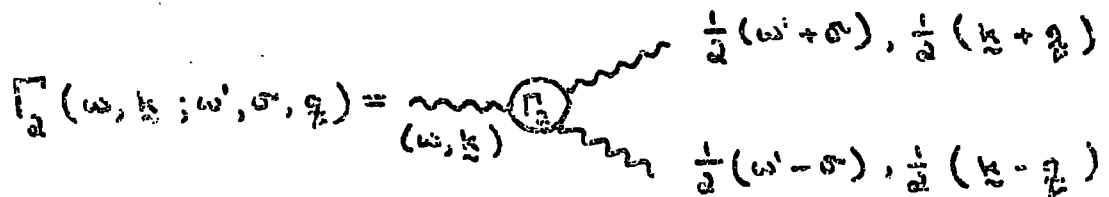
at $t = 0$. From (4.22), the contribution from the pole enhanced graph will be

$$\sim \quad \frac{g\, Z_0}{(J - \alpha)} \qquad (4.25)$$

where g is the coupling of the Pomeron to the external particles. Finally, the residue of the Pomeron pole in (4.23) has a double zero, which is consistent with the triple Pomeron coupling posessing a first order zero.

Cardy[76] has generalised this formalism to include the triple Pomeron inclusive vertex.

The relationship between it and the energy conserving Gribov vertex (Γ_G') is

$$\Gamma_G' \equiv \Gamma_a' (\omega, k ; \omega, \sigma q)$$

The inclusive vertex Γ_{inc}, may have $w \neq w'$ (i.e. the α's not all the same), but is evaluated at $w = 0$, $\underline{k} = 0$. In both cases the final state Pomerons must satisfy the mass shell condition.

$$w + \alpha' \underline{k}^2 = 0$$

where we have now included the Pomeron trajectory slope explicitly. For the final state Pomerons this becomes

$$\tfrac{1}{2} (w' \pm \sigma) + \frac{\alpha'}{4} (\underline{k}^2 + \underline{q}^2 \pm 2\, \underline{k}\cdot\underline{q}) = 0 \qquad (4.26)$$

Therefore

$$w' + \frac{\alpha'}{2} (\underline{k}^2 + \underline{q}^2) = 0 \qquad (4.27)$$

$$\sigma + \alpha' \, \underline{k}\cdot\underline{q} = 0$$

By studying the behaviour of the kernal K in (4.15),
Cardy concludes that the triple Pomeron vertex must vanish for
small q^2 like

$$\Gamma(\omega, \underline{k}; \omega', \sigma', \underline{q}) \sim -\tfrac{1}{2} a \underline{q}^2 + b(\omega - \omega') + O(\sigma^2, (\underline{q}^2)^2) \qquad (4.28)$$

Thus, setting $w = w'$ and using (4.27), the energy conserving
Gribov vertex has the behaviour

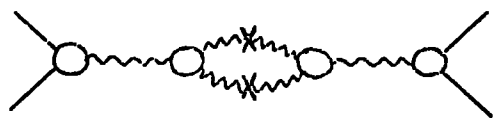$$\Gamma_G \sim a (w + \tfrac{\alpha'}{2} \underline{k}^2) \qquad (4.29)$$

Which means that

$$\Gamma_G \sim a (J - \alpha_c(t)) \qquad (4.30)$$

where $\alpha_c(t)$ is the trajectory of the two Pomeron cut. The function
Z_o which produces the zero in the triple Pomeron vertex is
therefore a moving zero, having the same trajectory as the two
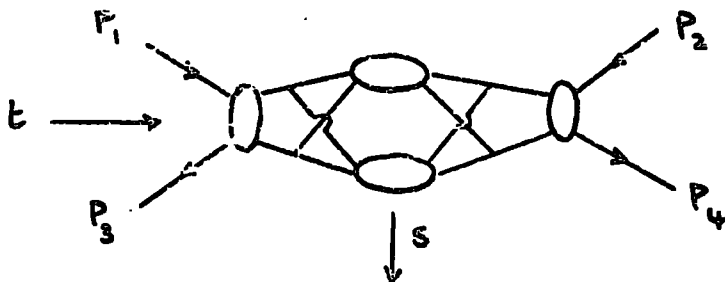Pomeron cut.

$$Z_o \sim \lambda (J - \alpha_c(t)) \qquad (4.31)$$

So when we include enhancement, the leading contribution
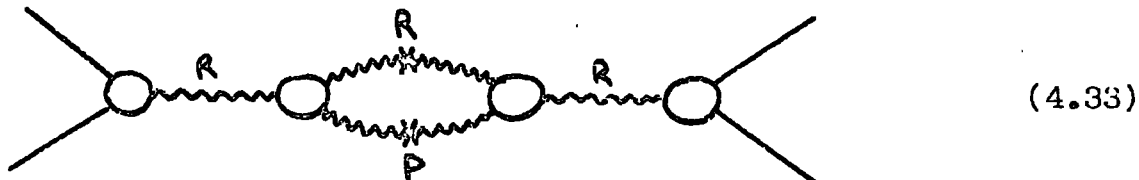to the two Pomeron cut has the behaviour

$$ (4.32)$$

$$\sim (J - \alpha_c(t))^2 (J - \alpha(t))^{-2} \ln(J - \alpha_c(t))$$

Note that if we exhibit the structure which is present in the
Gribov vertices in the diagram of (4.32), we obtian the diagram
below.

We can extend the analysis outlined above to include the case where we have non vacuum quantum numbers exchanged in the t-channel. If we consider the diagram

(4.33)

(where R represents a Reggeon having $\alpha_R(t) = \alpha_R(0) + \alpha_R' t$), then (4.32) again gives the leading contribution to the R ⊠ P cut even when the trajectories have different slopes[76]. In this case the mass shell condition is

$$w + \alpha_R' \underline{k}^2 = \alpha_R(0) - 1$$

The Reggeon calculus therefore, provides us with a representation (4.32) of the Reggeon-Pomeron cut discontinuity which vanishes at the tip of the cut and is strongly peaked about the Regge pole position. The derivation of (4.32) relies heavily on the vanishing of the triple Pomeron coupling (which in turn is a consequence of demanding $\alpha_P(0) = 1$) and indeed on the vanishing of the Regge-Regge-Pomeron coupling, at zero momentum transfer. It is possible to estimate the size of these couplings directly from the inclusive data[77] and unfortunately for the Reggeon calculus they do not appear to vanish in the required limit. However, neither does the Pomeron intercept seem to be exactly at one but slightly above[11].

Nevertheless, given that enhancement occurs we would still naively expect (4.33) to have the form

$$F(J,t) \sim f(J,t) (J - \alpha_R(t))^{-2} \ln(J - \alpha_c(t))$$

(4.34)

The Bronzan and Jones analysis[15] into the effect of t-channel

unitarity further suggests that

$$f(\alpha_c(t), t) = 0$$

i.e. We have a soft cut. Hence (4.32) may still be a reasonable parameterisation even though its exact derivation is suspect.

In the next chapter we shall investigate the consequences of this type of parameterisation for Regge cut phenomenology. In particular, we shall use (4.32) as the basis for an explicit model of the Regge-Pomeron cut which we shall apply to π N CEX and neutral pion photoproduction.

CHAPTER FIVE

5.1 PARAMETERIZATION OF THE REGGE-POMERON CUTS

In Chapter two, we assembled a great deal of evidence to support the view that all hadronic two-body scattering amplitudes show strong Regge pole like shrinkage out to large values of $|t|$, at least $|t| < 2.0$ (Gev/c)^2. (We shall return to the problem of photo-induced processes which appear not to shrink, later in this chapter.) Furthermore, we have shown how the absorptive/eikonal model can be made consistent with the amplitude analysis by the inclusion of lower lying contributions - namely R ⊗ P' cuts. However, the one characteristic feature of the eikonal model - the energy dependence of the cuts which it generates - is in severe conflict with the results of Chapter two. The problem therefore, is how to modify the energy dependence of the cuts to produce strong shrinkage at large $|t|$.

We have indicated in the previous chapter how t-channel unitarity, by softening the nature of the cut discontinuity and causing it to peak around the position of the pole, can produce precisely this effect. Equation (4.32) is a parameterization of the cut discontinuity which is zero at the tip of the branch cut $J = \alpha_c(t)$, and also includes a double pole $(J - \alpha_R(t))^{-2}$. When this is inserted into the Sommerfield-Watson transform, the peaking of the integrand near $J = \alpha_R(t)$ should ensure that the cut behaves like $s^{\alpha_R(t)}$ over a finite range of s and t. Of course as $s \rightarrow \infty$ we shall begin to see the contribution from $J \approx \alpha_c(t)$. We therefore expect that the effective trajectories of Chapter two should begin to show some deviation from linearity as this term becomes important. We shall indicate just when this effect should become observable on the basis of our fit to $\pi^- p \rightarrow \pi^0 n$ (section 5.2).

To evaluate the contribution of a Regge-Pomeron cut to the

scattering amplitude, we insert the form of the discontinuity (4.32) into the Sommerfeld-watson transform. For the particular case of an odd signature Regge pole, this gives

$$
A^{RP}(s,t) = \frac{1}{2\pi i} \int_{-i\infty+\gamma}^{i\infty+\gamma} G(t) \left(i \, e^{-i\pi J/a} \right) e^{aJ} s^J \left(\frac{J-\alpha_c}{J-\alpha_R} \right)^2 \ln(J-\alpha_c) \quad (5.1)
$$

$$
\equiv i \, G(t) \, F(s,t) \quad (5.2)
$$

where $\alpha_c(t)$ is the branch point as given by the usual Mandelstam formula, $\alpha_R(t)$ is the Regge pole trajectory and $G(t)$ is an arbitrary residue function. We have also included in (5.1) an exponential cut-off in the discontinuity function (e^{aJ}). By analogy to chapter three we now define
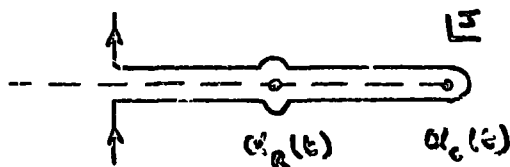
$$
c = a + \ln(s) - i\pi/2 \quad (5.3)
$$

we can then write

$$
F(s,t) = \frac{1}{2\pi i} \int_{-i\infty+\gamma}^{i\infty+\gamma} e^{cJ} \left(\frac{J-\alpha_c}{J-\alpha_R} \right)^2 \ln(J-\alpha_c) \, dJ \quad (5.4)
$$

$$
\equiv D(s,t) - P(s,t) \quad (5.5)
$$

In (5.5) we have divided the integral into two parts — the contribution from the dipole at $J = \alpha_R$ and the principal value integral. The integration contour is shown below.

(a) <u>Dipole</u>

$$D(s,t) = \frac{d}{dJ}\left[e^{cJ}(J-\alpha_c)^2 \ln(J-\alpha_c)\right]_{J=\alpha_R}$$

$$= e^{c\alpha_R}(\alpha_R-\alpha_c)\left[1 + \ln|\alpha_R-\alpha_c|\left(c(\alpha_R-\alpha_c)+2\right)\right] \quad (5.6)$$

(b) <u>Principal value integral</u>

$$P(s,t) = \int_{-\infty}^{\alpha_c} e^{cJ}(J-\alpha_c)^2(J-\alpha_R)^{-2}\, dJ \quad (5.7)$$

If we make the change of variable

$$x = (\alpha_c - J)\ln(s) \quad (5.8)$$

then (5.7) becomes

$$P(s,t) = \frac{e^{c\alpha_c}}{\ln(s)}\int_0^\infty \frac{x^2 e^{-\frac{cx}{\ln(s)}}}{\left[x+(\alpha_R-\alpha_c)\ln(s)\right]^2}\, dx \quad (5.9)$$

Now

$$\frac{d}{dx}\left[\frac{e^{-cx/\ln s}}{(x+\beta)}\right] = -\frac{c}{\ln s}\frac{e^{-cx/\ln s}}{(x+\beta)} - \frac{e^{-cx/\ln s}}{(x+\beta)^2}$$

Therefore, we can write (5.9) as

$$P(s,t) = -\frac{c e^{c\alpha_c}}{(\ln s)^2}\int_0^\infty \frac{x^2 e^{-cx/\ln s}}{\left[x+(\alpha_R-\alpha_c)\ln s\right]}\, dx \quad (5.10)$$

$$-\frac{e^{c\alpha_c}}{\ln s}\int_0^\infty x^2 \frac{d}{dx}\left\{\frac{e^{-cx/\ln s}}{\left[x+(\alpha_R-\alpha_c)\ln s\right]}\right\}$$

$$= \frac{-c e^{c\alpha_c}}{(\ln s)^2}\int_0^\infty \frac{x\, e^{-cx/\ln s}}{\left[x+(\alpha_R-\alpha_c)\ln s\right]}\, dx$$

$$(5.11)$$

$$+\frac{e^{c\alpha_c}}{\ln s}\int_0^\infty \frac{2x\, e^{-cx/\ln s}}{\left[x+(\alpha_R-\alpha_c)\ln s\right]}\, dx$$

where we have integrated by parts the second term of (5.10).
The integrals in (5.11) may be evaluated in terms of the exponential integral function $Ei(x)$[78] to give

$$P(s,t) = -\frac{c e^{c\alpha_c}}{(\ln s)^2}\left[-\beta^2 e^{c\beta/\ln s}\, Ei\left(-\frac{c\beta}{\ln s}\right) + \left(\frac{\ln s}{c}\right)^2\right.$$

$$\left. -\frac{\beta \ln s}{c}\right] + \frac{2 e^{c\alpha_c}}{\ln s}\left[\beta e^{c\beta/\ln s}\, Ei\left(-\frac{c\beta}{\ln s}\right) + \frac{\ln s}{c}\right] \tag{5.12}$$

where

$$\beta = (\alpha_R - \alpha_c)\ln(s) \tag{5.13}$$

If we use the expansion[78]

$$Ei(x) = \gamma + \ln|x| + \sum_{n=1}^{\infty}\frac{x^n}{n\,n!} \tag{5.14}$$

($\gamma = 0.5772$ is Euler's constant), we can simplify (5.12)

$$P(s,t) = e^{c\alpha_R}(\alpha_R - \alpha_c)(2 + (\alpha_R - \alpha_c)c)\left[\gamma + \ln c + \ln|\alpha_R - \alpha_c|\right]$$

$$+ e^{c\alpha_R}(\alpha_R - \alpha_c)(2 + (\alpha_R - \alpha_c)c)\left[\sum_{n=1}^{\infty}\frac{[(\alpha_c - \alpha_R)c]^n}{n\,n!}\right] \tag{5.15}$$

$$+ e^{c\alpha_c}\left(\frac{1}{c} + (\alpha_R - \alpha_c)\right)$$

Finally, by combining (5.6) and (5.15) we obtain

$$F(s,t) = e^{c\alpha_R}(\alpha_R - \alpha_c)$$

$$- e^{c\alpha_R}(\alpha_R - \alpha_c)(2 + (\alpha_R - \alpha_c)c)\left[\gamma + \ln c\right] \tag{5.16}$$

$$- e^{c\alpha_R}(\alpha_R - \alpha_c)(2 + (\alpha_R - \alpha_c)c)\left[\sum_{n=1}^{\infty}\frac{[(\alpha_c - \alpha_R)c]^n}{n\,n!}\right]$$

$$- e^{c\alpha_c}\left(\frac{1}{c} + (\alpha_R - \alpha_c)\right)$$

5.2 A REGGE CUT MODEL FOR $\pi^- p \to \pi^0 n$.

For the odd signature rho pole contribution to the two independent s-channel helicity amplitudes, we write

$$A_N^\rho (s,t) = i \left(\tfrac{s}{s_0} e^{-i\pi/2} \right)^{\alpha(0)} (-t)^{N/2} \alpha_\rho(t) \, G_N \, e^{c_N t} \tag{5.17}$$

Where, as usual

$$c_N = a_N + \alpha_\rho' (\ln(s/s_0) - i\pi/2) \tag{5.18}$$

$$\alpha_\rho(t) = \alpha_\rho(0) + \alpha_\rho' t$$

and we label the amplitudes by $N \; (= 0,1)$, the net s-channel helicity flip.

The presence of $\alpha_\rho(t)$ in both the flip and non flip amplitudes means that the rho chooses nonsense. We did in fact try a model in which $\alpha_\rho(t)$ appeared in only the flip amplitude (sense choosing). However, in order to obtain a good description of the large $|t|$ differential cross section we had to add extra exponentials to the pole residues. A better description of the data is obtained with (5.17), which has just a single exponential plus the nonsense factors (and fewer variable parameters).

Before we write down the cut amplitudes we recall from chapter two that the amplitude analysis strongly suggest that the flip amplitude in πN CEX is well described by a simple (nonsense choosing) rho pole, i.e. the cuts are small in this amplitude. We therefore include cuts only in the non flip amplitude and in the notation of chapter three we write for the $\rho \otimes P$ cut

$$A_{+-}^{\rho P} (s,t) = i \left(\tfrac{s}{s_0} e^{-i\pi/2} \right)^{\alpha_\rho(0)} G_\infty \times \tag{5.19}$$

$$\times \left\{ (-G_P) \, F_{c_\rho}(s,t) \, (1 + bt) \right\}$$

Where $F_{c_p}(s,t)$ is the function defined in (5.16) with

$$c \longrightarrow c_p = \frac{a_o a_p}{a_o + a_p} + \ln s - \frac{i\pi}{2} \qquad (5.20)$$

a_p is related to the slope of the Pomeron contribution to the forward πN cross section and a_o is the exponent which appears in the residue of the non flip pole (N = 0) through (5.18). We adopt (5.20) so that the exponential $|t|$ dependence of the cut is related to that of the pole in a similar way to the eikonal model. Since our model is basically concerned with the energy dependence of the cut and says little about the $|t|$ dependence, we have also included the factor (1 + bt) in (5.19) to allow for the presence of $\alpha_\rho(t)$ in the pole.

We require that the model describe the following features of the πN CEX data:-[79]

(i) The 6.0 Gev/c amplitude analysis.

(ii) The differential cross section data for the energy range $5 \leqslant P_{lab} \leqslant 50$ Gev/c.

(iii) The available polarization data.

(iv) The data on $\Delta\sigma = \sigma(\pi^-) - \sigma(\pi^+)$ which has recently become available up to $P_{lab} = 200$ Gev/c from NAL.

(v) The final piece of "data" is the $\alpha_{eff}(t)$ of fig.(2.1) which we do not fit, but nevertheless we regard it as extremely important that our model reproduce this data.

As our first attempt to fit the data we therefore had a simple ρ pole plus $\rho \boxtimes P$ cut model given by equations (5.17) and (5.19). However we encountered precisely the same problem as in the naive absorption model, namely the similarity in phase of pole and cut at small $|t|$. Thus demanding $\text{Im} A_{++} = 0$ at $t \sim -0.2$

$(\text{Gev/c})^2$ (the crossover zero) we also have an unwanted zero in Re A_{++} at approximately the same value of t. With our freely parameterised cut there are two possible courses of action.

(i) We could take the view that the phase of the $\rho \boxtimes P$ cut at 6.0 Gev/c is not the asymptotic phase. Looking at (5.16), the dominant contribution at small $|t|$ comes from the term e^{cu_c}/c , where c is given by (5.20). If we allow a_p to search over negative values we find that we can obtain an excellent fit to the 6.0 Gev/c amplitudes. However the parameters are such that

$$ C_p = \frac{a_o a_p}{a_o + a_p} + \ln S - \frac{i\pi}{2} \approx -\frac{i\pi}{2} $$

and we are essentially multiplying the small $|t|$ part of the cut by a factor "i". The energy dependence of the fit is now completely incompatible with the Serpukhov data. In fact the model α_{eff} is approximately linear for $|t| > 0.4$ $(\text{Gev/c})^2$, but curves over at small $|t|$ until $\alpha(0) \sim 0.25$. For this reason we reject this possibility.

(ii) The most sensible solution to the problem, remembering the arguments presented in chapters two and three, is to again add Regge-Regge cuts – in particular the $\rho \boxtimes P'$ cut. If we do this we should first remember that the cut trajectory will be given by

$$ \alpha_{\rho P'}(t) = \alpha_{\rho}(o) + \alpha_{P'}(o) - 1 + \frac{\alpha'_{\rho} \alpha'_{P'}}{\alpha'_{\rho} + \alpha'_{P'}} t \tag{5.21} $$

$$ \equiv \alpha_{\rho P'}(o) + \alpha'_{\rho P'} t \tag{5.22} $$

So that in this case the pole and cut do not coincide at $t = 0$.

Hence there is no reason to suppose that the pole "enhancement" of chapter four will occur. (Alternatively, the integration from $-\infty$ to $\alpha_c(t)$ which appears in the Sommerfeld-Watson transform does not include the pole at $J = \alpha_R(t)$.) We therefore expect that the discontinuity across the $\wp \boxtimes P'$ cut will take the form

$$\Delta_{PP'}(J,t) \sim \left(J - \alpha_c(t)\right)^n$$

Which gives a contribution to the amplitude

$$A^{\wp P'}(s,t) \sim \frac{s^{\alpha_c(t)}}{(\ln s)^{n+1}}$$

For simplicity we take $n = 0$, and we therefore have a normal absorption/eikonal model parameterisation for the $\wp \boxtimes P'$ cut.

$$A^{\wp P'}_{++}(s,t) = i \left(s/s_0 \, e^{-i\pi/2}\right)^{\alpha_\wp(0)} G_{++}$$

$$\left\{ G_{P'} \left(s/s_0 \, e^{-i\pi/2}\right)^{\alpha_{\wp P'}(0)} \frac{e^{c_{P'} \alpha'_{\wp P'} t}}{c_{P'}} (1+bt) \right\} \tag{5.23}$$

$$c_{P'} = \frac{a_\wp a_{P'}}{a_\wp + a_{P'}} + \ln s - \frac{i\pi}{2} \tag{5.24}$$

The full helicity amplitudes are

$$A_{++}(s,t) = A^\wp_{++}(s,t) + A^{\wp P}_{++}(s,t) + A^{\wp P'}_{++}(s,t) \tag{5.25}$$

$$A_{+-}(s,t) = A^\wp_{+-}(s,t) \tag{5.26}$$

where the various terms are defined in equations (5.17),(5.19) and (5.23). As we have already mentioned, the best description of the

secondary maximum in the CEX differential cross section near $t \sim -0.8$ (Gev/c)^2 is obtained using a nonsense choosing rho pole coupling. Collins and Swetman[27] found that the use of the A' and B invariant amplitudes improved the quality of their fit in this region. However, in our case such a description is of little practical value because of the extra parameters we would have to generate the cuts.

The final values of the parameters are shown in table (5.1). Because of the rather arbitrary t dependence of the cuts, we are unable to compare most of these parameters with those of the eikonal model fit described in Chapter three. However, the flip/non flip ratio of the rho couplings is in general agreement with all other estimates, as also are the trajectory parameters for the various exchanges. In particular $\alpha_p' \approx 0.28$ is consistent with the value obtained from the small t shrinkage of the pp differential cross section over the ISR range. [11]

In fig.(5.1) we plot the helicity amplitudes at 6.0 Gev/c. These are obviously in excellent agreement with the amplitude analysis – the cuts having modified the non flip amplitude to produce both the crossover zero and the approximate double zero in Re A_{++}. The fit to the differential cross section data is shown in fig.(5.2) where we have shown a selection of the available low energy data ($P_{lab} \leqslant 18$ Gev/c) along with the data from Serpukhov ($21 \leqslant P_{lab} \leqslant 50$ Gev/c). The shrinkage present in the data is clearly reproduced by the fit. The intercept $\alpha'(0)$ is fixed by the fit to $\Delta\sigma$ (fig.(5.4)), with the full model α_{eff} in fig.(5.3). The recent NAL data at 50, 100, 150 and 200 Gev/c has cast doubt on the overall normalisation of the Serpukhov data and in the fit to $\Delta\sigma$ we have used only the low energy plus NAL data. Finally we

show our fit to the available polarization data in fig.(5.5).
It is clearly consistent with the more recent data of Hill et al,
giving a polarization $\sim 20\%$ for $|t| \leqslant 0.5$ (Gev/c)^2, in contrast
to the CERN measurement of $\sim 60\%$ in this region. An interesting
prediction (which can just be observed in fig.(5.5d)), is the
appearance of a substantial negative polarization in the range
$1.0 \leqslant |t| \leqslant 2.0$ (Gev/c)^2 as we go to higher energies.

The only data which we have not included in our fit is
the wide angle CEX data from which Barger and Phillips extracted
$\alpha_{eff}(t)$ for $|t| \leqslant 5.0$ (Gev/c)^2. However, in fig.(5.6) we plot
$\alpha_{eff}(t)$ at large $|t|$ calculated from the model for three diff-
erent energy ranges. Below 5.0 Gev/c (which is the range analysed
by Barger and Phillips), the shrinkage in our model is consistent
with the "data" (fig.(2.3)) for $|t| \leqslant 3.0$ (Gev/c)^2, which is well
beyond the range over which we might reasonably expect Regge theory
to apply at such low energies, as we explained in chapter two.
Fig.(5.6) also predicts that we shall observe some deviation of
α_{eff} from (approximate) linearity as large $|t|$ data becomes
available at Serpukhov or NAL.

A further appealing property of the model is the way in
which it extrapolates down to low energy. In chapter two we
discussed how the lower lying contributions present in the new
absorption models to give the correct phase structure at 6.0 Gev/c,
are so strong that they overwhelm the pole at low energy, moving
the crossover zero in towards $t = 0$. If we look at the non flip
amplitude in our fit at 2.0 Gev/c, we find that the crossover zero
has moved in, but only to $t \sim -0.14$ (Gev/c)^2 compared with its
position of $t \sim -0.2$ (Gev/c)^2 at $P_{lab} = 6.0$ Gev/c. We should
contrast this with the eikonal model fit of Collins and Swetman

in which the crossover zero has moved to $t \sim -0.7$ (Gev/c)^2 at 2.0 Gev/c.

Thus we have demonstrated that a simple model which incorporates a $\rho \boxtimes P$ cut discontinuity peaked at the position of the pole, can describe all the features of the π N CEX data above $P_{lab} \sim 5.0$ Gev/c, provided we also include the $\rho \boxtimes P'$ cuts in order that our amplitudes have the correct phases. There are two predictions which can be made on the basis of this model:-

(i) We expect the strong shrinkage apparent in the currently available data to be modified according to fig.(5.6) when we look beyond $t \sim -2.0$ (Gev/c)^2 at Serpukhov and NAL.

(ii) A weaker prediction is the appearance of a substantial negative polarization at higher energy in the region $1.0 \leqslant |t| \leqslant 2.0$ (Gev/c)^2.

5.3 THE R ⊠ P CUT DISCONTINUITY IN PHOTOPRODUCTION

As we indicated in chapter two, the only reactions in which we do not observe Regge shrinkage are the photo-induced processes. These reactions have a much richer amplitude structure with non flip, single flip and double flip amplitudes all contributing to the cross section. One possibility is that the cut discontinuity is still peaked at the pole, as in π N, with the observed structure in the photoproduction α_{eff} near $t \sim -0.5$ (Gev/c)^2 and the lack of shrinkage at large $|t|$, being due to pole-cut interference which postpones the strong shrinkage beyond the limit of the available data.

To investigate this problem we have attempted to reproduce the photoproduction amplitudes obtained from the eikonal model fit of section 3.5 - which we know have the correct phases to satisfy

both the FESR's and the high energy asymmetry data – using diff-
erent parameterisations of the discontinuity function $\Delta(J,t)$.
We rely heavily on the formalism of section 5.2 and because the
cuts are freely parameterised, we require a new set of cut param-
eters $(a_p, a_{p'}, G_p, G_{p'})$ for each helicity amplitude. However, to
economise we set them equal in the non/double flip amplitudes, so
that there are in fact eight free parameters (four for the non/
double flip and four for the two single flip amplitudes) in all
to describe the absorption.

As in πN CEX we write (R $\boxtimes$ P cuts)

$$A^{RP}_{\mu'\mu}(s,t) = i \left({}^{s}/_{s_0} e^{-i\pi/2} \right)^{\alpha_R(0)} G^R_{\mu'\mu} (-t)^{N/2} \left\{ (-G_p) F_{c_p}(s,t) \right\} \qquad (5.27)$$

where

$$c_p = \frac{a_N a_p}{a_N + a_p} + \ln s - \frac{i\pi}{2} \qquad (5.28)$$

And for the R $\boxtimes$ P' cuts

$$A^{RP'}_{\mu'\mu}(s,t) = i \left({}^{s}/_{s_0} e^{-i\pi/2} \right)^{\alpha_R(0)} G^R_{\mu'\mu} (-t)^{N/2}$$
$$\left\{ G_{p'} \left({}^{s}/_{s_0} e^{-i\pi/2} \right)^{\alpha_{p'}(0)} \frac{e^{c_{p'} \alpha_{\mu p'} t}}{c_{p'}} \right\} \qquad (5.29)$$

with

$$c_{p'} = \frac{a_N a_{p'}}{a_N + a_{p'}} + \ln s - \frac{i\pi}{2} \qquad (5.30)$$

The R $\boxtimes$ P' trajectory is defined in a similar way to (5.22) and
we have dropped the helicity labels on c_p and $c_{p'}$ as well as on
all the absorption parameters.

For the N = 0, x = 2 amplitudes we allow some extra

freedom (compare equation (3.66)) by multiplying both (5.27) and (5.29) by a function of t, $(b_1 + b_2 t)$. The full amplitude is then, as usual, the sum of terms $R + R \boxtimes P + R \boxtimes P'$.

As in section 5.1, the function $F_{c_p}(s,t)$ depends on the form of the Reggeon Pomeron cut discontinuity, by analogy to (5.4).

$$F_{c_p}(s,t) = \frac{1}{2\pi i} \int_{-i\infty+\gamma}^{i\infty+\gamma} e^{c_p J} \Delta(J,t) \ln(J - \alpha_c) \, dJ \qquad (5.31)$$

We now look at some different possibilities for $\Delta(J,t)$. (Note that the full cut discontinuity always has an exponential e^{aJ} dependence which is included in the term e^{cJ} of (5.31).)

Our first consideration is

$$\Delta(J,t) = \left(\frac{J - \alpha_c}{J - \alpha_p} \right)^2 \qquad (5.32)$$

This is simply the paremeterisation used in section (5.2) to fit πN CEX and therefore $F_{c_p}(s,t)$ is given by (5.16). With this choice of discontinuity it is certainly possible to obtain the required zero in $\text{Im } A_{++}$ at $t \sim -0.5$ $(\text{Gev/c})^2$. However, when we try to fit the non flip and double flip amplitudes (see fig.(3.7)) the results are rather poor, the model being unable to reproduce any of the structure present in these amplitudes, particularly $\text{Im } A_{-+}$. In fact the "fit" tends to make the cuts very weak in A_{-+} and A_{+-}. Since, with just rho and omega poles, the polarised photon asymmetry measures the strength of the non and double flip cuts it is particularly badly described in this model (being essentially one for all t). In fig.(5.7) we show the polarised target asymmetry resulting from our best fit. The descrepancy between the model and the data is obvious. Our final check is to compare $\alpha_{eff}(t)$ calculated from the model, with fig.(2.6a). Because the cuts are small

in the non and double flip amplitudes, there is no structure induced into α_{eff} by pole-cut cancellations in these amplitudes and the model shows typical Regge shrinkage, contrary to the data. However, if we look at just the single flip amplitude we obtain the α_{eff} of fig.(5.8). Here there is a zero in the imaginary part of the amplitude at $t \sim -0.5$ $(Gev/c)^2$, which is reflected in the slight deviation of α_{eff} from linearity in this region. It is clear that the reason why we do not see the effect characteristic of the absorption model (fig.(2.2)) is that at this value of t our new type of cut has approximately the same phase and energy dependence as the pole - namely that corresponding to the trajectory $\alpha_R(t)$. Thus the cancellation is simply between two different functions of t (coming from two different exponential slopes), which does not produce any wild fluctuations of α_{eff}.

This could have important consequences for Regge cut phenomenology. In particular it could make the need for NWSZ redundant. In section 5.2 we used a nonsense choosing rho pole with no cuts in the flip amplitude to fit the πN CEX data. Since the flip amplitude in πN has the same form as the single flip photoproduction amplitude, it should be possible to obtain a zero in Im $A_{+-}(\pi N)$ at $t \sim -0.5$ $(Gev/c)^2$ by pole-cut interference whilst still maintaining the approximate linearity of α_{eff}.

However, it is apparent that (5.32) is not the correct form of cut discontinuity with which to fit the photoproduction amplitudes. We next tried two parameterisations in which we increase the contribution from the tip of the branch cut $J = \alpha_c$. Firstly

$$\Delta(J,t) \sim \frac{J - \alpha_c}{J - \alpha_R} \tag{5.33}$$

which gives

$$F_{c_p}(s,t) = -(\alpha_R - \alpha_c) e^{c\alpha_R} \left[\sum_{n=1}^{\infty} \frac{[(\alpha_c - \alpha_R)c]^n}{nn!} \right]$$

$$- (\alpha_R - \alpha_c) e^{c\alpha_R} (\gamma + \ln c) - \frac{e^{c\alpha_c}}{c} \qquad (5.34)$$

And secondly

$$\Delta(J,t) \sim \frac{1}{(J - \alpha_R)^2} \qquad (5.35)$$

from which we obtain

$$F_{c_p}(s,t) = \frac{e^{c\alpha_R} - e^{c\alpha_c}}{(\alpha_R - \alpha_c)} - c e^{c\alpha_R} (\gamma + \ln c)$$

$$- c e^{c\alpha_R} \left[\sum_{n=1}^{\infty} \frac{[(\alpha_c - \alpha_R)c]^n}{nn!} \right] \qquad (5.36)$$

Again we find it impossible to reproduce the amplitudes of chapter three using either of these parameterisations for the R ⊗ P cut. Equation (5.33) undoubtably gives a better description of the single flip amplitudes than (5.36) or (5.32), but the non and double flip amplitudes are once again, very poor. The model α_{eff} is very similar for both these parameterisations and in fact shows considerably more structure than the previous attempt using (5.32). In fig.(5.9) we show α_{eff} from the best fit to the amplitudes using (5.33). However, because of the bad description of A_{+-} and A_{-+} the fit to the polarised target and polarised photon asymmetries (fig.(5.10)) is clearly inadequate.

Our final choice for the discontinuity is

$$\Delta (J,t) \sim \text{constant} \qquad (5.37)$$

which is of course similar to the usual absorptive/eikonal model cut discontinuity and gives

$$F_{c_p}(s,t) \sim -\frac{e^{c\,\alpha_c}}{c}$$

(5.38)

Using this simple parameterisation of the R ⊠ P cut we find that our fit to the non and double flip amplitudes is much better than with any of our other choices of $\Delta(J,t)$. We can also obtain a good description of the single flip amplitudes.

We know from our previous work (chapter three), that (5.37) is likely to be able to fit the photoproduction data. (This is not certain because the discontinuity may be more complex in the eikonal model.) However, the systematic approach which we have adopted makes it clear that this form for the discontinuity is crucial, particularly in obtaining a good description of the non and double flip amplitudes and hence the asymmetry data. The only point which is unclear from this analysis is the choice of $\Delta(J,t)$ for the single flip amplitudes. It is impossible to choose between (5.33) and (5.37) on the basis of a fit to the amplitudes of chapter three at a single energy. We therefore confronted two simple model directly with the photoproduction data over a range of energies ($3.0 \lesssim P_{lab} \lesssim 15.0$ Gev/c).

(A) $\Delta(J,t) \sim$ constant in all amplitudes.

(B) $\Delta(J,t) \sim$ constant in A_{+-} and A_{-+}, with $\Delta(J,t) \sim \left(\frac{J - \alpha_c}{J - \alpha_R}\right)$ in A_{++} and A_{--}.

By first fitting the amplitudes at 6.0 Gev/c, we immediately obtain good agreement with the phase sensitive asymmetry data which only exists at low energies. When we try to describe the differential cross section over the full energy range we find that model (A) is udoubtably the better of the two. In particular the dip at $t \sim -0.5$ (Gev/c)^2 appears to deepen with energy when we fit with (B), contrary to the data (fig.(5.11)). For this reason we can clearly state that the best description of the Reggecn-

Pomeron cut discontinuity in photoproduction is provided by the usual eikonal/absorptive type model, (A). We emphasise that in comparing the different parameterisations of $\Delta(J,t)$, all of the possibilities were treated on exactly the same basis as outlined above.

Having established that $\Delta(J,t) \sim$ constant gives the best results, we then changed the parameterisation slightly to enable us to compare the results of the fit with that of chapter three. We have no more free parameters, but we now write the R $\otimes$ P cut as

$$A^{RP}_{\mu'\mu}(s,t) = i\left(s/s_0\, e^{-i\pi/2}\right)^{\alpha_R(0)} G^R_{\mu'\mu}\, (-t)^{N/2} \times$$

$$\times \left\{ \left(\frac{-G_P}{c+c_P}\right) \left(s/s_0\, e^{-i\pi/2}\right)^{\alpha'_{RP}t}\, \exp\left(\frac{a\,\alpha_P}{a+\alpha_P}\right)t \right\} \tag{5.39}$$

where
$$\alpha_{RP}(t) = \alpha_R(0) + \alpha_P(0) - 1 + \left(\frac{\alpha'_R\,\alpha'_P}{\alpha'_R + \alpha'_P}\right)t.$$

And in the case of the N = 0, x = 2 amplitude we multiply (5.39) by $(b_1 + b_2 t)$. The R $\otimes$ P' cuts are parameterised in a similar fashion.

The results of this fit[80] are shown in figs.(5.11) to (5.16) and in table (5.2). We should emphasise that the parameterisation is rather crude, particularly in the non flip (N = 0, x = 2) amplitude. A much better description is the full eikonal approach described in section 3.5.

In conclusion, the eikonal model is successful in photoproduction because it has the correct behaviour of $\Delta(J,t)$. Any model which seeks to shift the dominant contribution to the discontinuity away from the tip of the cut towards the position of the pole $J = \alpha_R$, will necessarily be inadequate in photoproduction.

POLE PARAMETERS		CUT PARAMETERS	
a_0	4.60	a_P	0.02
a_1	1.46	$a_{P'}$	3.40
G_0	28.51	G_P	0.05
G_1	131.53	$G_{P'}$	-1.15
(0)	0.55	b	-0.09
α'	0.93	α'_P	0.28
		$\alpha_{P'}(0)$	0.45
		$\alpha'_{P'}$	1.08

TABLE 5.1

The values of the parameters obtained in the fit to the π N CEX data using the model of section 5.2. The Pomeron intercept was fixed at $\alpha_P(0) = 1$.

EXCHANGE PARAMETER	RHO	OMEGA	POMERON	P'
a_o	3.36	9.48	4.94	9.90
a_1	0.15	1.03	5.10	6.35
G_o (G_T)	44.13	19.58	0.40	-3.61
G_1 (G_v)	1.15	13.61	2.13	-1.89
b_1	-0.53			
b_2	5.96			

TABLE 5.2

The values of the parameters obtained in the fit to the photoproduction data using the model of section 5.3. Parameters for the double flip amplitude $(N = 2)$ are identical to those shown for the non flip amplitude $(N = 0)$ and b_1, b_2 are the same for both rho and omega exchanges.

The rho and omega trajectories are those of section 3.5, whilst the P and P' trajectories were fixed (from table 5.1) to be

$$\alpha_p(t) = 1.0 + 0.25\ t$$

$$\alpha_{p'}(t) = 0.45 + 1.08\ t$$

CONCLUSIONS

There are two important points which we must bear in mind in order to obtain the correct behaviour of Regge cut amplitudes.

(i)   It is crucial in fixing the phase of the full cut amplitude to include contributions from the region $-1 < J < 0$. We have chosen to do this by using Regge-Regge cuts, although several other methods have been proposed [81]. This phase problem, inherent in the old absorption models but only made transparent by the amplitude analysis, has obscured the other basic flaw in the absorption model approach - namely the form of the cut discontinuity.

(ii)   It now seems clear that the strong shrinkage observed in hadronic processes is due to some kind of pole enhancement mechanism, which peaks the R Ⓧ P cut discontinuity at the position of the pole.   In this respect, the absorption model which gives $\Delta(J,t) \sim$ constant (by this we mean that the discontinuity has no singularities or zeros), is clearly inadequate. However, it appears that in photoinduced processes, this mechanism does not operate and the absorption model (provided we have the correct phase structure) is sufficient to describe the data.

Finally we note that pole enhancement of the cut discontinuity in hadronic reactions, may make NWSZ unnecessary in order to "explain" the dips observed at $t \sim -0.5$ $(Gev/c)^2$ in $\pi^- p \to \pi^0 n$ and $\gamma p \to \pi^0 p$. The structure in the photoproduction α_{eff} at this point supports the pole-cut interference mechanism. However, if this is the case, there is then the puzzling inconsistency of the absence of structure in the πN CEX α_{eff}. Why should the Argonne model work best in hadronic reactions and the Michigan model be most successful in photoproduction?

Also, factorisation of the ρ residue would suggest that if we have a NWSZ, we should observe a dip in $\gamma p \to \rho^0 p$ (which is dominated by ρ exchange). In general, factorisation tests of this nature support the Michigan approach.

If we make the hypothesis that there are no NWSZ and that all dips are produced by pole-cut interference, we arrive at a consistent picture provided we assume that pole enhancement of the cut discontinuity occurs in hadronic processes (and not in photoproduction). Then, as we have seen in section (5.3), pole-cut cancellation can still take place at $t \sim -0.5$ (Gev/ c)^2 (in πN CEX for example) without destroying the linear behaviour of α_{eff} in this region, whereas in $\gamma p \to \pi^0 p$, pole-cut interference produces the observed structure in α_{eff}.

It would be interesting to extend this type of analysis to other processes in an attempt to confirm this peculiarity of the photon. There are two areas where good, accurate data could provide a stringent test of our hypothesis.

(i) Vector meson production, which is related to photoproduction by Vector Dominance may show that the pole enhancement effect is not a property of particular helicity amplitudes (e.g. those with one unit of helicity flip at the "meson" vertex ($\pi \pi \gamma$, $\pi \pi \rho$, etc.)). Fig.(2.15) shows that the unnatural parity exchanges in ρ and ω production (π and B respectively) appear to shrink at large $|t|$, indicating that $\Delta(J,t) \sim$ constant is a property of the photon.

(ii) A second set of reactions is backward πN and backward photoproduction. Examples of these along with the allowed (baryon) exchanges are shown below[4].

(a) $\pi^+ p \to p \pi^+$ $\qquad$ N_α, N_γ, Δ_δ

(b) $\pi^- p \to \gamma \pi^-$ $\qquad$ Δ_δ
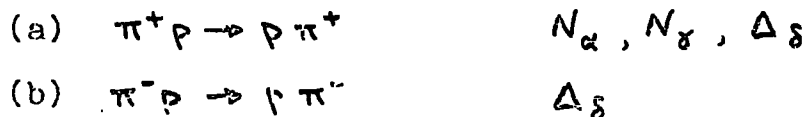
(c) $\gamma p \rightarrow p \pi^0$ $N_\alpha, N_\gamma, \Delta_\delta$

(d) $\gamma p \rightarrow n \pi^+$ $N_\alpha, N_\gamma, \Delta_\delta$

All of the arguments presented above for the forward reactions also apply here[82]. Firstly, factorisation is again a problem. Reaction (a) has a dip at $u \sim -0.15$ $(Gev/c)^2$ which may be associated with a zero in the N_α amplitude at $\alpha_{Nucleon} = -\frac{1}{2}$. However, we then have to assume that the N_γ coupling is small to avoid filling in the dip (in the EXD limit). Factorisation would now suggest a dip in (c), which is not observed experimentally. Also, the photoproduction reactions show very little shrinkage whilst the hadronic processes do appear to shrink[28], although the data only extends to $u \sim -0.5$ $(Gev/c)^2$ (reaction (a)). So here again, experiment seems to support the hypothesis of a disc-ontinuity dominated by the pole in hadronic processes and by the tip of the branch cut in photoproduction.

A systematic analysis of Regge cuts in these and other processes obviously provides a useful extension to this line of research.

FIGURE CAPTIONS - CHAPTER FIVE

5.1 $I_t = 1$ helicity amplitudes for the reaction $\pi^- p \rightarrow \pi^0 n$.

5.2 Fit to the differential cross section for $\pi^- p \rightarrow \pi^0 n$.

5.3 The effective trajectory calculated from the model of section (5.2) compared with the "data" of fig.(2.1).

5.4 Fit to the data for $\Delta\sigma(\pi N)$.

5.5 Fit to the polarization data for $\pi^- p \rightarrow \pi^0 n$.

5.6 The effective trajectory calculated from the model of section (5.2) out to $|t| \leq 4.0$ $(Gev/c)^2$ for different incident beam momenta.

5.7 Fit to the polarised target asymmetry data for $\gamma p \rightarrow \pi^0 p$ with $\Delta(s,t) \sim \left(\frac{s-\alpha_c}{s-\alpha_R}\right)^2$ in all helicity amplitudes.

5.8 The effective trajectory of the single flip amplitude in $\gamma p \rightarrow \pi^0 p$ with $\Delta(s,t) \sim \left(\frac{s-\alpha_c}{s-\alpha_R}\right)^2$ in this amplitude.

5.9 The effective trajectory for $\gamma p \rightarrow \pi^0 p$ with $\Delta(s,t) \sim \left(\frac{s-\alpha_c}{s-\alpha_R}\right)$ in all helicity amplitudes.

5.10 Fit to the polarized target and polarized photon asymmetry for $\gamma p \rightarrow \pi^0 p$ with $\Delta(s,t) \sim \left(\frac{s-\alpha_c}{s-\alpha_R}\right)$ in all helicity amplitudes.

5.11 Fit to the differential cross section for $\gamma p \rightarrow \pi^0 p$. The solid curve is the final fit with $\Delta(s,t) \sim$ constant in all helicity amplitudes. The dashed curve shows the fit with $\Delta(s,t) \sim \left(\frac{s-\alpha_c}{s-\alpha_R}\right)$ in A_{++} and A_{--}, and $\Delta(s,t) \sim$ constant in A_{+-} and A_{-+}.

5.12 Fit to the differential cross section for $\gamma p \rightarrow \eta^0 p$ with $\Delta(s,t) \sim$ constant in all helicity amplitudes.

5.13 Fit to the polarized target asymmetry data for $\gamma p \rightarrow \pi^0 p$ with $\Delta(s,t) \sim$ constant in all helicity amplitudes.

5.14 Fit to the polarized photon asymmetry data for $\gamma p \to \pi^\circ p$ with $\Delta(s,t) \sim$ constant in all helicity amplitudes.

5.15 Fit to the neutron/proton ratio (R) for π° photoproduction with $\Delta(s,t) \sim$ constant in all helicity amplitudes.

5.16 The effective trajectory for $\gamma p \to \pi^\circ p$, calculated with $\Delta(s,t) \sim$ constant in all helicity amplitudes.
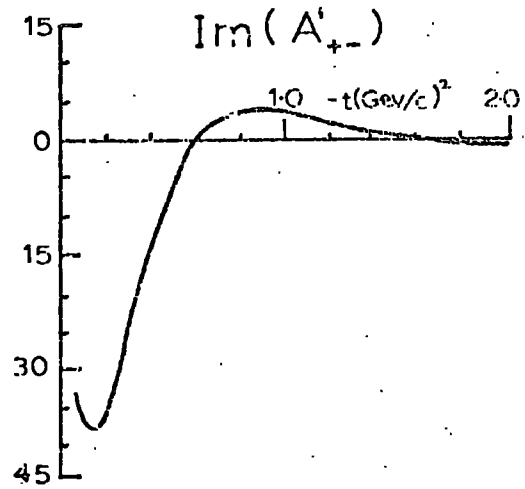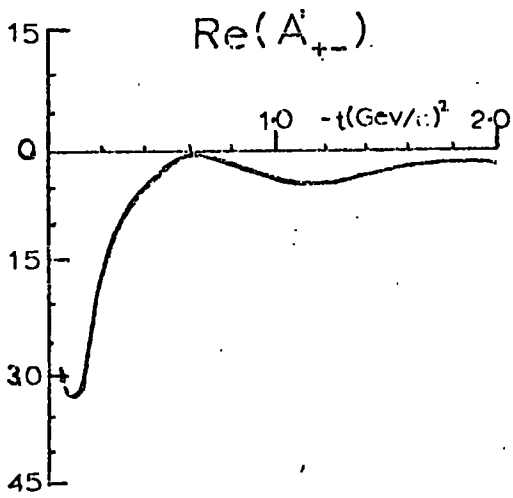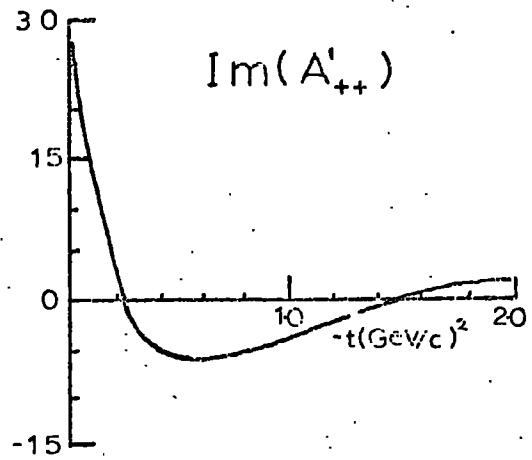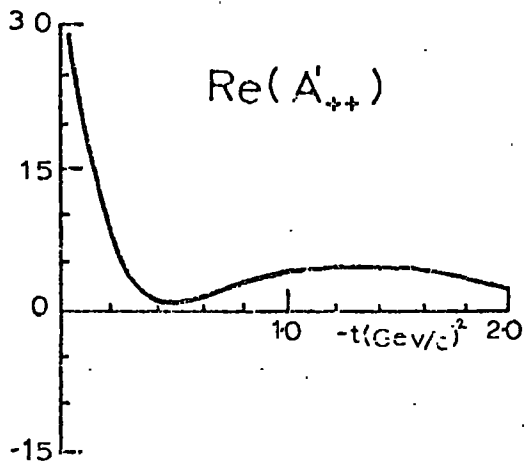
Fig 5·1
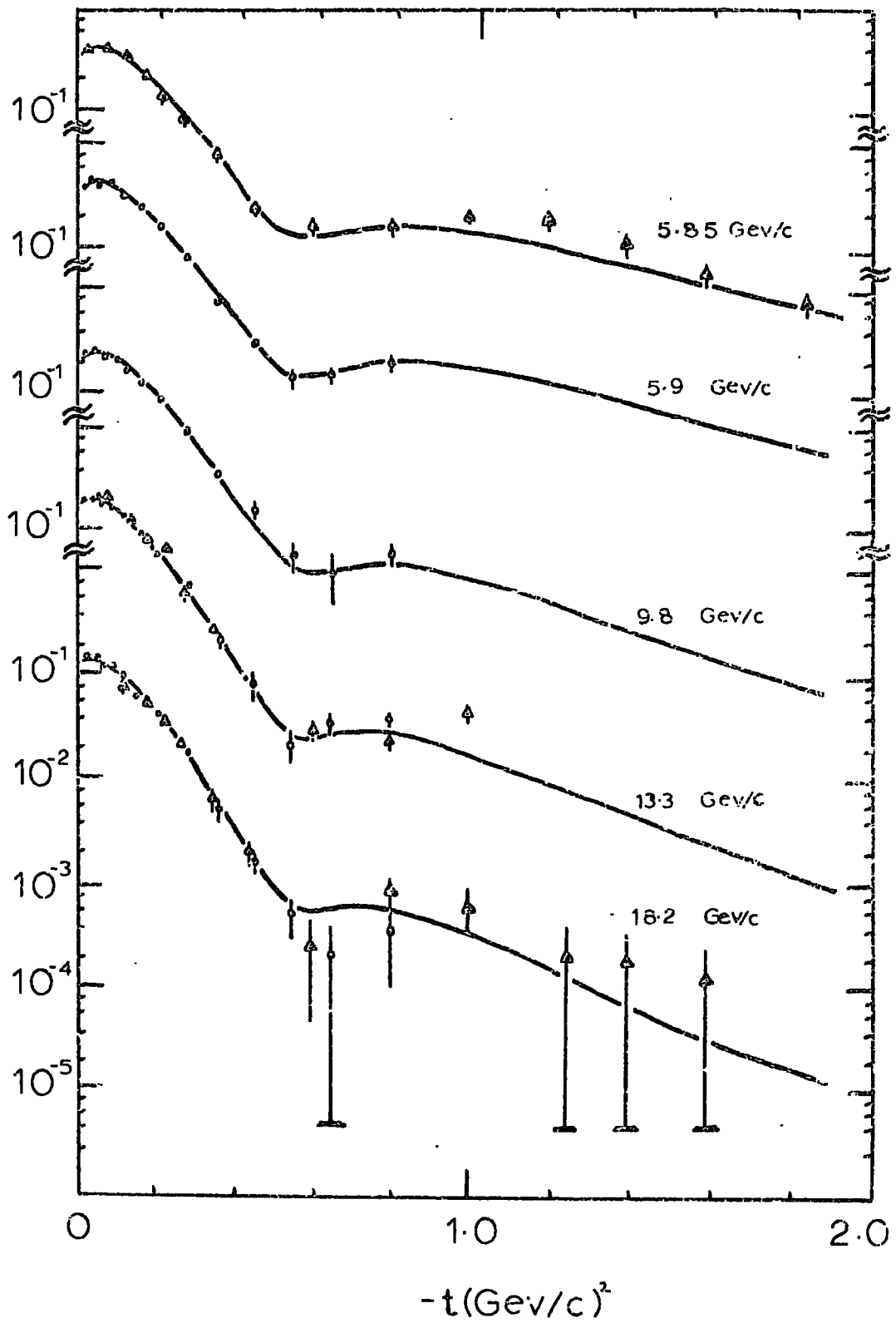
Fig 5·2

$-t(Gev/c)^2$
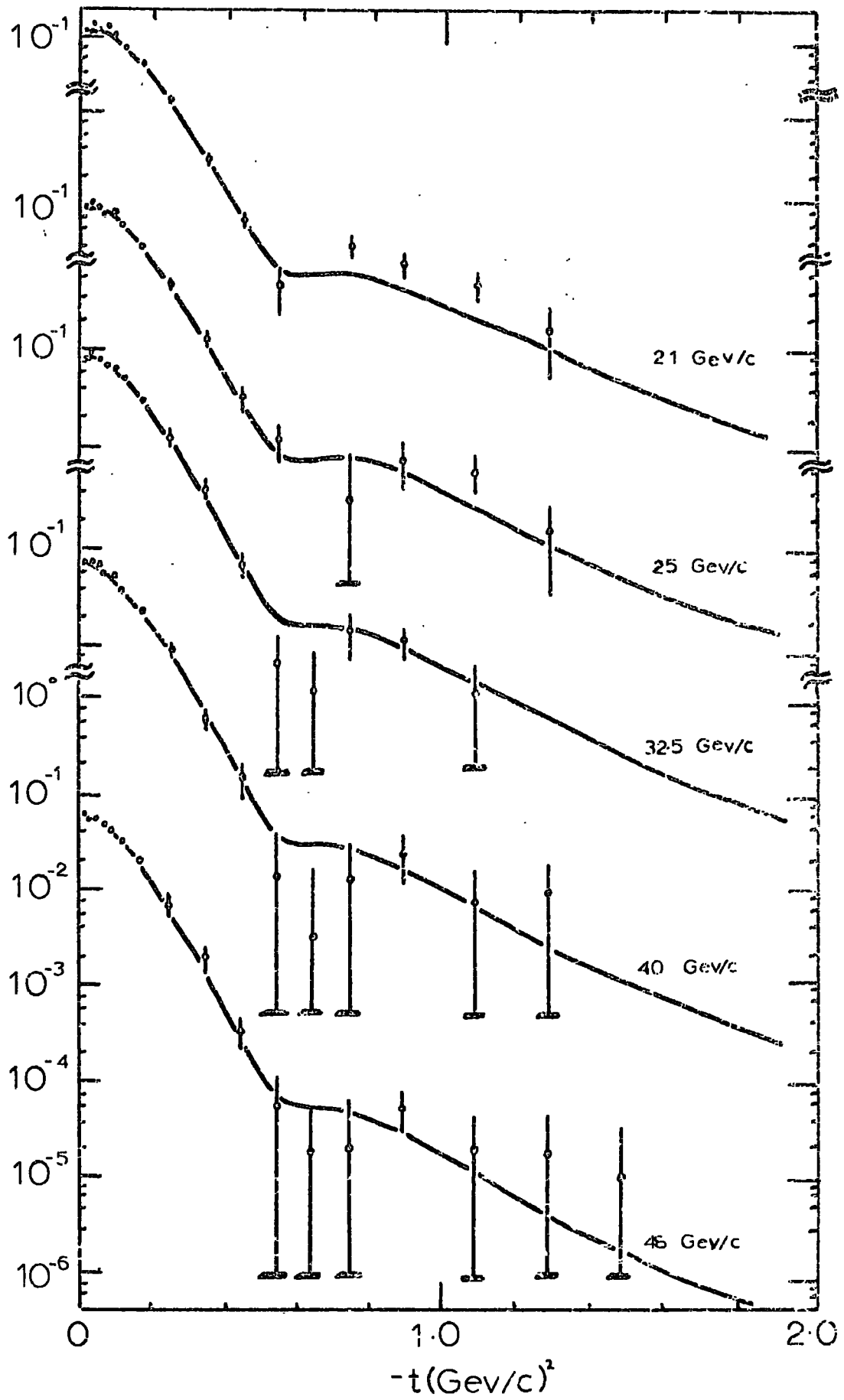
Fig 5·2 (cont.)
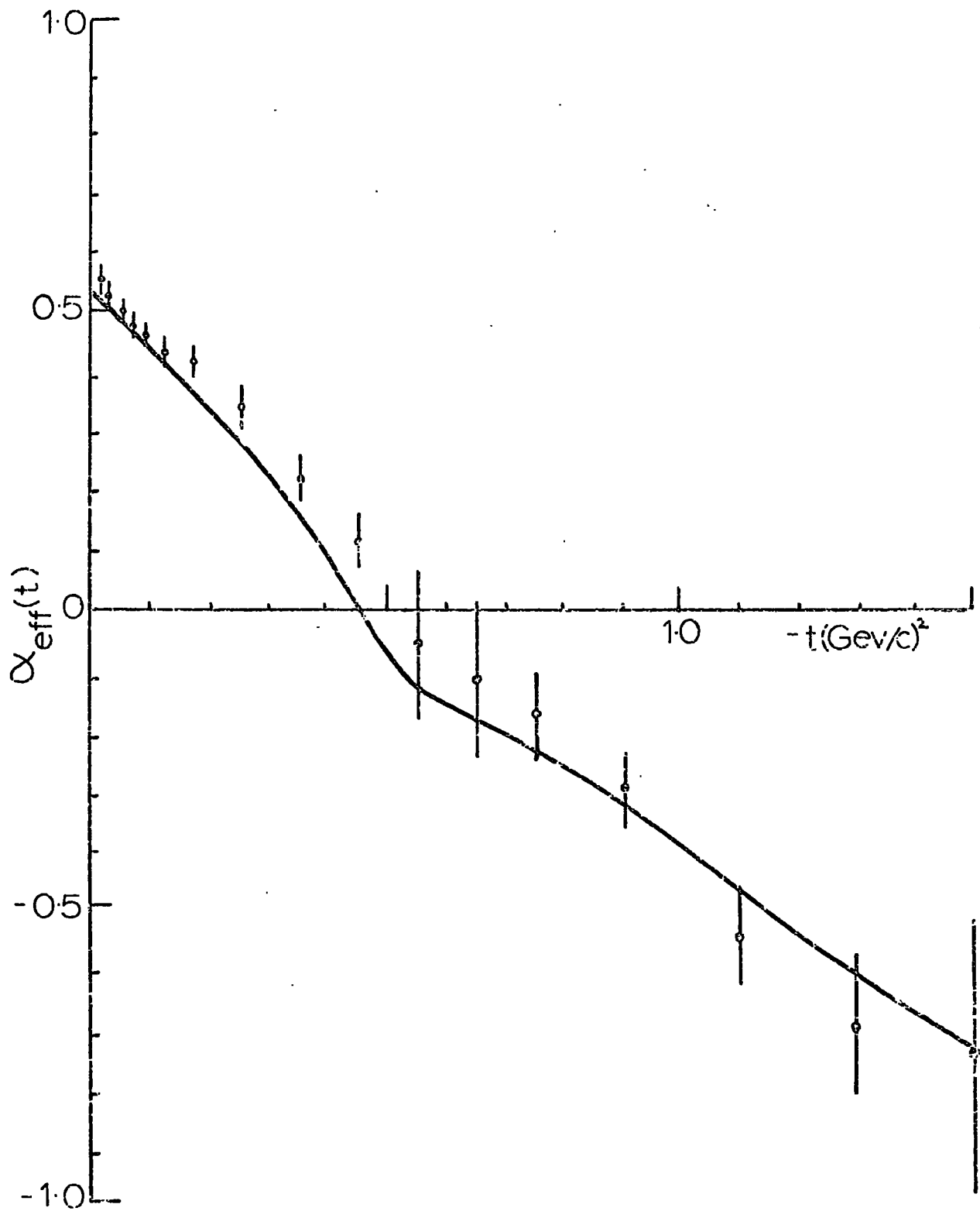
Fig 5·3
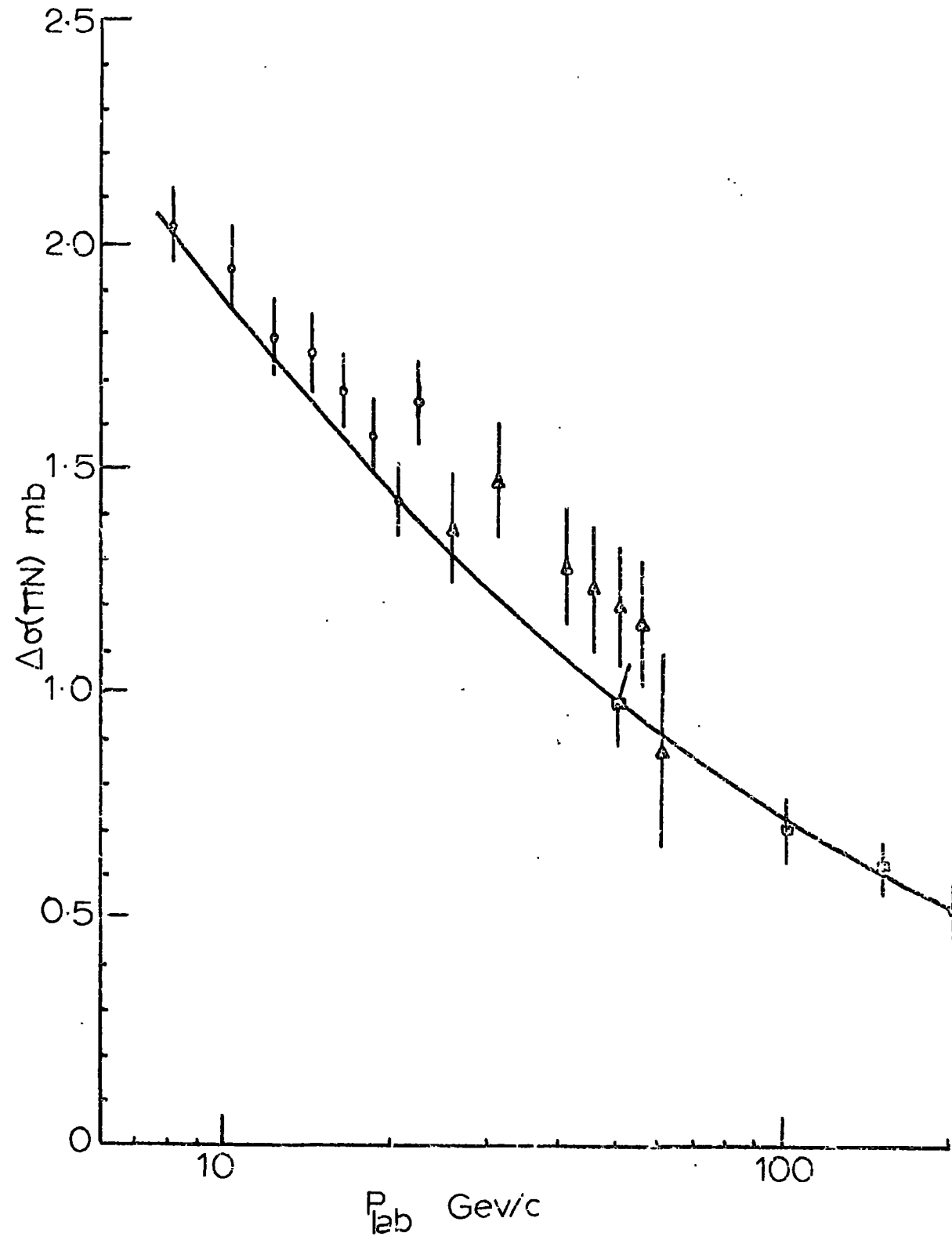
Fig 5·4
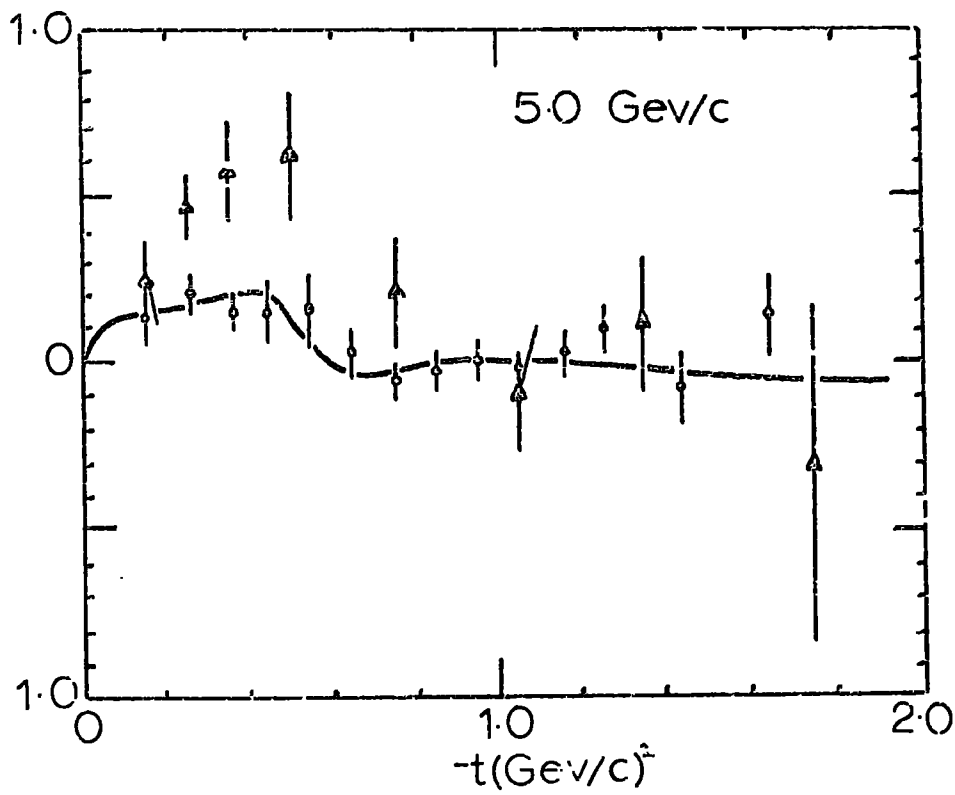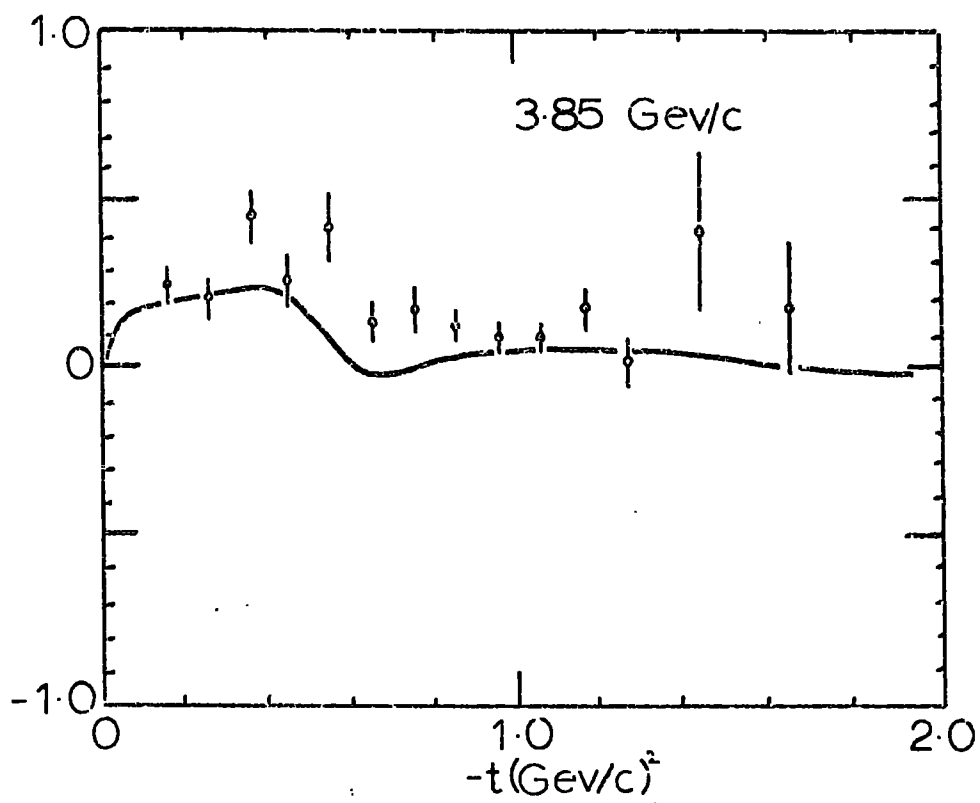
Fig 5·5
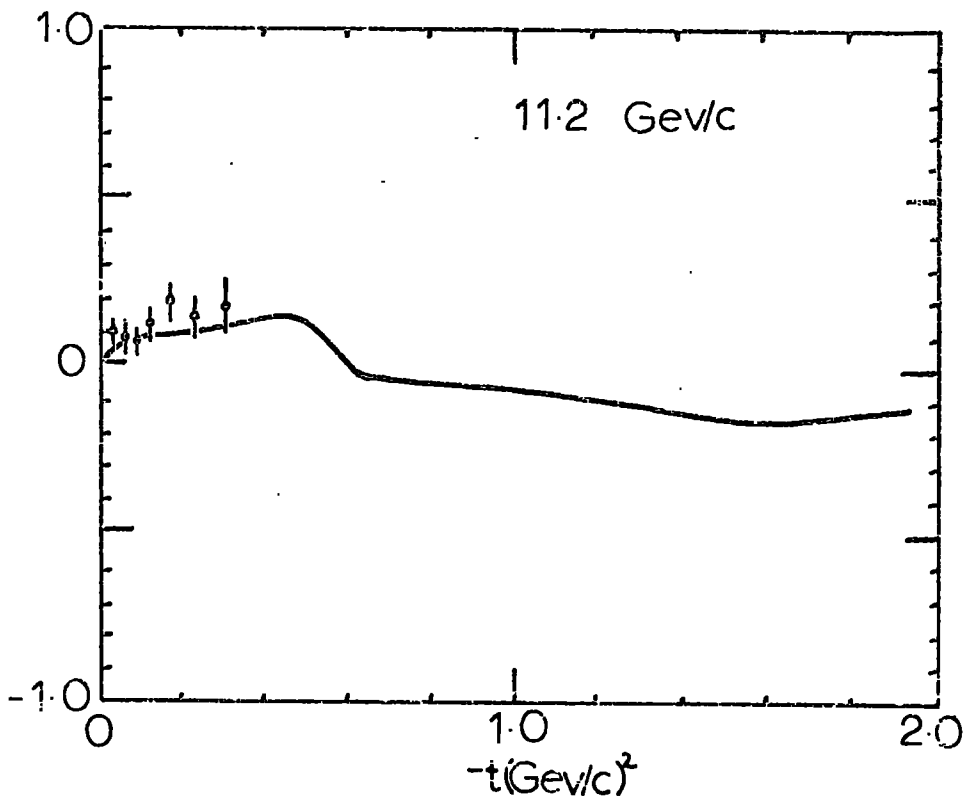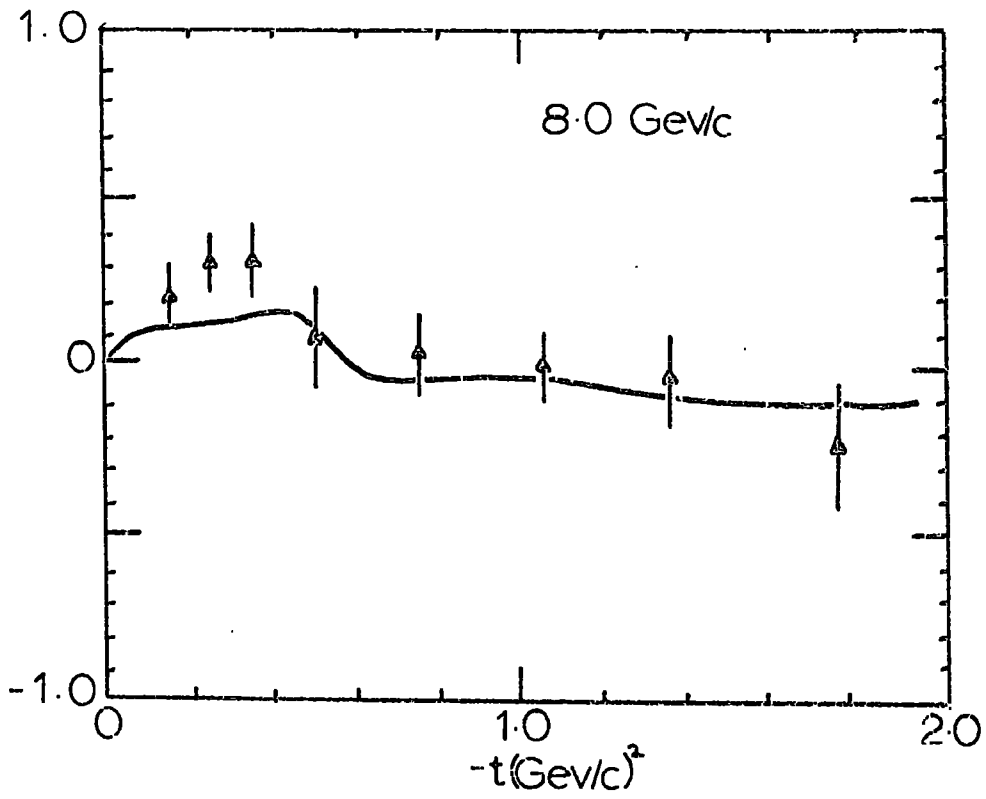
Fig 5·5(cont.)

Fig 5·6

Fig 5·7

Single Flip only
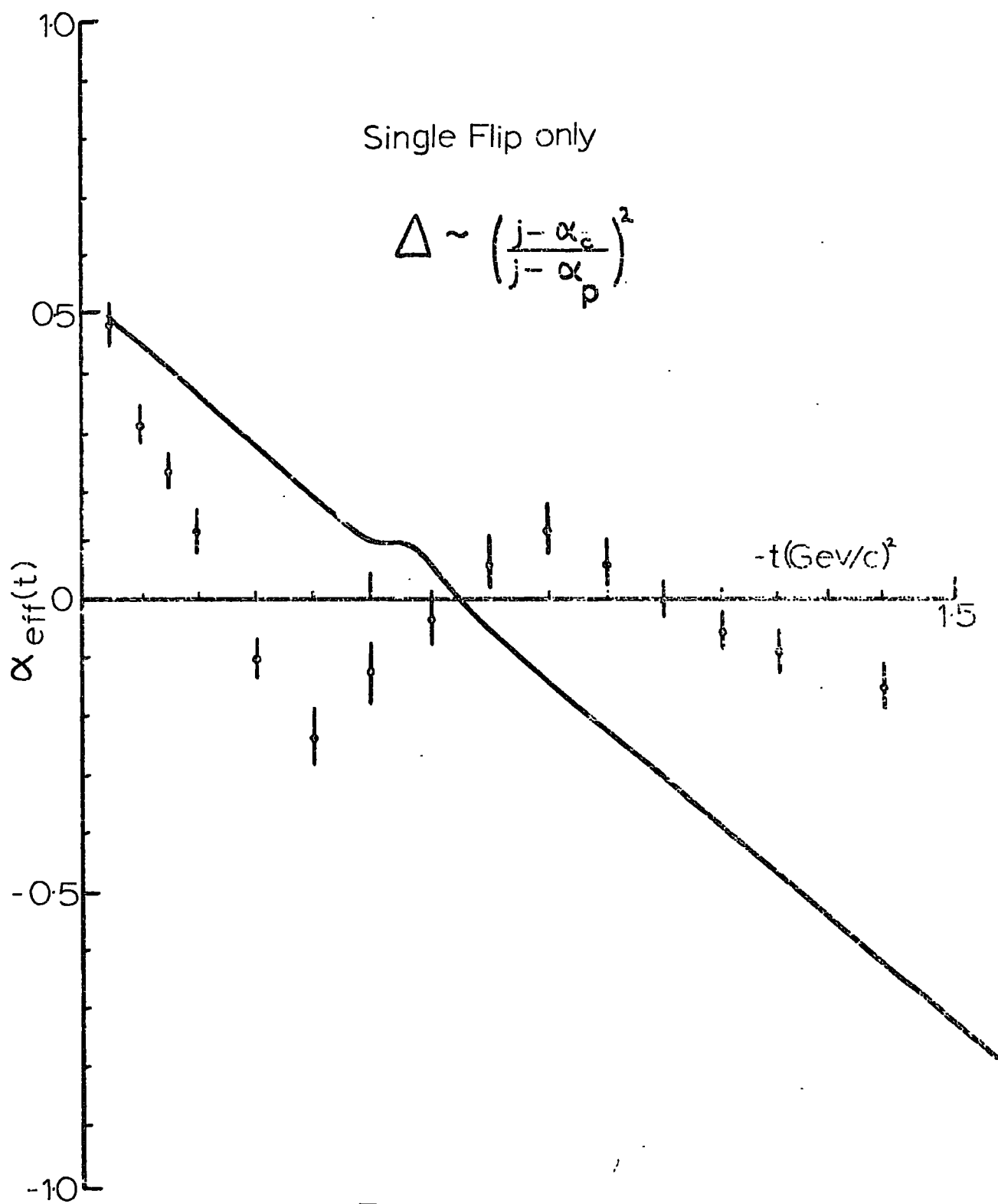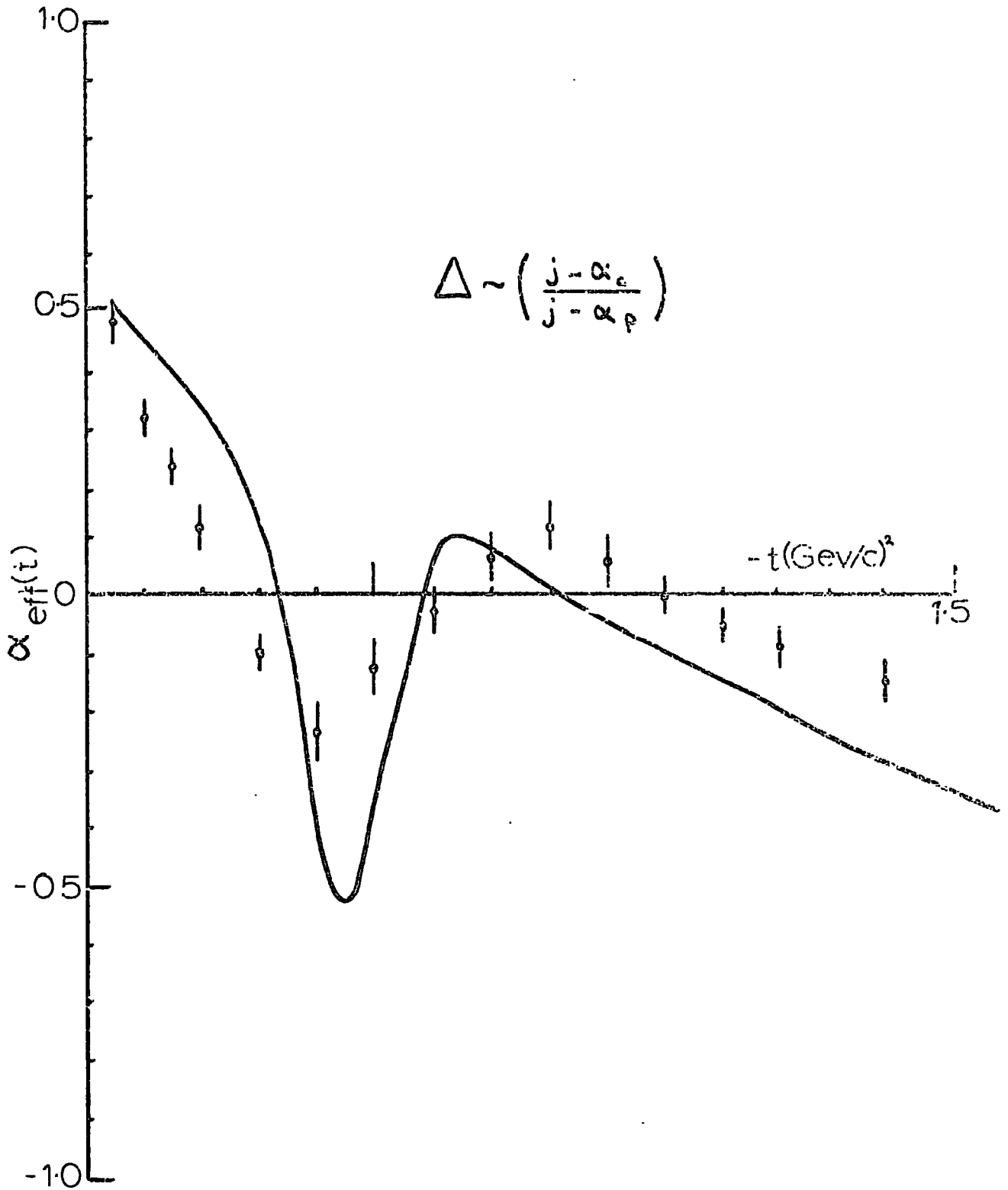
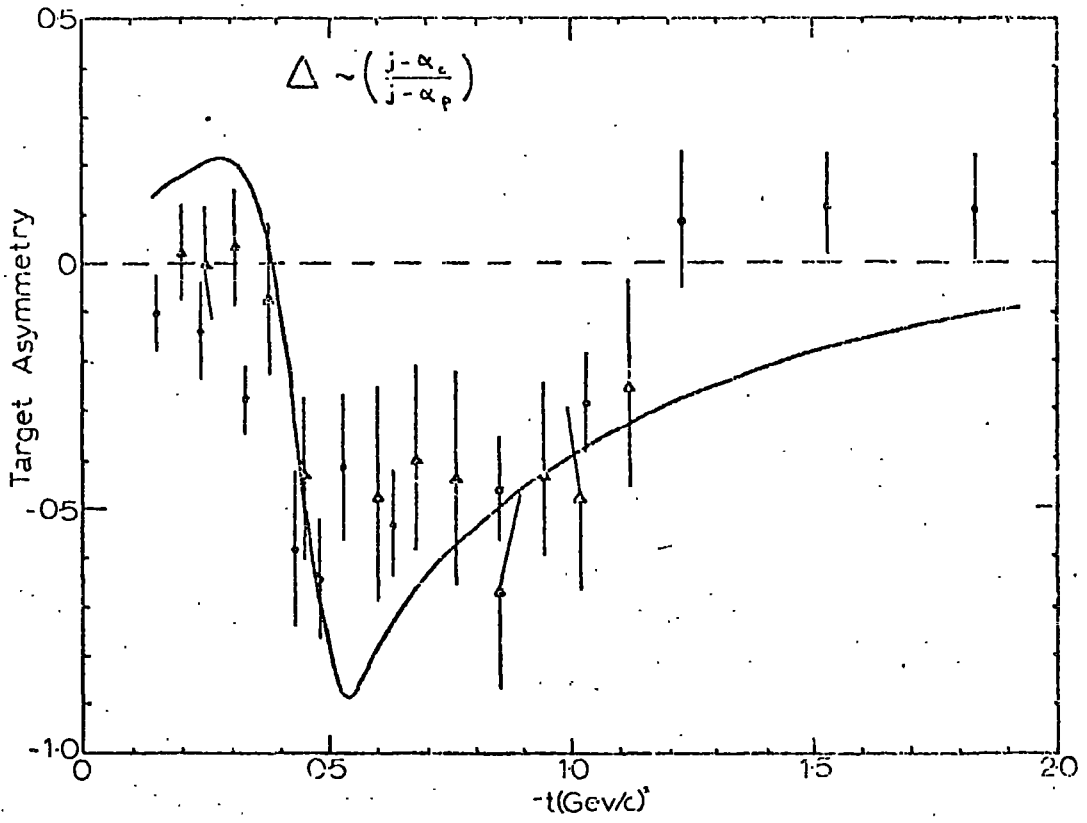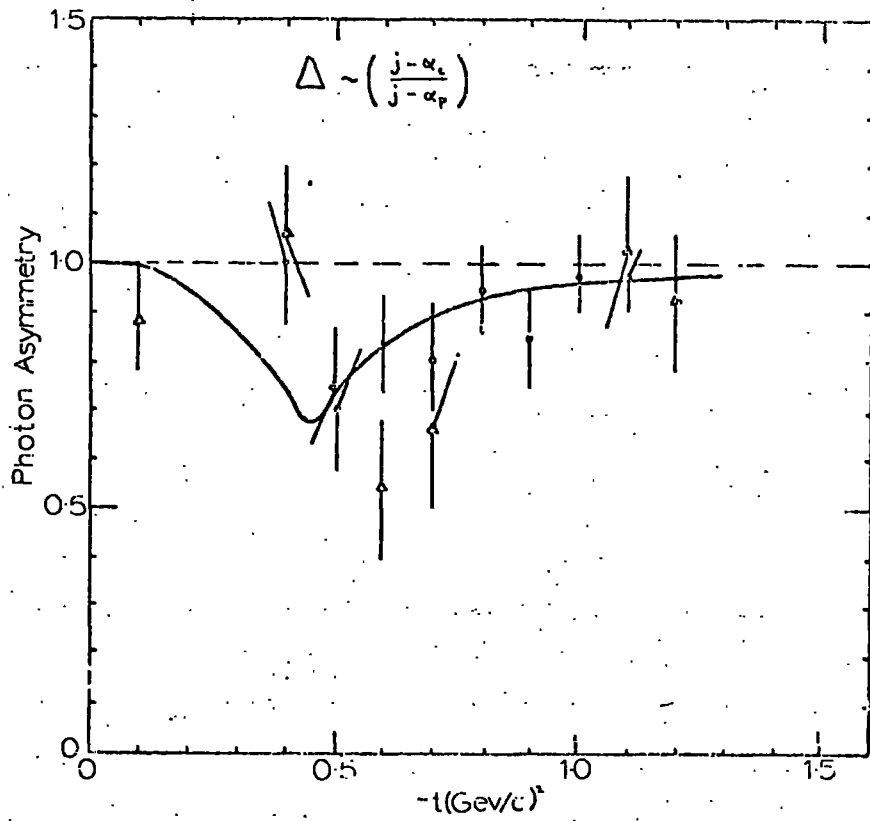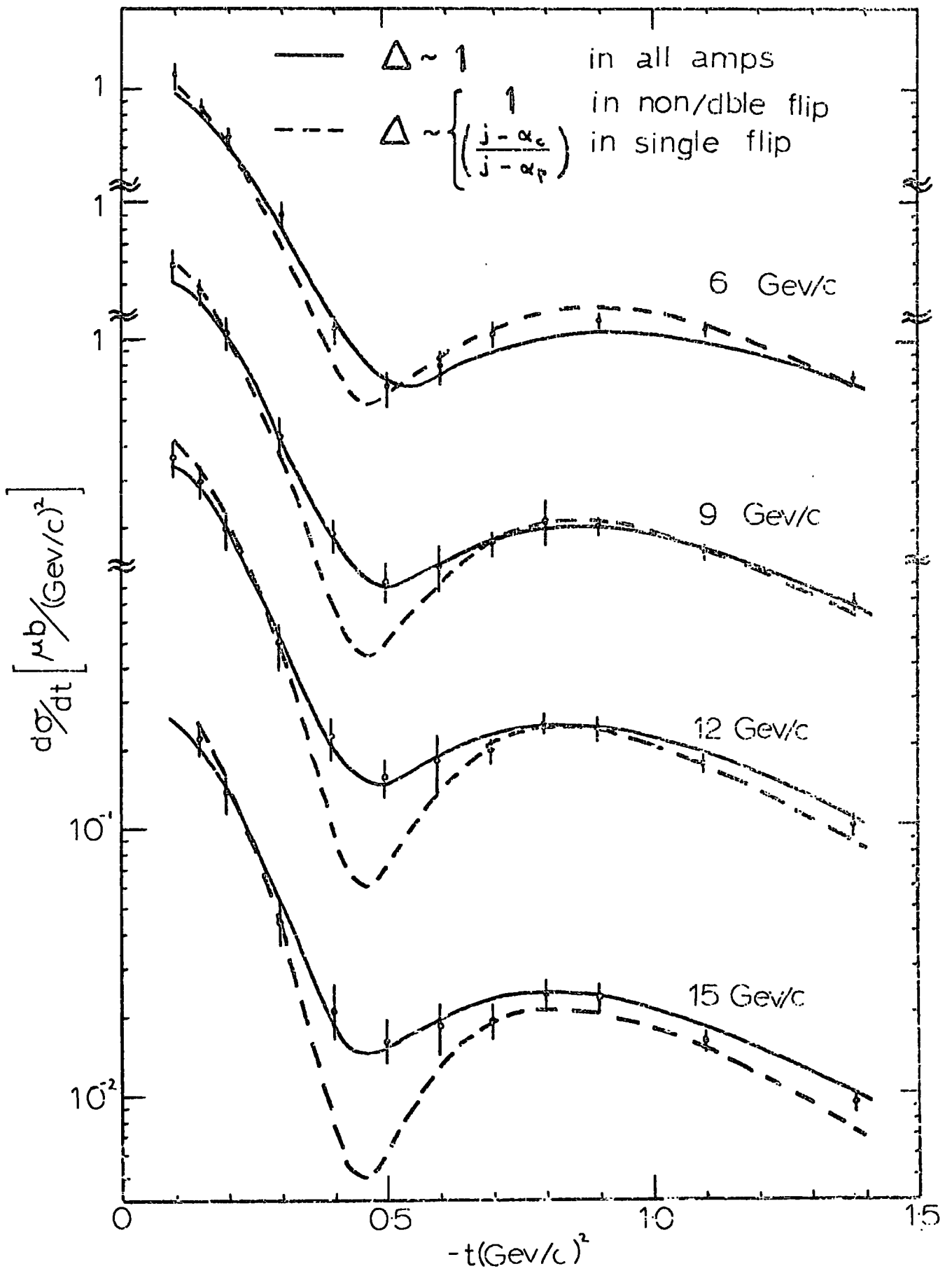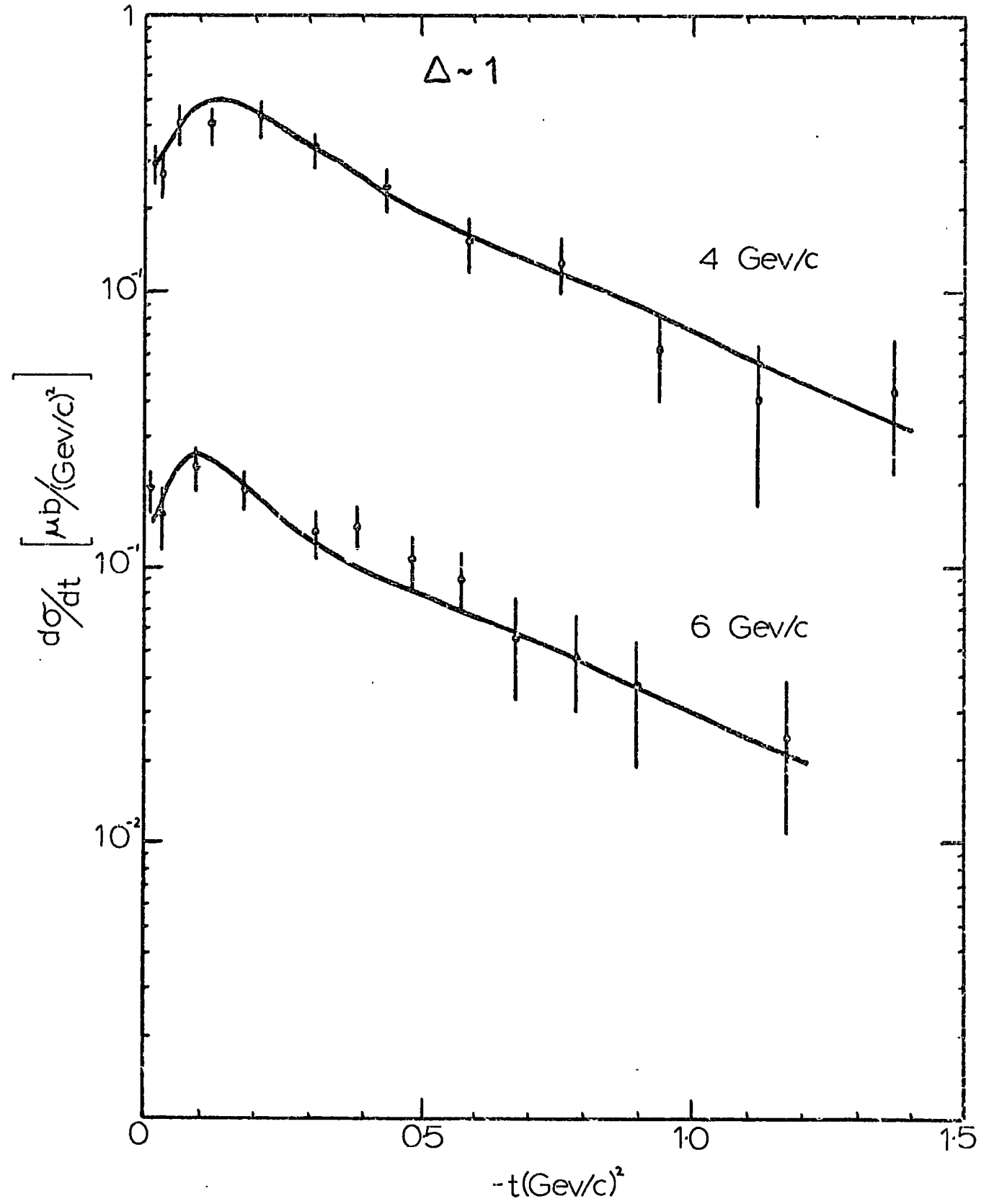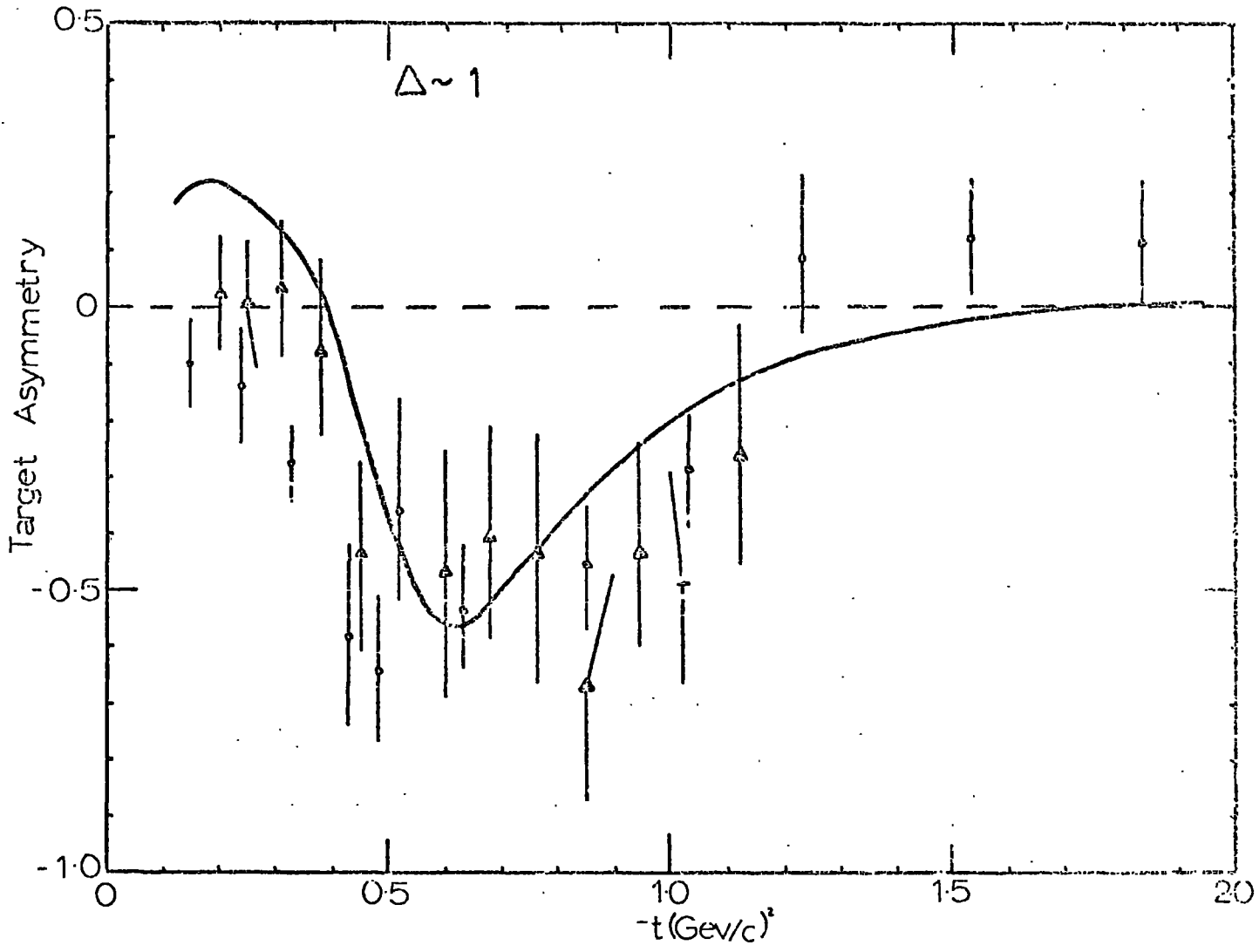$$\Delta \sim \left(\frac{j - \alpha_c}{j - \alpha_p} \right)^2$$
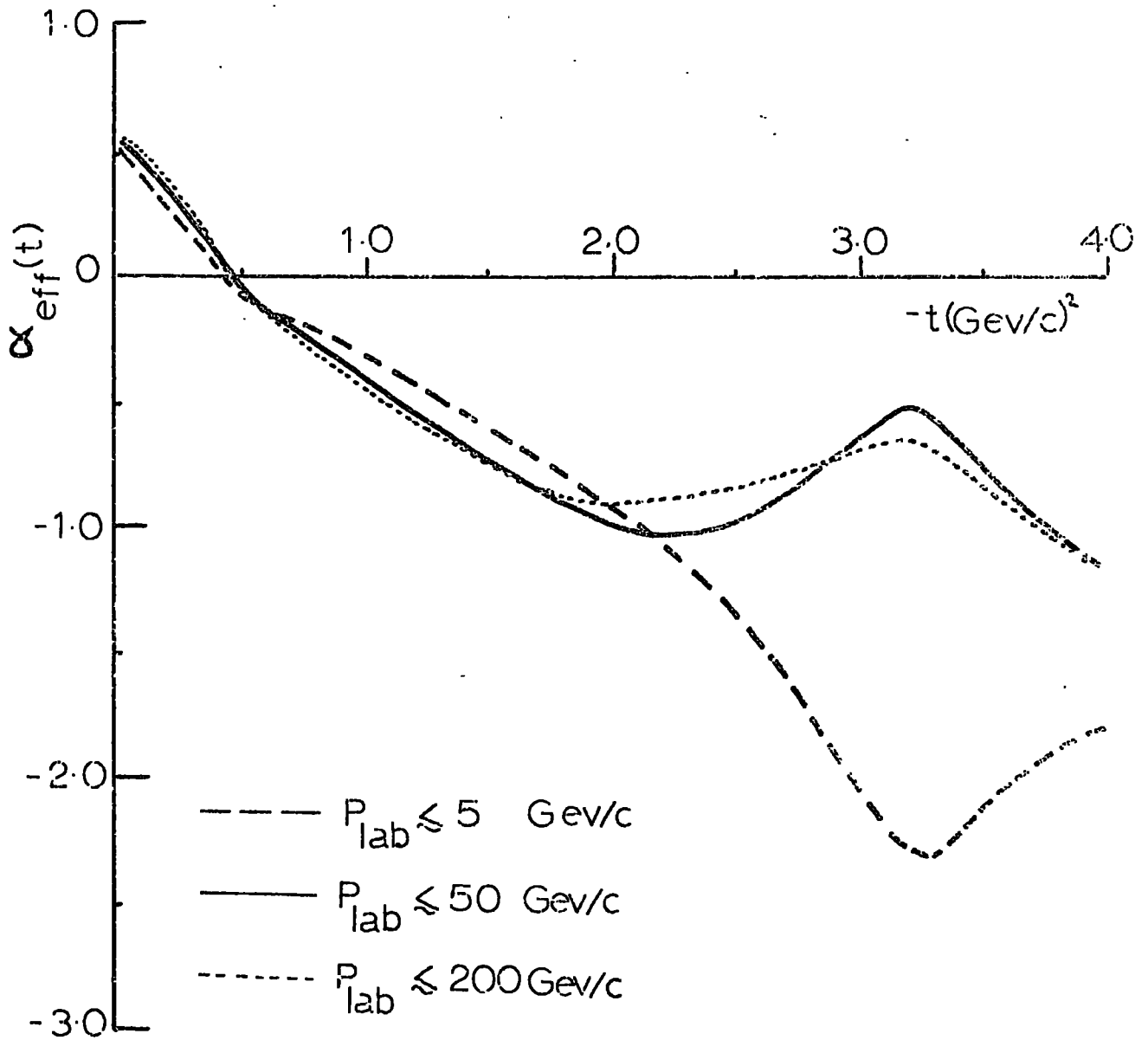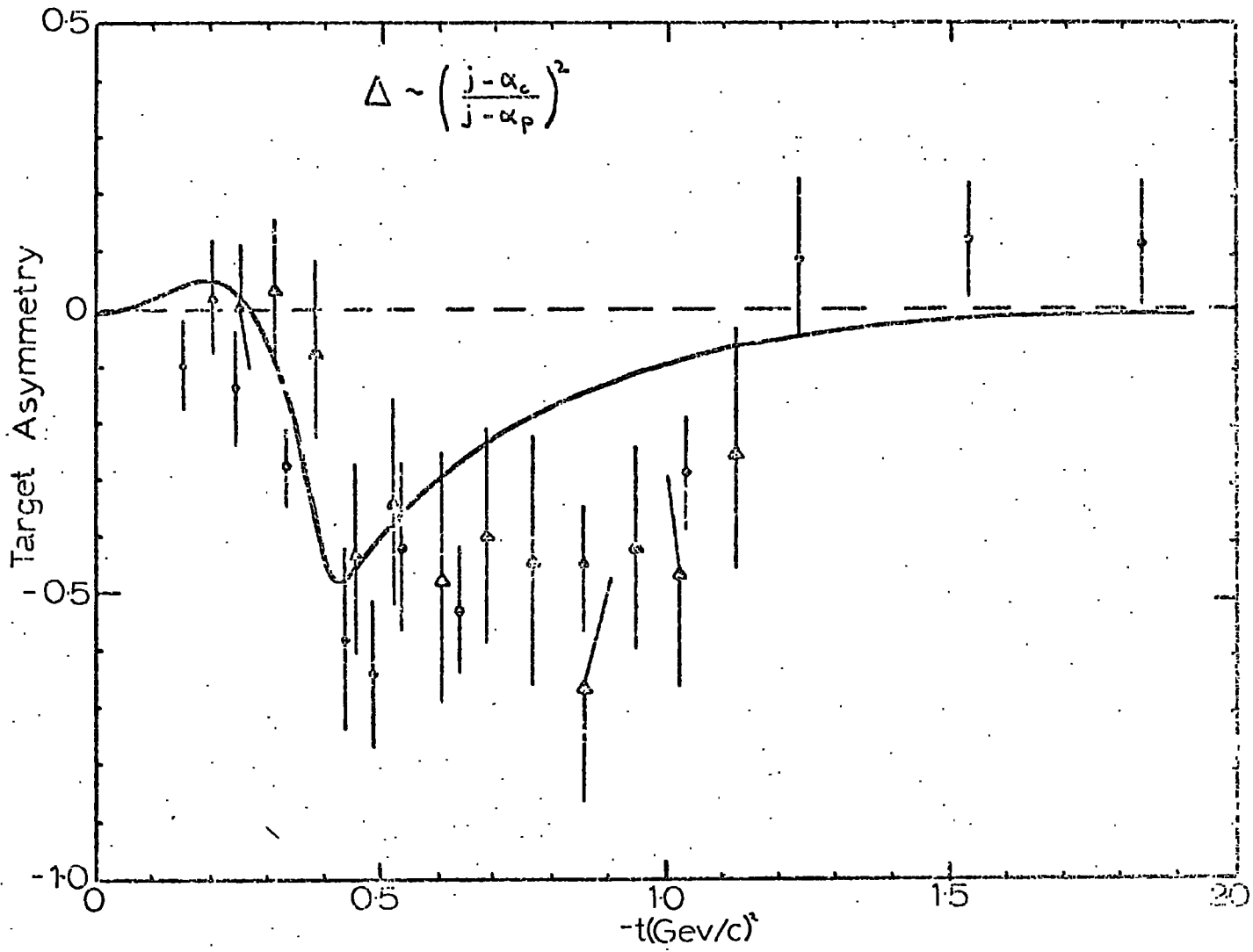
Fig 5·8

Fig 5·9

Fig 5·10a

Fig 5·10b

Fig 5·11
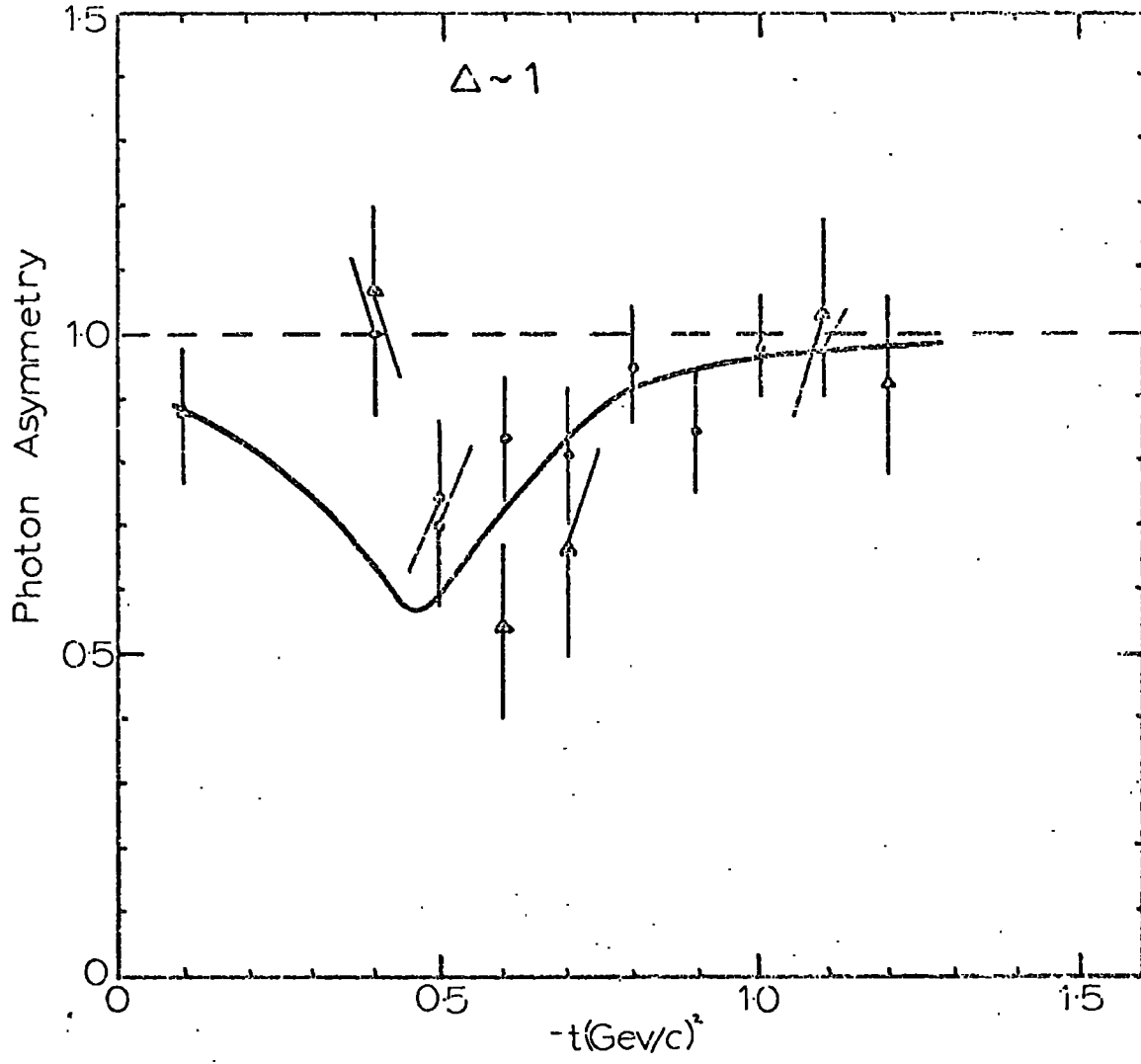
Fig 5·12

Fig 5·13

Fig 5·14
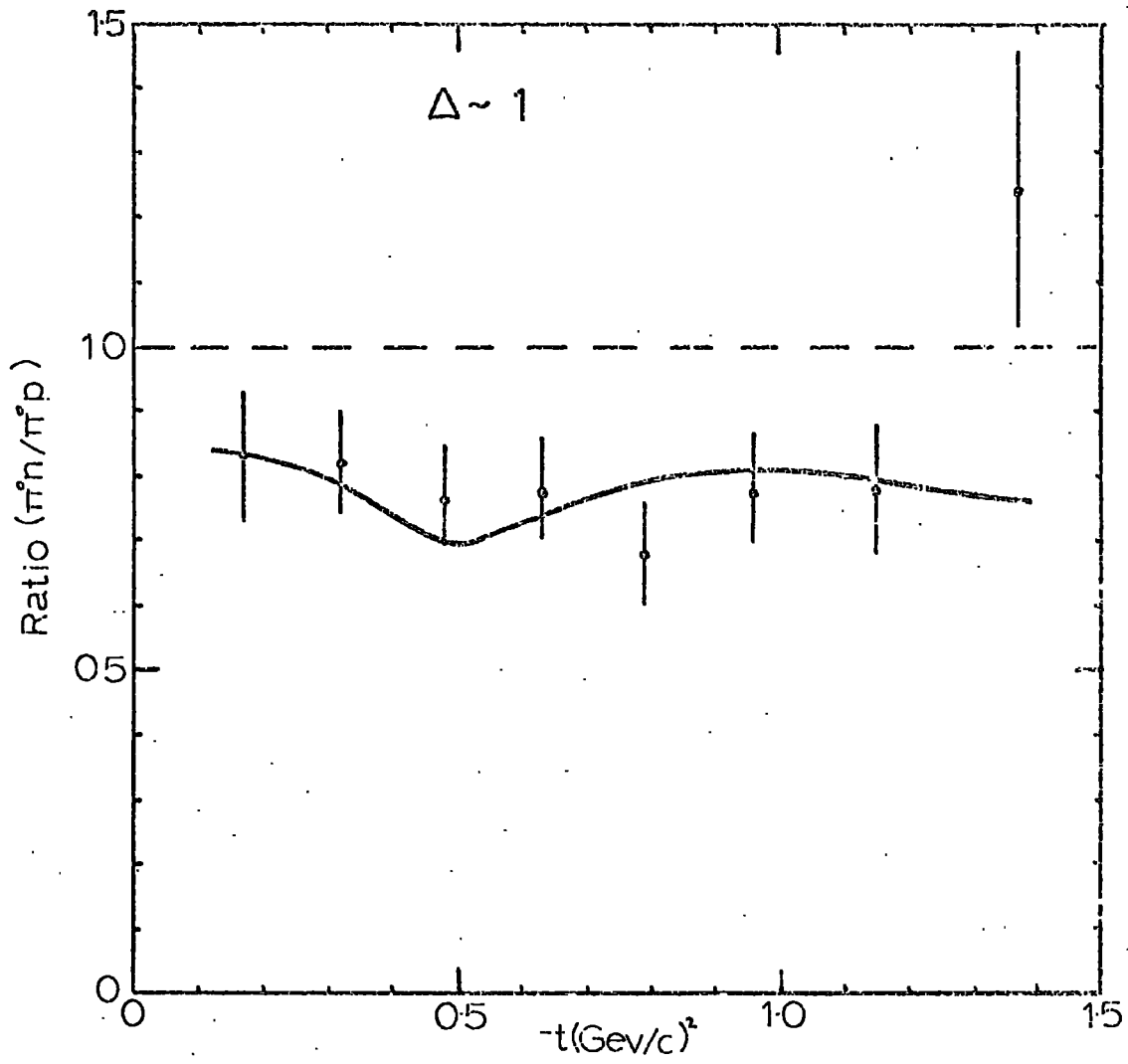
Fig 5·15
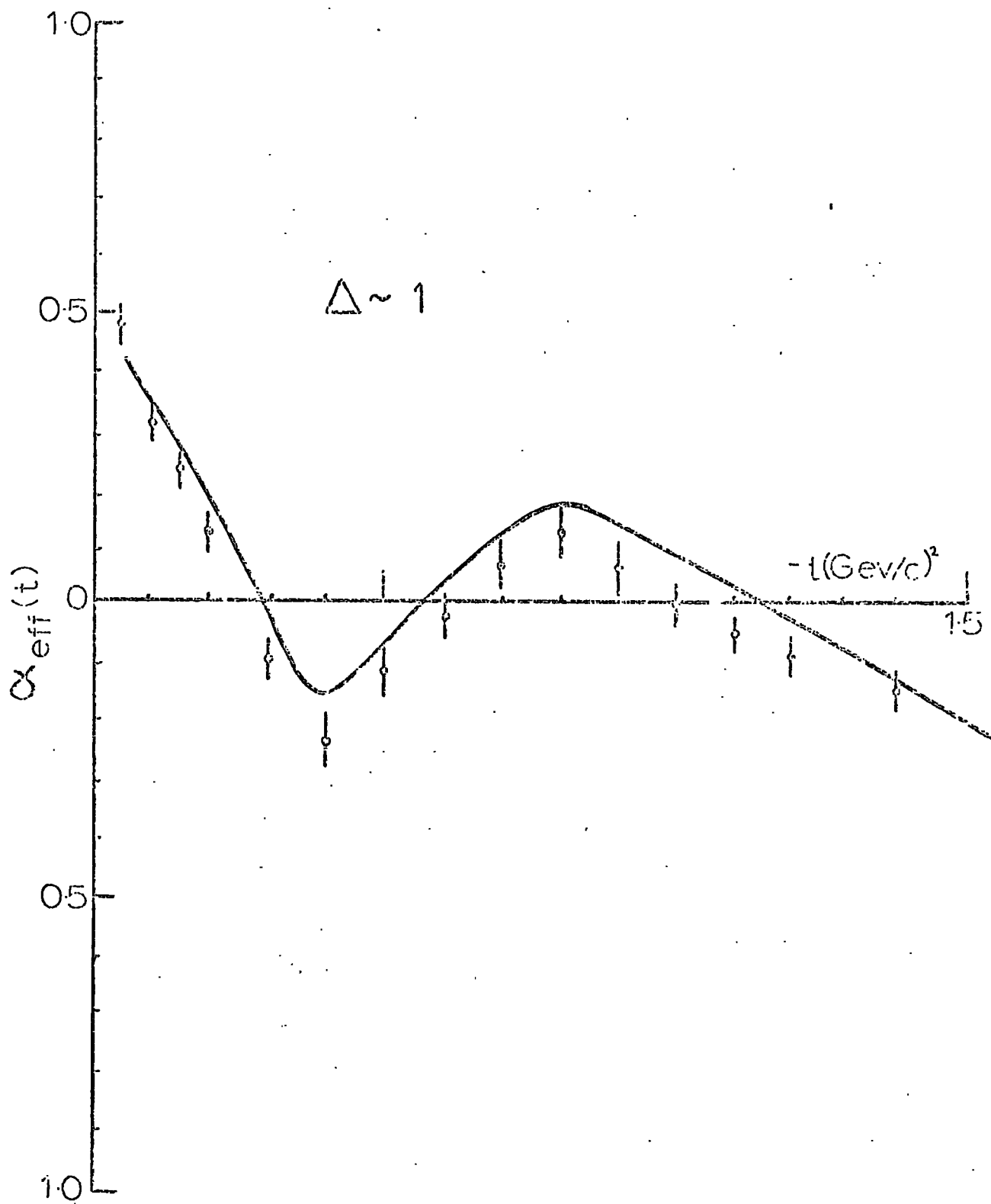
Fig 5.16

APPENDIX ONE

A1.1 KINEMATICS.

We shall use the following notation for the general scattering process

$$1 + 2 \longrightarrow 3 + 4$$

$$P_1 = (E_1, \; q_{s_{12}}) \qquad P_2 = (E_2, \; -q_{s_{12}})$$

$$P_3 = (E_3, \; q_{s_{34}}) \qquad P_4 = (E_4, \; -q_{s_{34}})$$
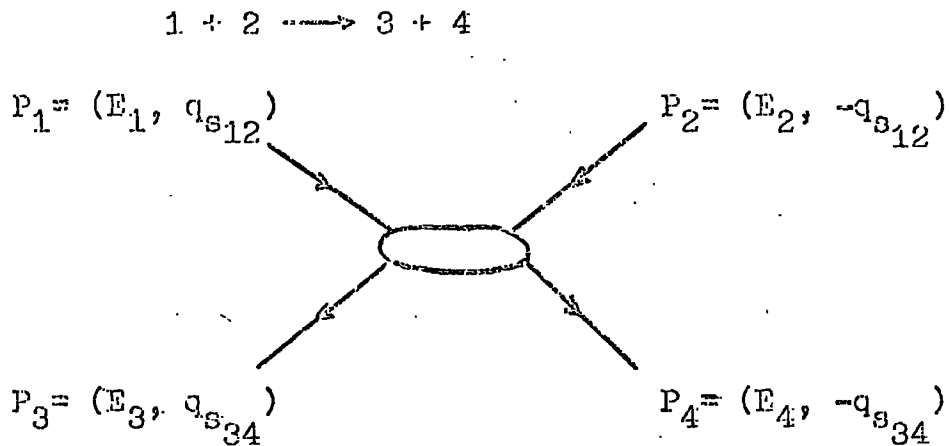
The invariant quantities s, t and u are defined by

$$s = (P_1 + P_2)^2 = (P_3 + P_4)^2$$
$$t = (P_1 - P_3)^2 = (P_2 - P_4)^2 \qquad (A1.1)$$
$$u = (P_1 - P_4)^2 = (P_2 - P_3)^2$$

with the constraint

$$s + t + u = \sum_{i=1}^{4} m_i^2 - \sum \qquad (A1.2)$$

The s (t or u) channel process is that for which s (t or u) corresponds to the square of the total centre of mass energy. Thus

s	channel	$1 + 2 \longrightarrow 3 + 4$
t	channel	$1 + 3 \longrightarrow 2 + 4$
u	channel	$1 + 4 \longrightarrow 3 + 2$

The laboratory frame is taken to be the rest frame of particle 2 . In terms of laboratory quantities

$$S = m_1^2 + m_2^2 + 2 m_2 (E_{lab})_1$$

$$t = m_2^2 + m_4^2 - 2 m_2 (E_{lab})_4 \qquad (A1.3)$$

$$u = m_2^2 + m_3^2 - 2 m_2 (E_{lab})_3$$

The incoming centre of mass three-momentum for the s-channel process is

$$q^2_{s_{12}} = (s - (m_1 + m_2)^2)(s - (m_1 - m_2)^2)/4s \qquad (A1.4)$$

with a similar expression for $q^2_{s_{12}}$.

If the s-channel centre of mass scattering angle is θ_s, then

$$t = m_1^2 + m_3^2 - 2q_{s_{12}} q_{s_{34}} \cos \theta_s + 2E_1 E_3 \qquad (A1.5)$$

and

$$\cos \theta_s \equiv Z_s = \frac{s(t-u) + (m_1^2 - m_2^2)(m_3^2 - m_4^2)}{4 q_{s_{12}} q_{s_{34}}}$$

$$\qquad (A1.6)$$

$$= 1 + \frac{t - t_0}{4 q_{s_{12}} q_{s_{34}}}$$

where t_0 is the value of t corresponding to $\theta_s = 0$. At high energy, a useful approximation is

$$t_0 \sim - \frac{1}{s} \left[(m_1^2 - m_3^2)(m_2^2 - m_4^2) + \right.$$
$$\left. \frac{1}{s} (m_1^2 m_2^2 - m_3^2 m_4^2)(m_1^2 + m_2^2 - m_3^2 - m_4^2) + \cdots \right] \qquad (A1.7)$$

Therefore, if either $m_1 = m_3$ or $m_2 = m_4$, $t_0 \sim 1/s^2$ and becomes negligible extremely quickly. (Of course if all masses are equal $t_0 = 0$). In the reactions which we are principally concerned with t_0 can safely be ignored.

Equations (A1.4) to (A1.7) may be redefined for the t or u channel process. In particular $\cos \theta_t \equiv Z_t$ can be obtained from (A1.6) by the substitution

$$(s, t, m_2, m_3) \longrightarrow (t, s, m_3, m_4)$$

A1.2 HELICITY AMPLITUDES AND NORMALISATION

In the notation of reference 4, the centre of mass helicity amplitudes for the s-channel process are

$$A_{H_s}(s,t) = \langle \mu_3 \mu_4 | A(s,t) | \mu_1 \mu_2 \rangle$$

and for the t-channel process

$$A_{H_t}(s,t) = \langle \lambda_2 \lambda_4 | A(s,t) | \lambda_1 \lambda_3 \rangle$$

where μ_i represent the s-channel helicities and λ_i the t-channel ones.

The amplitudes are normalised so that the optical theorem becomes

$$\sigma_T(mb) = \frac{0.3893}{2 q_{s_{12}} \sqrt{s}} \, \text{Im} \, \langle \mu_1 \mu_2 | A(s,o) | \mu_3 \mu_4 \rangle \qquad (A1.8)$$

And the differential cross section is

$$\frac{d\sigma}{dt}\left(mb/(Gev/c)^2\right) = \frac{0.3893}{64 \pi q_{s_{12}}^2 s} \frac{1}{(2\sigma_1+1)(2\sigma_3+1)} \sum_{H_s} |A_{H_s}(s,t)|^2 \qquad (A1.9)$$

where σ_i is the spin of particle one etc.

With this normalisation the amplitudes are dimensionless. (Note that 1 mb = 0.3893 $(Gev/c)^{-2}$.)

A1.3 PION NUCLEON AMPLITUDES AND OBSERVABLES

In all $0^- + \frac{1}{2}^+ \longrightarrow 0^- + \frac{1}{2}^+$ reactions, there are four helicity amplitudes reduced to two by parity conservation. If we label each amplitude by the baryon helicity state, then the experimental observables are

$$\frac{d\sigma}{dt}\left(mb/(Gev/c)^2\right) = \frac{0.3893}{64 \pi q_{s_{12}}^2 s} \left[|A_{++}|^2 + |A_{+-}|^2 \right] \qquad (A1.10)$$

$$\sigma_T(mb) = \frac{0.3893}{2 q_{s_{12}} \sqrt{3}} \text{ Im } A_{++}(t=0) \qquad (A1.11)$$

$$P = \frac{2 \text{ Im } A_{++} A_{+-}}{|A_{++}|^2 + |A_{+-}|^2} \qquad (A1.12)$$

To describe the particular case of πN scattering we use the t-channel isospin amplitudes $A^{It=0}$ and $A^{It=1}$ in terms of which

$$A(\pi^{\pm} p \to \pi^{\pm} p) = A^0 \mp A'$$

$$A(\pi^- p \to \pi^0 n) = \sqrt{2} \, A' \qquad (A1.13)$$

A1.4 PHOTOPRODUCTION AMPLITUDES AND OBSERVABLES

In this case we have eight amplitudes reduced to four by parity conservation. We label them $A^{\lambda}_{\mu'\mu}$ for the general process

$$\gamma_{\lambda} + N_{\mu} \to 0^- + N_{\mu'}$$

We only need to consider $\lambda = 1$ because of parity conservation so we now drop this superscript. The four independent amplitudes are

A_{-+}	$N = 0$
A_{++}	$N = 1$
A_{--}	$N = 1$
A_{+-}	$N = 2$

where n is the net s-channel helicity flip. In terms of these amplitudes the experimental observables are:-

(i) Differential cross section.

$$\frac{d\sigma}{dt}\left(\frac{mb}{(GeV/c)^2}\right) = \frac{0.3893}{128\pi(s-m^2)^2} \sum_{\mu'\mu} |A_{\mu'\mu}|^2 \qquad (A1.14)$$

(m is the nucleon mass)

(ii) Polarised photon asymmetry

$$\Sigma = \frac{2 \, Re[A_{++}A_{--}^{*} - A_{-+}A_{+-}^{*}]}{\sum_{\mu'\mu} |A_{\mu'\mu}|^2} \qquad (A1.15)$$

(iii) Polarised target asymmetry

$$A = \frac{2 \, Im[A_{-+}^{*}A_{--} - A_{+-}^{*}A_{++}]}{\sum_{\mu'\mu} |A_{\mu'\mu}|^2} \qquad (A1.16)$$

(iv) Recoil nucleon polarisation

$$P = \frac{2 \, Im[A_{-+}^{*}A_{++} - A_{+-}^{*}A_{--}]}{\sum_{\mu'\mu} |A_{\mu'\mu}|^2} \qquad (A1.17)$$

(v) π^0 photoproduction from neutrons

$$R\left(\frac{\gamma n \to \pi^0 n}{\gamma p \to \pi^0 p}\right) = \frac{\sum_{\mu'\mu} |(A_{\mu'\mu})_s - (A_{\mu'\mu})_v|^2}{\sum_{\mu'\mu} |(A_{\mu'\mu})_s + (A_{\mu'\mu})_v|^2} \qquad (A1.18)$$

Where the subscripts s and v refer to the isoscalar and isovector parts of the amplitude respectively.

Finally the amplitudes for η^0 photoproduction are related to the above amplitudes by SU(3).

$$A(\eta^0) = \frac{a}{\sqrt{3}}\left[\frac{\partial \gamma_\rho}{\partial \gamma_\omega} A^\rho(\pi^0) + \frac{\partial \gamma_\omega}{\partial \gamma_\rho} A^\omega(\pi^0)\right] \qquad (A1.19)$$

Where a = 1.23 from the $\eta - \eta'$ mixing as given by the quadratic mass formula.

APPENDIX TWO

A2.1 THE EFFECTIVE TRAJECTORY $\alpha_{eff}(t)$

For the single Regge pole exchange $\alpha(t)$, the forward differential cross section takes the form

$$\frac{d\sigma}{dt} \sim \beta(t) \left(\frac{s}{s_0}\right)^{2\alpha(t) - 2} \tag{A2.1}$$

If $\alpha(t)$ is a linear function of t,

$$\alpha(t) = \alpha(0) + \alpha' t$$

we can write

$$s^{\alpha(t)} = e^{\alpha(t) \ln(s)} = s^{\alpha(0)} e^{\alpha' \ln(s) t}$$

Then (A2.1) becomes

$$\frac{d\sigma}{dt} \sim \beta(t) \left(\frac{s}{s_0}\right)^{2\alpha(0) - 2} \exp\left[2\alpha' \ln\left(\frac{s}{s_0}\right) t\right]$$

So we expect that the width of the forward peak in the differential cross section will "shrink" logarithmically with energy.

The behaviour of $\frac{d\sigma}{dt}$ is usually more complicated because of additional poles and other singularities such as Regge cuts which may contribute in a given process. However, in this case it is possible to define an "effective trajectory" $\alpha_{eff}(t)$, and a computer programme has been written to calculate it from the experimental data. To do this we change (A2.1) slightly and write

$$P_L^2 \frac{d\sigma}{dt} \sim N_i \beta(t) \left(\frac{\nu}{\nu_0}\right)^{2\alpha_{eff}(t)} \tag{A2.2}$$

Where P_L is the laboratory beam momentum and

$$\nu = \frac{(s - u)}{2}$$

N_i is a t independent normalisation parameter associated with a

particular momentum (say P_i). This parameter may also be associated with data at more than one momentum to allow a complete renormalisation of all the data from (say) a particular experimental group which may be suspect.

To determine α_{eff} at $t = t_i$, the available data is interpolated to obtain values at $t = t_i$ using a linear interpolation in $\ln (d\sigma/dt)$ from data at adjacent values of t. α_{eff} is then calculated by a least squares fit of $\ln (d\sigma/dt)$ against $\ln \nu$, and the error estimated using the variance covariance matrix. Naturally the errors reflect the interpolation which has to be performed to obtain data at the same t value but different energies. From this point of view it is very useful to have available data on $d\sigma/dt$ over a wide range of energy measured at the same t values at each energy.

The kinematic corrections to (A2.2) have been examined by Spiro and Deram. [40] For equal mass scattering (such as $\pi^- p \rightarrow \pi^0 n$) they are completely negligible, even at low energies ($P_L \sim 3$ Gev/c). For unequal masses their inclusion produces an upward shift of α_{eff}, which may be impotant if we try to calculate α_{eff} at large $|t|$ using only low energy data in, for example, processes such as $\pi^+ p \rightarrow K^+ \Sigma^+$. However, to obtain the effective trajectories of chapter two, such corrections have been ignored, although we have included t_0 correctly as indicated in Appendix 1.

REFERENCES

REFERENCES

1. P.D.B. Collins and E.J. Squires, Regge poles in particle physics (Springer, Berlin, 1968).

2. A.D. Martin and T.D. Spearman, Elementary particle theory (North Holland, Amsterdam, 1970).

3. E.J. Squires, Complex angular momentum and particle physics (Benjamin, New York, 1963).

4. P.D.B. Collins, Physics Reports 1C No. 4 (1971).

5. G. Cohen-Tannoudji and Ph. Salin, Nuovo Cimento 55A 412 (1968).

6. A.C. Irving, A.D. Martin, V. Barger, Nuovo Cimento 16A 573 (1973).

7. F.J. Gilman, Phys Rev 171 1453 (1968).

8. P.D.B. Collins, "How Important are Regge Cuts?", Springer Tracts in Modern Physics 60 204 (1971).

9. P.L. Bonamy et al, Phys Lett 23 501 (1966).

10. J.V Allaby et al, Phys Lett 30B 500 (1969).

11. P.D.B. Collins, F.D. Gault, A. Martin, University of Durham preprint (April 1974).

12. F.D. Gault, A.D. Martin, G.L. Kane, Nucl Phys B32 429 (1971).

13. G.M. Cicuta and R.L. Sugar, Phys Rev D3 970 (1971).

14. S. Mandelstam, Nuovo Cimento 30 1127, 1148 (1963).

15. J.B. Bronzan and C.E. Jones, Phys Rev 160 1494 (1967).
    P.V. Landshoff and J.C. Polkinghorne, Phys Rev 181 1989 (1969).

16. D. Amati, S. Fubini, A. Stanghellini, Phys Lett 1 29 (1962).

17. R.J. Eden, P.V. Landshoff, D.I. Olive and J.C. Polkinghorne, The Analytic S-matrix (Cambridge University Press, 1966).

18. F. Elvekajeer, T. Inami, G.A. Ringland, Phys Lett 44B 91 (1973).

19. F. Henyey, G.L. Kane, Jon Pumlin, M.H. Ross, Phys Rev 182 1579 (1969).

20. R.C. Arnold and M.L. Blackmon, Phys Rev _176_ 2082 (1968).

21. R.C. Arnold, Phys Rev _183_ 1523 (1967).

22. B.J. Hartley and G.L. Kane, University of Michigan preprint, (January 1973).

23. G.A. Ringland, R.G. Roberts, D.P. Roy, J. Tran Thanh Van, Nucl Phys _B44_ 395 (1973).

24. B. Sadoulet, Nucl Phys _B53_ 135 (1973).

_._ S.E. Egli, D.W. Duke, N.W. Dean, Phys Rev _D9_ 1365 (1974).

25. R.J.N. Phillips and W. Rarita, Phys Rev _139B_ 1336 (1965).
G. Höhler et al, Phys Lett _20_ 79 (1966).

26. V.N. Bolotov et al, Institute of High Energy Physics—Serpukhov (preprint 1973).

27. P.D.B. Collins and R.A. Swetman, Nuovo Cimento Lett _5_ 793 (1972

28. G.C. Fox, Talk at the 1969 Stony Brook Conference (unpublished)

29. V. Barger and R.J.N. Phillips, Nucl Phys _B33_ 22 (1971).

30. P. Bonamy et. al.,Nucl Phys _B16_ 335 (1970), _B52_ 392 (1973).
D. Hill et al, Phys Rev Lett 30 239 (1973).

31. F. Halzen and C. Michael, Phys Lett _36B_ 367 (1971).
R.L. Kelly, Phys Lett _39B_ 635 (1972).

32. M. Borghini et al, Phys Lett 31B 405 (1970).

33. C.B. Chiu, "Phenomenology in Particle Physics 1971",
Editors C.B. Chiu, G.C. Fox, A.J.G. Hey.

34. F. Elvekajeer, T. Inami, R.J.N. Phillips, Nucl Phys _B64_ 301 (1973).

35. V. Barger, K. Geer, F. Halzen, Nucl Phys _B44_ 475 (1972).

36. W.D. Apel et al, XVII London Conference on High Energy Physics, July 1974.

37. G.R. Goldstein and J.T. Owens, Phys Rev _D7_ 865 (1973).

38. R.P. Worden, Nucl Phys _B53_ 205 (1973).

39. V. Barger and R.J.N. Phillips, Phys Rev 187 2210 (1969).

40. R.J.N. Phillips and W. Rarita, Phys Lett 19 598 (1965).

  M. Spiro and A. Derem, Nuovo Cimento Lett 1 81 (1971).

41. O. Guisan et al, Phys Lett 18 200 (1965).

42. R.L. Anderson et al, Phys Rev D4 1937 (1972).

  A.M. Osbourne et al, Phys Rev Lett 29 1621 (1972).

  W. Braunschweig et al, Nucl Phys B20 191 (1970).

43. R.L. Anderson et al, Phys Rev D1 27 (1970).

  W. Braunschweig et al, Phys Lett 33B 236 (1970).

44. M. Aguilar-Benitez et al, Phys Rev D4 2583 (1971).

  P. Astbury et al, Phys Lett 23 396 (1966).

45. Y. Goldschmidt-Clermont et al, Phys Lett 27B (1968).

  A. Firestone et al, Phys Rev Lett 25 958 (1970).

  D. Cline et al, Phys Rev Lett 23 1018 (1969).

46. G.W. Brandenburg et al, SLAC-PUB-1339 (November 1973).

47. R.D. Mathews, Nucl Phys B11 339 (1969).

48. S.M. Pruss et al, Phys Rev Lett 23 189 (1969).

  A. Bashian et al, Stony Brook preprint (1970).

49. W.F. Buhl et al, Phys Lett 48B 388 (1974).

50. P. Estabrooks and A.D. Martin, Phys Lett 42B 229 (1972).

51. R.J. Glauber, "Lectures in Theoretical Physics", Vol.1 (New York, Wiley, 1959).

52. For example ref.(8) and references therein.

53. G.M. Cicuta and R.L. Sugar, Phys Rev D3 970 (1971).

54. J.L. Cardy, Nucl Phys B28 445, 477 (1971).

55. For example ref. (8).

56. W. Magnus and F. Oberhettinger, "Special functions of mathematical physics" (Chelsea, New York, 1949).

57. R.P. Worden, Nucl Phys 40B 260 (1972).

58. J. Finkelstein, Nuovo Cimento 5A 413 (1971).

59. P.D.B. Collins and P.K. Hutt, Nuovo Cimento Lett 4 347 (1972).

60. H. Harari, Phys Rev Lett 22 582 (1969).

    J.L. Rosner, Phys Rev Lett 22 689 (1969).

61. G. Giradi et al, Nucl Phys B47 445 (1972).

62. G. Chadwick et al, SLAC-PUB-1093 (August 1972).

63. R.P. Worden, Nucl Phys B37 253 (1972).

64. P.D.B. Collins and A. Fitton, Nucl Phys B68 125 (1974).

65. Data references:

$\frac{d}{dt}(\gamma p \to \pi^0 p)$	Reference 42
$\frac{d}{dt}(\gamma p \to \eta^0 p)$	Reference 43
$R(\pi^0 n / \pi^0 p)$	A.M. Osbourne et al, Phys Rev Lett 29 1621 (1972).
Target asymmetry	P.S.L. Booth et al, Nucl Phys B38 339 (1973).
	H. Bienlein et al, Phys Lett 46B 131 (1973)
Photon asymmetry	R.L. Anderson et al, Phys Rev Lett 26 30 (1971).

66. J.L. Alonso and D. Schiff, Nucl Phys B51 557 (1973).

67. V.N. Gribov, I. Ya Pomeranchuk, K.A. Ter-Martiroysan, Phys Rev 139 B184 (1965).

68. N. Mukherji and B.P. Desai, Phys Rev D7 470 (1973).

69. V.N. Gribov, Soviet Physics JETP 26 414 (1968).

    (Zh. Eksp. Teor. Fiz 53 654 (1967).)

70. I.J. Muzinich, F.E. Paige, T.L. Trueman, Ling-Lie Wang, Phys Rev D6 1048 (1972).

d

71. V.N. Gribov, I. Ya Pomeranchuk, K.A. Ter-Martirosyan, Phys Lett $\underline{9}$ 269 (1964).

72. A review of the arguments used is given in ref.(74).

73. V.N. Gribov and A.A. Migdal, Sov J. Nucl Phys $\underline{8}$ 583 (1969). (Yad Fiz $\underline{8}$ 1002 (1968).)

74. J.L. Cardy and A.R. White, TH 1740 - CERN (unpublished)

75. J.B. Bronzan, Phys Rev $\underline{D4}$ 1097 (1971).

76. J.L. Cardy, Daresbury preprint DL/P 202 (April 1974).

77. R.G. Roberts, Proceedings of the fourteenth Scottish Universities Summer School in Physics, July - August 1973.

78. I.S. Gradsteyn and I.M. Ryzhik, "Tables of Integrals, Series and Products", (Academic Press, New York, 1965).

79. Data References:

$\frac{d\sigma}{dt}(\pi^- p \to \pi^0 n)$ P. Sonderegger et al, Phys Lett $\underline{20}$ 75 (1966)
(5.85, 13.3, 18.2 Gev/c)
A.V. Stirling et al, Phys Rev Lett $\underline{14}$ 763 (1965) (5.5, 9.8, 13.3, 18.2 Gev/c)
Reference 26
(21, 25, 32.5, 40, 48 Gev/c)

$\Delta\sigma (\pi N)$ K.J. Foley et al, Phys Rev Lett $\underline{11}$ 425 (1963)
Reference 26.
Reference 36.

Polarisation   Reference 30.

80. The data used in the fit is the same as in the eikonal model fit of chapter three, Reference 65.

81. See for example References 22 and 23.

82. For a SCRAM fit to backward scattering R.L. Kelly, G.L. Kane, F. Henyey, Phys Rev Lett $\underline{24}$ 1511 (1970) and for a general discussion of backward scattering E.L. Berger and G.C. Fox, Nucl Phys $\underline{B30}$ 1 (1971).